Logo

جامعة سيدي محمد بن عبد الله بفاس
UNIVERSITÉ SIDI MOHAMED BEN ABDELLAH DE FES

كلية العلوم ظهر المهراز فاس
FACULTE DES SCIENCES DHAR EL MAHRAZ FES

N° d'ordre : **82/2024**

Centre des Etudes : ***Sciences et Techniques et Sciences Médicales***

Formation Doctorale : ***Mathématiques et Applications***

Discipline : ***Mathématiques***
Spécialité : ***Mathématiques Appliquées***
Laboratoire : ***Analyse Mathématique et Applications***

THÈSE de DOCTORAT

Modeling Infectious Disease Dynamics with Fractional-Order Differential Equations: Applications to HIV, COVID-19, and Marine Parasites

Présentée par :

Safae L'KIMA

Soutenue le 26/12/2024 devant le jury :

Nom et Prénom	Grade	Établissement	Qualité
Pr. HACHIMI Hanaa	PES	École Nationale des Sciences Appliquées-Kénitra	Présidente
Pr. RAGUSA Maria Alessandra	PES	Université de Catania, Italie	Rapporteur& examinateur
Pr. HATTAF Khalid	PES	Centre Régional des Métiers de l'Education et de la Formation-Casablanca	Rapporteur& examinateur
Pr. ELMASSOUDI Mhamed	MCH	Faculté des Sciences Dhar EL Mahraz-Fès	Rapporteur& examinateur
Pr. LAHMI Badr	MCH	Faculté des Sciences Moulay Ismail, Meknès	Examinateur
Pr. MELIANI Said	PES	Faculté des Sciences et Techniques-Beni Mellal	Examinateur
Pr. AIT HAMMOU Mustapha	MCH	Faculté des Sciences Dhar EL Mahraz-Fès	Examinateur
Pr. AZROUL Elhoussine	PES	Faculté des Sciences Dhar EL Mehraz-Fès	Directeur de thèse

Résumé de la thèse

La modélisation mathématique est un outil essentiel pour les décideurs politiques dans la conception d'interventions efficaces et aide les gestionnaires de la santé à développer des programmes de santé publique ciblés. Au cours des dernières années, l'utilisation des équations différentielles d'ordre fractionnaire dans les modèles biologiques, en particulier dans les modèles épidémiologiques a considérablement augmenté. Cette thèse exploite le calcul fractionnaire pour explorer les modèles épidémiologiques et éco-épidémiologiques.

Tout d'abord, nous développons un modèle du VIH qui capture la dynamique complexe de l'épidémie, en intégrant les effets de la migration à l'aide des opérateurs Caputo et Atangana-Baleanu (ABC). En utilisant des équations différentielles d'ordre fractionnaire, ce modèle offre une représentation plus détaillée et précise des processus biologiques par rapport aux modèles d'ordre entier classiques, en tenant compte des interactions à long terme, des périodes de latence et des temps de récupération, qui sont essentiels pour modéliser la progression et le contrôle de la maladie.

Ensuite, nous analysons la dynamique de transmission des parasites marins en utilisant les dérivées de Caputo et ABC. Cette approche offre des perspectives plus approfondies que les méthodes traditionnelles, en soulignant le rôle crucial des effets de mémoire dans la détermination des dynamiques de transmission des parasites marins.

Enfin, nous présentons un nouveau modèle de transmission du COVID-19 utilisant la dérivée ABC. Nos résultats soulignent l'importance de classer les individus infectés en deux groupes : détectés et non détectés, et de mettre en œuvre une stratégie de contrôle optimal, telle que des campagnes de sensibilisation, pour gérer efficacement la propagation du COVID-19.

Cette recherche fournit une analyse approfondie des propriétés mathématiques des modèles, y compris l'existence et l'unicité des solutions, ainsi que leur positivité et leur bornitude. De plus, la stabilité des points d'équilibre et la sensibilité des paramètres utilisés dans ces modèles sont établies. L'étude intègre également des analyses numériques utilisant diverses méthodes. En capturant les effets de mémoire et les interactions non-locales qui caractérisent les systèmes épidémiologiques et éco-épidémiologiques complexes, cette recherche améliore notre compréhension des dynamiques des maladies infectieuses.

Mots clés : *Calcul fractionnaire, effets de mémoire, modèles épidémiologiques, modèles éco-épidémiologiques, VIH/SIDA, parasites marins, dynamique de la COVID-19, analyse numérique, méthodes numériques.*

Sidi Mohamed Ben Abdellah University-Fez Faculty of Sciences Dhar El Mahraz Laboratory LAMA, Department of Mathematics Doctoral Research in Mathematics

==========

Modeling Infectious Disease Dynamics with Fractional-Order Differential Equations: Applications to HIV, COVID-19, and Marine Parasites

==========

By

Safae L'KIMA

A Ph. D. Thesis

submitted to Sidi Mohamed Ben Abdellah University In Partial Fulfillment of the Requirements for the Degree of

Doctor of Mathematics

Specialty: Partial Differential Equations and numerical analysis

Defended on December 26, 2024.

A.Y. 2024-2025

Dedication




To my parents, for their endless love and encouragement,
To my sisters and brothers, for their constant support and belief in me,
To my friends, for their companionship and uplifting presence,
To all my professors, for their guidance and invaluable knowledge,
And to everyone who inspired me to strive for excellence.




ACKNOWLEDGEMENTS

The work accomplished during this thesis would not have been possible without the support, guidance, and encouragement of many individuals, to whom I extend my heartfelt gratitude.

First and foremost, I wish to express my deepest gratitude to my thesis supervisor, **Prof. El Houssine Azroul**, for his exceptional guidance, insightful feedback, and unwavering support throughout this research journey. His expertise and belief in my abilities have been a constant source of inspiration, motivating me to strive for excellence.

I am profoundly thankful to the esteemed members of the jury for dedicating their time and expertise to review and evaluate my work. I am particularly grateful to **Prof. Hanaa Hachimi** from the National School of Applied Sciences (ENSA), Kenitra, for graciously serving as the president of the jury.

My sincere thanks go to the rapporteurs, **Prof. Maria Alessandra Ragusa** from the University of Catania, Italy, **Prof. Khalid Hattaf** from the Faculty of Sciences Ben M'Sik, Casablanca, and **Prof. Mhamed Elmassaoudi** from the Faculty of Sciences Dhar El Mahraz, Fez. Their thoughtful reviews, detailed feedback, and the interest they have shown in my work have greatly enriched this thesis.

I would also like to express my appreciation to the examiners, **Prof. Said Meliani** from the Faculty of Sciences and Techniques, Beni Mellal, **Prof. Badr Lahmi** from the Faculty of Sciences, Moulay Ismail University, Meknès, and **Prof. Mustapha Ait Hammou** from the Faculty of Sciences, Dhar El Mahraz, Fez, for their insightful evaluations and constructive suggestions, which have been instrumental in refining this work.

To all the professors and administrative staff of the Department of Mathematics at the Faculty of Sciences Dhar El Mahraz, Fez, I extend my sincere gratitude for their warm welcome and unwavering support. Their exceptional professionalism and kindness have made this journey more meaningful.

I am deeply thankful to **Prof. Mohammed Shimi** and **Prof. Athmane Boumazourh** for their constant support, encouragement, and positivity, which have been a pillar of strength throughout my academic journey.

My heartfelt thanks go to my colleagues **Sara Bouda**, **Ghizlane Diki**, **Nezha Kamali**, and **Nassira Madani**. The camaraderie, collaboration, and shared moments in our research laboratory have been invaluable in overcoming challenges and fostering progress.

To my beloved parents, **Khadija** and **Larbi**, and my dear sisters and brothers, your unwavering belief in me, unconditional love, and encouragement have been the foundation of my achievements. This work is dedicated to you.

Finally, I express my sincere gratitude to my friends **Houria El Yahyaoui**, **Meryem El Lekhlifi**, **Jihane Tankoul**, **Fatima Hmidani**, **Ilham El Ouardi**, and **Omar Kchit** for their friendship, support, and the positive atmosphere they have created. Your encouragement and assistance have made this journey truly rewarding.

List of Symbols and Abbreviations

Mathematical Notations	
$\mathbb{N}$	The set of natural numbers.
$\mathbb{C}$	The complex plane.
$\mathbb{R}$	The set of real numbers.
$\mathbb{R}^+ = [0, +\infty)$	The set of non-negative real numbers.
e^z	Exponential function
$\mathrm{Re}(z)$	The real part of the complex number z.
$H^1(a,b)$	Sobolev space $W^{2,1}$.
$C(\Omega)$	Banach space of all real-valued, continuous functions on Ω.
D_t^α	Non-integer derivative of order α with respect to t.
${}^{\mathrm{RL}}\mathrm{D}_{a^+}^\alpha$	Riemann-Liouville left-sided derivative.
${}^{\mathrm{RL}}D_{b^-}^\alpha$	Riemann-Liouville right-sided derivative.
${}^{C}\mathrm{D}_t^\alpha$	Caputo derivative.
${}^{ABC}\mathrm{D}_t^\alpha$	Atangana-Baleanu derivative in Caputo sense.
${}^{ABR}\mathrm{D}_t^\alpha$	Atangana-Baleanu derivative in Riemann-Liouville sense.

List of Abbreviations	
RL	Riemann-Liouville
FDEs	Fractional Differential Equations
ODEs	Ordinary Differential Equations
ABC	Atangana-Baleanu-Caputo
ABR	Atangana-Baleanu-Riemann-Liouville
HIV	Human Immunodeficiency Virus
AIDS	Acquired Immunodeficiency Syndrome
COVID-19	Coronavirus Disease of 2019

ABSTRACT

Mathematical modeling is a critical tool for policymakers in designing effective interventions and supports health managers in developing targeted public health programs. In recent years, the application of fractional-order differential equations, particularly in epidemiological models, has grown significantly. This thesis leverages fractional calculus to explore both epidemiological and eco-epidemiological models.

Firstly, we develop an HIV model that captures the complex dynamics of the epidemic, incorporating migration effects through both the Caputo and Atangana-Baleanu (ABC) operators. By utilizing fractional-order differential equations, this model provides a more detailed and accurate representation of biological processes compared to conventional integer-order models, accounting for long-term interactions, latency periods, and recovery times, which are essential for modeling disease progression and control.

Secondly, we analyze the transmission dynamics of marine parasites using the Caputo and ABC derivatives. This approach offers deeper insights than traditional methods, emphasizing the critical role of memory effects in shaping the transmission dynamics of marine parasites.

Finally, we present a new model for COVID-19 transmission using the ABC derivative. Our findings underscore the importance of categorizing infected individuals into two groups: detected and undetected, and implementing an optimal control strategy, such as public awareness campaigns, to effectively manage the spread of COVID-19.

This research provides a thorough analysis of the mathematical properties of the models, including the existence and uniqueness of solutions, as well as their positivity and boundedness. Furthermore, the stability of equilibrium points and the sensitivity of the parameters used in these models are established. The study also incorporates numerical analyses using various schemes. By capturing the memory effects and non-local interactions that characterize complex epidemiological and eco-epidemiological systems, this research enhances our understanding of diverse infectious disease dynamics.

Keywords: Fractional Calculus, Memory Effects., Epidemiological Models, Eco-Epidemiological Models, HIV/AIDS, Marine Parasites, COVID-19 Dynamics, Numerical Analysis, Numerical Methods.

RÉSUMÉ

La modélisation mathématique est un outil essentiel pour les décideurs politiques dans la conception d'interventions efficaces et aide les gestionnaires de la santé à développer des programmes de santé publique ciblés. Au cours des dernières années, l'utilisation des équations différentielles d'ordre fractionnaire dans les modèles biologiques, en particulier dans les modèles épidémiologiques a considérablement augmenté. Cette thèse exploite le calcul fractionnaire pour explorer les modèles épidémiologiques et éco-épidémiologiques.

Tout d'abord, nous développons un modèle du VIH qui capture la dynamique complexe de l'épidémie, en intégrant les effets de la migration à l'aide des opérateurs Caputo et Atangana-Baleanu (ABC). En utilisant des équations différentielles d'ordre fractionnaire, ce modèle offre une représentation plus détaillée et précise des processus biologiques par rapport aux modèles d'ordre entier classiques, en tenant compte des interactions à long terme, des périodes de latence et des temps de récupération, qui sont essentiels pour modéliser la progression et le contrôle de la maladie.

Ensuite, nous analysons la dynamique de transmission des parasites marins en utilisant les dérivées de Caputo et ABC. Cette approche offre des perspectives plus approfondies que les méthodes traditionnelles, en soulignant le rôle crucial des effets de mémoire dans la détermination des dynamiques de transmission des parasites marins.

Enfin, nous présentons un nouveau modèle de transmission du COVID-19 utilisant la dérivée ABC. Nos résultats soulignent l'importance de classer les individus infectés en deux groupes : détectés et non détectés, et de mettre en œuvre une stratégie de contrôle optimal, telle que des campagnes de sensibilisation, pour gérer efficacement la propagation du COVID-19.

Cette recherche fournit une analyse approfondie des propriétés mathématiques des modèles, y compris l'existence et l'unicité des solutions, ainsi que leur positivité et leur bornitude. De plus, la stabilité des points d'équilibre et la sensibilité des paramètres utilisés dans ces modèles sont établies. L'étude intègre également des analyses numériques utilisant diverses méthodes. En capturant les effets de mémoire et les interactions non-locales qui caractérisent les systèmes épidémiologiques et éco-épidémiologiques complexes, cette recherche améliore notre compréhension des dynamiques des maladies infectieuses

Mots clés : Calcul Fractionnaire, Effets de Mémoire, Modèles Épidémiologiques, Modèle Éco-Épidémiologiques, VIH/SIDA, COVID-19, Parasites Marins, Méthodes Numériques, Analyse Numériques.

الملخص:

تُعد النمذجة الرياضية أداة بالغة الأهمية لواضعي السياسات في تصميم التدخلات الفعالة وتدعم مديري الصحة في وضع برامج الصحة العامة المستهدفة. في السنوات الأخيرة، نما تطبيق المعادلات التفاضلية ذات الترتيب الكسري، لا سيما في النماذج الوبائية، بشكل كبير. تستفيد هذه الأطروحة من حساب التفاضل والتكامل الكسري لاستكشاف النماذج الوبائية والبيئية الوبائية

أولاً، نقوم بتطوير نموذج لفيروس نقص المناعة المكتسبة يجسد الديناميكيات المعقدة للوباء، مع دمج تأثيرات الهجرة من خلال مشتقات كابوتو وأتانغانا-باليانو. من خلال استخدام المعادلات التفاضلية ذات الترتيب الجزئي، يوفر هذا النموذج تمثيلًا أكثر تفصيلاً ودقة للعمليات البيولوجية مقارنةً بالنماذج التقليدية ذات الترتيب الصحيح، مع مراعاة التفاعلات طويلة الأجل وفترات الكمون وأوقات التعافي. هذه الجوانب ضرورية لنمذجة تطور المرض ومكافحته

ثانيًا، نقوم بتحليل ديناميكيات انتقال الطفيليات البحرية باستخدام مشتقات كابوتو وأتانغانا-باليانو. يقدم هذا النهج رؤى أعمق من الطرق التقليدية، مع التأكيد على الدور الحاسم لتأثيرات الذاكرة في تشكيل ديناميكيات انتقال الطفيليات البحرية

وأخيرًا، نقدم نموذجًا جديدًا لانتقال كوفيد-19 باستخدام مشتقة أتانغانا-باليانو. تؤكد النتائج التي توصلنا إليها على أهمية تصنيف الأفراد المصابين إلى مجموعتين: المكتشفة وغير المكتشفة، وتنفيذ استراتيجية مكافحة مثلى، مثل التوعية العامة

LIST OF PUBLICATIONS

Refereed Journals/Manuscripts Under Preparation

1. A.Alla Hamou, E.Azroul, **S.L'Kima** (2024). The effect of migration on the transmission of HIV/AIDS using a fractional model: Local and global dynamics and numerical simulations. *Mathematical Methods in the Applied Sciences*.

2. A.Alla Hamou, E.Azroul, **S.L'Kima** (2024). Fractional order modeling of parasite-produced marine diseases with memory effect. *Modeling Earth Systems and Environment*.

3. E.Azroul, **S.L'Kima**. Mathematical modeling of marine parasite diseases with non-singular fractional derivative. *Proceedings of the International Conference on Fractional Calculus and Applications (ICFCA 2024)*.

4. E.Azroul, **S.L'Kima**. Fractional-order analysis of COVID-19 transmission: A study using the Atangana–Baleanu–Caputo derivative and optimal control, *(submitted)*.

5. E.Azroul, **S.L'Kima**. Fractional Calculus in HIV/AIDS Dynamics: A Study of Solution Behavior and Memory Effects. *(submitted)*.

List of Tables

Table **Page**

2.1 The parameter values used in the SIA model without migration. 26
2.2 Sensitivity analysis of $\mathscr{R}_0$ concerning the parameters of model SIA 33
2.3 The parameter values used in the SIA model with migration. 35

3.1 The parameter values used in the fractional order SIP model. 60
3.2 Sensitivity index results for the SIP model parameters. 69

4.1 Sensitivity indices of various model parameters. 103
4.2 Parameter values for the fractional model SEI^uI^dR. 106

List of Figures

Figure **Page**

0.1 Schematic representation of transitions in an SIR compartment model. 6
0.2 Compartmental diagram of the SIR model. 6

2.1 Schematic diagram of HIV and AIDS transmission. 25
2.2 HIV/AIDS transmission pattern with migration. 34
2.3 Dynamic behavior of the SIA model without migration as a function of Time (years) for different ρ values using the Adams-Bashforth-Moulton fractional method 45
2.4 Dynamic Behavior of the SIP model with migration as a function of time (Years) for different ρ values using the Adams-Bashforth-Moulton fractional method 46
2.5 System behavior with migration for different values of p and q. 47
2.6 Dynamics of the SIA model over time (in years) for various values of ρ using the Taoufik–Atangana scheme 53
2.7 Comparison of the ABC and Caputo fractional derivatives in the dynamics of the SIA model with $\rho = 0.95$. 54
2.8 Comparison of the ABC and Caputo fractional derivatives in the dynamics of the SIA model with $\rho = 0.75$. 55
2.9 Comparison of the ABC and Caputo fractional derivatives in the dynamics of the SIA model with $\rho = 0.60$. 56

3.1 Schematic diagram representing the SIP model. 62
3.2 Histogram showing sensitivity indices of $\mathscr{R}_0$ with respect to the parameters of the fractional SIP model. 70
3.3 The illustration of the numerical solution of the SIP fractional model at different fractional order α, with $\mathscr{F}(P) = \beta P$ and $\mathscr{R}_0 = 0.9309 < 1$. 72
3.4 The illustration of the numerical solution of the SIP fractional model at different fractional order α, with $\mathscr{F}(P) = \beta P$ and $\mathscr{R}_0 = 1.3861 > 1$. 73

3.5 Variations in solution trajectories: three-dimensional model SIP with different α values and $\mathscr{F}(P) = \beta P$. 73
3.6 The illustration of the numerical solution of the SIP fractional model at different fractional order α, with $\mathscr{F}(P) = \beta P/(1 + k_1 P)$ and $\mathscr{R}_0 = 0.9309 < 1$. . . . 75
3.7 The illustration of the numerical solution of the SIP fractional model at different fractional orders α, with $\mathscr{F}(P) = \beta P/(1 + k_1 P)$ and $\mathscr{R}_0 = 1.3861 > 1$ . . . 76
3.8 Variations in solution trajectories: three-dimensional model SIP with different α values and $\mathscr{F}(P) = \beta P/(1 + k_1 P)$. 76
3.9 Variation of $\mathscr{R}_0$ as a function of the most influential parameters. 77
3.10 Numerical solution of the SIP fractional ABC model at different fractional orders α, with $\mathscr{R}_0 = 0.93087$. 83
3.11 Numerical solution of the SIP fractional ABC model at different fractional orders α, with $\mathscr{R}_0 = 1.3861$. 84

4.1 Diagram of the $SEI^u I^d R$ model of COVID-19. 89
4.2 Bar plot representing the sensitivity indices of various model parameters. . . 103
4.3 Dynamics of the $SEI^d I^u R$ model over time (in years) for various values of α using the Taoufik–Atangana scheme. 109
4.4 The effect of τ on the dynamics of the exposed population. 110
4.5 The effect of τ on the dynamics of the infected undetected population for different values of α. 111
4.6 The effect of τ on the dynamics of the infected detected population for different values of α. 112
4.7 The effect of the transmission rate within the community β_u on the dynamics of the exposed population for different values of the fractional order α. 113
4.8 The effect of the transmission rate within the community β_u on the dynamics of the infected undetected population for different values of α. 114
4.9 The effect of the transmission rate within the community β_u on the dynamics of the infected detected population for different values of α. 115
4.10 Comparison of the evolution of COVID-19 dynamics with and without Control. 116

TABLE OF CONTENTS

Dedication i

Acknowledgements ii

List of Symbols and Abbreviations iii

List of Puplications iv

Abstract v

Résumé vi

List of Tables vii

List of Figures viii

Table of Contents x

General Introduction 1

1 Preliminaries on Fractional Calculus 10

1.1 Special Functions in Fractional Calculus 10

1.1.1 Gamma Function 10

1.1.2 Mittag-Leffler Function 11

1.2 Fundamental concepts of fractional integration and differentiation 12

1.2.1 Riemann–Liouville fractional integral and derivative 12

1.2.2 Caputo derivative 13

1.2.3 Atangana–Baleanu Fractional Derivative and Integral 16

1.3 Fractional Laplace transform 16
1.4 Analysis of existence, uniqueness, and stability for fractional differential systems 18
1.4.1 Temporal System Equilibria 18
1.4.2 Existence and uniqueness of solution 18
1.4.3 Stability of equilibrium points 19
1.4.4 Sensitivity analysis 19
1.5 Numerical approximation of FDEs 20
1.5.1 Adams-Bashforth-Moulton fractional technique 20
1.5.2 Taoufik–Atangana scheme: two-step Lagrange polynomial approximation 21

2 The effect of migration on the transmission of HIV/AIDS using a fractional model: local and global dynamics and numerical simulations 23
2.1 Caputo fractional model of HIV and AIDS: with and without migration . . 25
2.1.1 Formulation of a fractional model of HIV/AIDS without migration 25
2.1.2 Formulation of a fractional model of HIV/AIDS with migration . . 34
2.1.3 Numerical Solutions of FDEs using the Adams-Bashforth-Moulton fractional Technique 42
2.2 Dynamic analysis of the ABC fractional approach to HIV and AIDS with migration 47
2.2.1 ABC-Fractional equations: existence and uniqueness 47
2.2.2 Non-negativity and boundedness of solutions 50
2.2.3 Numerical schemes for FDEs using the Atangana–Taoufik fractional method 51
2.2.4 Numerical sumulations and discussions 52
2.3 Comparison of ABC and Caputo fractional derivatives in HIV and AIDS dynamics 53
2.4 Conclusion 57

3 Fractional order modeling of parasite-produced marine diseases with memory effect 58
3.1 Model formulation 59
3.2 Analyzing the dynamics of marine parasite diseases using the Caputo derivative 60
3.2.1 Existence and uniqueness of solution and non-negativity 61

3.2.2 Biologically feasible region of the solution . . . 63
3.2.3 Basic reproduction number and equilibrium . . . 64
3.2.4 Analysis of local stability for the fractional model . . . 67
3.3 Sensitivity analysis . . . 68
3.4 Numerical simulations and discussion of Caputo fractional derivative . . . 70
3.4.1 The impact of memory effect and incidence function on population dynamics . . . 70
3.4.2 The influence of the model parameters . . . 74
3.5 Investigating the SIP model through the ABC derivative . . . 78
3.5.1 Existence and uniqueness of solution . . . 78
3.5.2 Nonnegativity of the solutions . . . 80
3.5.3 Biologically feasible region of the solution . . . 81
3.5.4 Numerical results and discussion . . . 82
3.6 Conclusion . . . 85

4 Fractional-Order Analysis of COVID-19 Transmission: A Study Using the Atangana–Baleanu–Caputo Derivative and Optimal Control 86
4.1 Model formulation . . . 87
4.2 Mathematical analysis of the fractional model: existence, positivity, and stability . . . 89
4.2.1 Existence and uniqueness of the solution . . . 89
4.2.2 Nonnegativity of solutions . . . 95
4.2.3 Biologically feasible region of the solution . . . 96
4.2.4 Basic reproduction number . . . 97
4.2.5 The Equilibrium points . . . 97
4.2.6 Stability analysis . . . 98
4.3 Fractional control and sensitivity analysis of the SEI^uI^dR epidemic model 102
4.3.1 Sensitivity analysis of $\mathscr{R}_0$ . . . 102
4.3.2 Formulation of fractional control optimization for the SEI^uI^dR model . . . 104
4.4 Numerical simulations . . . 106
4.4.1 Effect of the ABC derivative on model dynamics . . . 107
4.4.2 Numerical simulation of the control problem . . . 108
4.5 Conclusion . . . 117

Conclusion and Future Perspectives 118

Bibliography **120**

General Introduction

Brief historical overview of fractional calculus

Fractional calculus is an extension of classical calculus in which the concepts of derivatives and integrals are generalized to non-integer (fractional) orders. Unlike traditional derivatives, which are limited to integer orders ($\alpha = 1, \ldots, n, n \in \mathbb{N}$), fractional derivatives provide a more flexible approach to differentiation and integration. This flexibility makes fractional calculus a powerful tool for modeling processes that exhibit memory effects and hereditary properties, allowing a system's past states to influence its present and future behavior [72]. An additional benefit of using fractional derivatives in mathematical models is the expansion of the stability region, as demonstrated in Matignon's work from 1996 [63].

Moreover, there are numerous definitions of fractional derivatives, each developed at different points in history to suit various applications. The most well-known definitions include:

- The **Grunwald-Letnikov derivative**, developed by Letnikov in 1868 [55].
- The **Riemann-Liouville derivative**, proposed in 1876 [74].
- The **Hadamard derivative**, introduced by Hadamard in 1892 [60].
- The **Weyl derivative**, proposed by Weyl in 1917 [91].
- The **Caputo derivative**, introduced by Caputo in 1967 [22].
- More recent definitions include the **Caputo–Fabrizio derivative** [23] and the **Atangana–Baleanu derivative**, introduced in 2016 [14, 16].

These definitions offer different perspectives on fractional calculus, enabling its application in a wide variety of fields, including the modeling of complex systems in epidemiology. They accommodate various modeling requirements, particularly for systems

exhibiting non-local behaviors, such as long-term memory or delayed responses. The applications of fractional calculus are rapidly expanding across numerous disciplines, such as mechanics [13], electrochemistry [28], biophysics [68], science and engineering [80], economics [77], and others [6, 24]. In many of these cases, traditional integer-order derivatives prove insufficient for accurately representing such phenomena.

Fractional calculus is often seen as a contemporary and innovative topic, but its origins can be traced back to a letter from Gottfried Wilhelm Leibniz to the Marquis de L'Hôpital in **1695**, where he answered a question about the implications of taking a derivative of order $\alpha = \frac{1}{2}$, expressed as $\frac{d^\alpha}{dx^\alpha}$. Although this question remained largely theoretical for many years, it laid the groundwork for future inquiry. Later, L. Euler **(1738)**, renowned for his vast contributions to mathematics, made significant progress by generalizing the concept of factorials, which led to the development of the gamma function. This work also laid the foundation for fractional integrals. Euler further provided the following definition for the fractional derivative [35]:

$$D^{\alpha}_{a^+} f(x) = \frac{\Gamma(1-\beta)}{\Gamma(1-\alpha-\beta)} \frac{1}{(x-a)^{\beta+\alpha}}. \tag{1}$$

Lagrange **(1772)** made an indirect contribution to the law of exponents for differential operators of integer order through the formulation of the following expression [53]:

$$\frac{d^m}{dx^m} \cdot \frac{d^n}{dx^n} y = \frac{d^{m+n}}{dx^{m+n}} y, \tag{2}$$

which holds for integer-order derivatives. This concept was later extended to fractional calculus, as demonstrated by A.V. Letnikov in 1868 [55].

Laplace **(1812)** was the first to introduce the concept of fractional derivatives using an integral-based approach [54]. However, it was Lacroix who provided the fractional derivative of arbitrary order for $d^n x^a / dx^n$, specifically for $n = 1$ and $\alpha = \frac{1}{2}$. Lacroix applied Euler's method, described in (1), and derived the following expression [52]:

$$\frac{d^{\frac{1}{2}}}{dx^{\frac{1}{2}}} x = \frac{2\sqrt{x}}{\sqrt{\pi}}. \tag{3}$$

Joseph B. J. Fourier (**1822**) was the first mathematician to propose a fractional derivative for trigonometric functions, which he expressed as follows [37].

$$\frac{d^\alpha f(x)}{dx^\alpha} = \frac{1}{2\pi} \int_{-\infty}^{+\infty} \lambda^\alpha d\lambda \int_{-\infty}^{+\infty} f(t) \cos(\lambda x - tx + p\pi/2) dt. \tag{4}$$

Niels Henrik Abel (**1823**) was the pioneer in applying fractional calculus to address an integral equation known as the Tautochrone problem, which remained one of the few examples of fractional calculus applications for an extended period [41].

A pivotal development took place with I. Liouville (**1835**), who provided a rigorous definition of fractional derivatives and integrals, thereby strengthening the theoretical framework of the discipline [64]. B. Riemann **(1847)** built upon these concepts by creating the Riemann-Liouville integral, which became essential to the study of fractional calculus [41].

$$D^{-\alpha}f(x) = \frac{1}{\Gamma(\alpha)}\int_c^x (x-t)^{\alpha-1} f(t)dt. \tag{5}$$

I. Hadamard (**1892**) made significant contributions by defining what are now known as Hadamard fractional derivatives, expressed as follows [62].

$$D_a^{(\alpha)}f(x) = \frac{1}{\Gamma(1-\alpha)} x\frac{d}{dx}\int_0^x \frac{f(t)}{\left(\ln\frac{x}{t}\right)^{\alpha}}\frac{dt}{t}, 0<\alpha<1, \tag{6}$$

H. Weyl (**1917**) significantly advanced fractional calculus by investigating the relationships between fractional integrals and complex analysis, which enhanced the understanding of mathematical structures in this domain, expressed as follows[91].

$$\begin{aligned} I_+^{\alpha}f(x) &= \frac{1}{\Gamma(\alpha)}\int_{-\infty}^x \frac{f(t)}{(x-t)^{1-\alpha}}dt, \\ I_-^{\alpha}f(x) &= \frac{1}{\Gamma(\alpha)}\int^{\infty} \frac{f(t)}{(x-t)^{1-\alpha}}dt. \end{aligned} \tag{7}$$

P. Lévy (**1923**) expanded the application of fractional calculus to probability theory, significantly influencing its development and uses in areas such as stochastic processes and anomalous diffusion. More recently, significant contributions to fractional calculus have been made by mathematicians such as Caputo, Jumarie, Caputo-Fabrizio, and Atangana. While these are just a few notable examples, their work, along with that of many others, has laid a robust foundation for this rapidly advancing field.

Over the last few decades, the use of fractional calculus has expanded significantly, particularly in systems where memory and hereditary properties are crucial, such as viscoelastic materials [61], anomalous diffusion [79], and biological processes [17]. The growing interest in fractional calculus within epidemiology also stems from its ability to model the spread of infectious diseases more realistically by accounting for time delays, latent periods, and the long-term impact of past infections on future dynamics. This thesis is devoted to the application of fractional calculus to classical mathematical models, with a specific focus on its use in epidemiology and eco-epidemiology. In the following section, we will explore the theoretical aspects of compartmental models in epidemiology and discuss their key properties relevant to this field.

Mathematical modeling in epidemiology: a historical and conceptual overview

Mathematical modeling has become a well-established and rapidly expanding interdisciplinary field. It is widely regarded as one of the most exciting applications of mathematics due to the inherent complexity of biological systems. This complexity necessitates collaboration across disciplines. For mathematicians, biology presents new challenges and opportunities to develop innovative mathematical approaches, while for biologists, mathematical modeling offers a powerful tool to gain deeper insights into biological phenomena.

In this thesis, we focus on the study of epidemiological and eco-epidemiological models. Both types of models play crucial roles in understanding the dynamics of diseases and their impact on populations. Epidemiology, which investigates disease dynamics within populations, has long relied on mathematical models as essential tools for analyzing, predicting, and controlling the spread of infectious diseases. These models allow researchers to simulate various scenarios, such as disease transmission and intervention strategies, providing valuable insights into potential outcomes. Over the past century, epidemiological models have evolved from basic deterministic frameworks into more sophisticated systems that incorporate stochastic elements and biological complexities.

While epidemiology focuses on disease transmission within human populations, eco-epidemiology extends this scope to encompass the interactions between diseases and ecological systems. By bridging the fields of ecology and epidemiology, eco-epidemiology examines how infections affect ecological populations and contribute to regulating their sizes. It is well recognized that many ecological communities are influenced by infectious diseases, making this interaction a significant area of research. The mathematical study of eco-epidemiological models has provided new insights into previously unexplored aspects of these complex systems.

The development of epidemiological models has a rich history, with its origins dating back to 1760, when Daniel Bernoulli used differential equations to model the effects of smallpox inoculation [20]. The foundations of mathematical epidemiology, particularly the compartmental approach, were laid not by mathematicians but by physicians at the start of the twentieth century. Sir Ronald Ross was awarded the Nobel Prize in Medicine in 1902 for demonstrating the dynamics of malaria transmission between mosquitoes and humans [75]. Modern epidemiological modeling is largely credited to William Ogilvy Kermack and Anderson Gray McKendrick, who introduced the influential SIR model in

1927 [47]. Building on their work, compartmental models divide the population studied into distinct groups based on the dynamics of disease transmission. These models assume specific movement patterns between compartments over time. Diseases that confer immunity have a different compartmental structure compared to non-immune or vector-borne diseases. The transitions between compartments are mathematically expressed through time derivatives of compartment sizes, with the models initially formulated as differential equations.

The SIR model is often visualized using a compartmental diagram, as depicted in Figure 0.1. In this model, the population is categorized into three distinct compartments: Susceptible (S), Infected (I), and Recovered (R). Individuals transition between these compartments based on the dynamics of disease spread. Susceptible individuals (S), who are at risk of contracting the disease, may become Infected (I) through contact with infected individuals, as denoted by the arrow labeled *new infections*. Once infected, individuals either recover and move into the Recovered (R) compartment, as shown by the *recovery* arrow, or are *removed* through death or other factors. Recovered individuals gain immunity, but in certain cases, they can lose this immunity and return to the susceptible group, as illustrated by the *loss of immunity* feedback loop. Additionally, each compartment has a *removal* flow, which represents the natural departure from the population due to reasons like death. The system captures how new susceptible individuals enter the population, the progression of infection, and the recovery process, providing insights into the dynamics of disease transmission over time. It is important to note that the number of compartments in these models depends on the nature of the disease and its historical context. Therefore, we can represent various models such as SI, SIR, or SEIR, depending on the specific characteristics of the disease.

Building upon the foundational concepts discussed earlier, we can illustrate the dynamics of disease transmission through a simple example: the SIR model, proposed by Kermack and McKendrick in 1927. In this model, the total population N is divided into three compartments: Susceptible (S), Infected (I), and Recovered (R), as illustrated in Figure 0.2. We make the following assumptions:

- Susceptible individuals can contract the disease and become infected at a rate proportional to the number of susceptible individuals and the number of infected individuals, denoted as rSI.
- Infected individuals can recover from the disease and move to the recovered category at a rate aI.

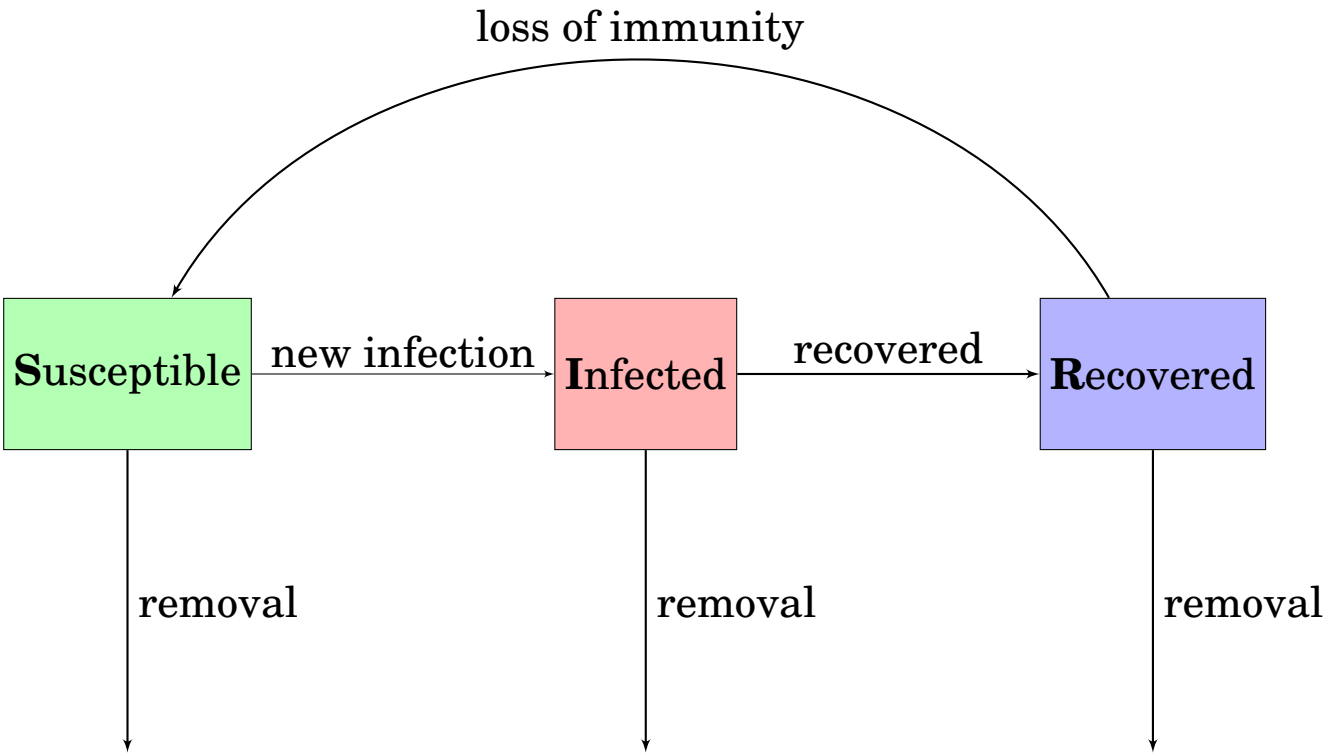


Figure 0.1: Schematic representation of transitions in an SIR compartment model.

- Recovered individuals gain immunity and cannot return to the susceptible state.

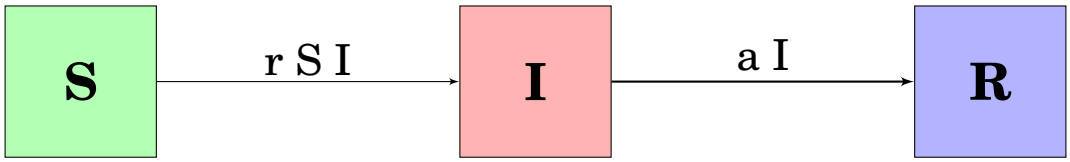


Figure 0.2: Compartmental diagram of the SIR model.

Based on these assumptions, we can describe the dynamics of the model using the following ordinary differential equations (ODEs):

$$\frac{dS}{dt} = -rSI, \tag{8}$$

$$\frac{dI}{dt} = rSI - aI, \tag{9}$$

$$\frac{dR}{dt} = aI. \tag{10}$$

Where $S_0 \geq 0$, $I_0 \geq 0$, and $R_0 \geq 0$ represent the initial numbers of susceptible individuals, infected individuals, and recovered individuals, respectively.

The equation (8) represents the rate at which susceptible individuals become infected. The negative sign indicates a decrease in the susceptible population as individuals contract the disease. The infection rate is proportional to both the susceptible population S and the infected population I, with r being the infection rate constant.

In equation (9), the infected population increases as susceptible individuals become infected (rSI) and decreases as infected individuals recover at a rate of aI, where a is the recovery rate constant.

Finally, in equation (10), the recovered population increases as infected individuals recover at the rate of aI. There is no loss from this compartment, as we assume that recovered individuals remain immune.

It is crucial to understand that the model described in (8)-(10) is valid only while $S(t)$ and $I(t)$ and $R(t)$ remain nonnegative. Therefore, if either $S(t)$ or $I(t)$ drops to zero, we interpret this as the end of the model. We find that $\frac{dS}{dt} < 0$ at all times, and $\frac{dI}{dt} > 0$ occurs only when $S > \frac{a}{r}$. This indicates that I will increase as long as S exceeds $\frac{a}{r}$. However, because S consistently declines over time, I will eventually decrease and approach zero. In cases where $S_0 < \frac{a}{r}$, I will decrease to zero, indicating no epidemic. Conversely, when $S_0 > \frac{a}{r}$, I will rise to a peak that occurs when $S = \frac{a}{r}$ before ultimately declining to zero, indicating an epidemic.

Understanding these dynamics is essential for determining the conditions under which an epidemic can occur. The value $\frac{rS_0}{a}$ acts as a critical threshold known as **the basic reproduction number** $\mathscr{R}_0$ [31], which determines the potential for an epidemic outbreak. If $\mathscr{R}_0 < 1$, the infection will eventually die out, whereas if $\mathscr{R}_0 > 1$, an epidemic is likely to occur. The basic reproduction number $\mathscr{R}_0$ represents the expected *number of secondary infections generated by a single infected individual introduced into a fully susceptible population*. In subsequent sections of this thesis, we will explore the computation of this threshold for more complex epidemic models.

Objective, framework, and outline of the thesis

The objective of this thesis is to apply fractional calculus to epidemiological modeling, focusing on the development of models that incorporate memory effects and non-local interactions within populations. This approach aims to provide a deeper understanding of the transmission dynamics of infectious diseases, leading to more accurate predictions

and improved strategies for controlling outbreaks.

In particular, this work seeks to:

- Introduce fractional-order derivatives in the formulation of epidemiological and eco-epidemiological models.
- Analyze the existence, uniqueness, and stability of solutions within these models.
- Conduct numerical simulations to study the behavior of fractional models and compare their predictions to those of classical models.
- Investigate the impact of fractional-order derivatives on the effectiveness of disease control measures.

The first chapter provides a review of some fundamental concepts. It introduces the theory of fractional calculus, focusing on key definitions and foundational results essential for the development of this study. Then, some elements of the theory of dynamical systems are presented, which allow us to analyze the stability of equilibrium points as well as the existence and uniqueness of solutions for fractional differential equations, including a sensitivity analysis. We conclude **Chapter** 1 by presenting several numerical methods that will be used throughout our study. To keep this chapter concise, we refer the reader to relevant reference works for more detailed explanations.

In **Chapter** 2, we present the analysis of a fractional-order mathematical model for HIV/AIDS infection, with a particular focus on the influence of migration on the dynamics of the model. We detail the modeling framework, which incorporates both the Caputo derivative and the Atangana–Baleanu–Caputo (ABC) derivative approach, allowing for a comparative study. First, we demonstrate that the solutions of the corresponding fractional differential equations are positive and bounded. We then compute the basic reproduction number $\mathscr{R}_0$ using the next-generation matrix method and conduct a sensitivity analysis of the model parameters in the absence of migration. We proceed by examining the equilibrium points of the system, analyzing their local and global stability. Finally, we validate our theoretical findings through numerical simulations for various values of the fractional order.

In **Chapter** 3, we shift our focus to diseases caused by marine parasites and propose a fractional-order mathematical model to investigate the effects of both the Caputo and ABC derivatives on parasite dynamics. The chapter provides a comprehensive mathematical analysis, including the existence and uniqueness of solutions, non-negativity of the state variables, and the characterization of the biologically feasible region. We

also conduct a sensitivity analysis of the model parameters and study the stability of the equilibrium points. Finally, numerical simulations are performed for both models to illustrate the impact of the different fractional derivatives on the dynamics of marine parasite infections.

Chapter 4 examines a fractional-order model for the COVID-19 pandemic using the Atangana–Baleanu derivative in the Caputo sense, emphasizing its implications for public health. We employ the Banach fixed-point theorem to demonstrate the existence and uniqueness of solutions. Furthermore, we establish the positivity and boundedness of the solutions, as well as analyze the local stability of equilibrium points. A central focus of this chapter is a sensitivity analysis that identifies key parameters, particularly the transmission coefficient β_u, which reflects transmission rates in isolation settings and has the greatest impact on the basic reproduction number $\mathscr{R}_0$. Numerical simulations, conducted using the Taoufik–Atangana scheme, validate the robustness of the model, highlighting the significance of the fractional-order parameter in delaying convergence and capturing unique peak behaviors not observed with integer-order derivative. Additionally, we propose an optimal control strategy aimed at reducing infection rates through increased public awareness, resulting in a significant reduction in both the exposed and infected populations, whether detected or undetected. Our findings underscore the potential of the ABC derivative in capturing complex epidemic trends, offering valuable insights for effective public health interventions and disease control.

The thesis concludes with a summary of the key findings and outlines future research directions.

CHAPTER 1

PRELIMINARIES ON FRACTIONAL CALCULUS

This chapter does not aim to provide an exhaustive theory of fractional calculus but rather to present the essential definitions and foundational concepts necessary for the discussions in subsequent chapters. In the previous section, we introduced key mathematical functions, such as the Gamma and Mittag-Leffler functions, which play a central role in fractional calculus. Here, we focus on the most widely used definitions of fractional integrals and derivatives and summarize the main results associated with these operators. Additionally, we address important topics, including the existence, uniqueness, and stability of solutions to fractional differential equations, as well as the numerical schemes and methods applied across various models. Furthermore, we introduce an important technique in mathematical biology: sensitivity analysis.

1.1 Special Functions in Fractional Calculus

1.1.1 Gamma Function

The Gamma function, also known as Euler's Gamma function, extends the concept of the factorial to real and complex numbers. In fractional calculus, it is typically defined using Euler's integral of the second kind, providing a foundation for its application in more advanced mathematical contexts

Definition 1.1. *([51, 72] For any real or complex number z such that* $\mathrm{Re}(z) > 0$*, the Euler*

gamma function $\Gamma(z)$ *is defined by the improper integral:*

$$\Gamma(z) = \int_0^\infty t^{z-1} e^{-t}\, \mathrm{d}t. \tag{1.1}$$

The gamma function satisfies key properties:

- $\Gamma(n+1) = n!$ for integer value n.
- $\Gamma(z+1) = z\Gamma(z)$ for $\mathrm{Re}(z) > 0$.

The first assertion can be deduced using (1.1), and the second property can be established using integration by parts. For further details regarding these properties, see [51, 72].

1.1.2 Mittag-Leffler Function

The Mittag-Leffler function is a generalization of e^z, denoted as $E_\alpha(z)$ for $\alpha > 0$, and is named in honor of the mathematician Magnus Gustaf Mittag-Leffler, who introduced it in the early 19th century. Subsequently, Agrawal extended these functions to include two parameters, ($\alpha > 0$ and $\beta \in \mathbb{C}$), referring to them as the two-parameter Mittag-Leffler functions noted by $E_{\alpha,\beta}(z)$. These functions play a crucial role in fractional-order differential equations.

Definition 1.2. *([72]). The one-parameter Mittag-Leffler function is defined as:*

$$E_\alpha(z) = \sum_{k=0}^{\infty} \frac{z^k}{\Gamma(\alpha k + 1)}, \quad z \in \mathbb{C},\ \alpha > 0. \tag{1.2}$$

To further generalize the Mittag-Leffler function, an additional parameter β is introduced, leading to the two-parameter Mittag-Leffler function:

Definition 1.3. *([72]). A two-parameter Mittag-Leffler function is expressed through the following series expansion:*

$$E_{\alpha,\beta}(z) = \sum_{k=0}^{\infty} \frac{z^k}{\Gamma(\alpha k + \beta)}, \quad (\alpha > 0, \quad \beta > 0). \tag{1.3}$$

The additional parameter β allows the function to model more complex behaviors than the one-parameter version. The parameter β provides more control over the shape of the function, influencing the decay or growth rate in the series. When $\beta = 1$, the two-parameter function reduces to the one-parameter version: $E_{\alpha,1}(z) = E_\alpha(z)$. In general, the Mittag-Leffler function $E_{1,\beta}(z)$ can be expressed as:

$$E_{1,m}(z) = \frac{1}{z^{m-1}} \left(\exp(z) - \sum_{k=0}^{\infty} \frac{z^k}{k!} \right).$$

Additionally, the hyperbolic cosh and sinh functions are specific cases of the Mittag-Leffler function:

$$E_{2,1}(z^2) = \sum_{k=0}^{\infty} \frac{z^{2k}}{(2k)!} = \cosh(z), \quad \text{since } \Gamma(2k+1) = (2k)!,$$
$$\text{and} \quad E_{2,2}(z^2) = \frac{1}{z} \sum_{k=0}^{\infty} \frac{z^{2k+1}}{(2k+1)!} = \frac{\sinh(z)}{z}.$$

The Mittag-Leffler function also satisfies the following equation, as presented in [50]:

$$E_{\alpha,\beta}(z) = zE_{\alpha,\alpha+\beta}(z) + \frac{1}{\Gamma(\beta)}. \tag{1.4}$$

This relationship highlights the versatility of the Mittag-Leffler function, showcasing its importance in various mathematical contexts, including its connection to fractional calculus and its applications in modeling dynamic systems.

1.2 Fundamental concepts of fractional integration and differentiation

In this part, we examine key properties of fractional integrals and derivatives that will be essential for the later analysis of our specific problems. The content presented here is drawn from a range of books and research papers[51, 72, 94].

1.2.1 Riemann–Liouville fractional integral and derivative

There are many definitions of the fractional derivative operator, and in this section, we will present the most commonly used ones. According to the Riemann-Liouville approach to fractional calculus, the concept of a fractional integral naturally arises from the well-known Cauchy formula, which simplifies the calculation of the n-th primitive of a function $f(t)$ to a single integral.

$$I_a^n f(t) = \int_a^t \int_a^{u_n} \int_a^{u_{n-1}} \dots \int_a^{u_3} \int_a^{u_2} f(u_1) du_1 du_2 \dots du_{n-1} du_n, \quad \forall t \in [a,b]. \tag{1.5}$$

Using Fubini's theorem, we obtain

$$I_a^n f(t) = \frac{1}{(n-1)!} \int_a^t (t-u)^{n-1} f(u) du, \quad \forall t \in [a,b]. \tag{1.6}$$

Utilizing the Gamma function ($\Gamma(n) = (n-1)!$), Cauchy's formula can be generalized to a fractional order α(where α is not necessarily an integer) in the following manner.

Definition 1.4. *([51, 72]) Let $\alpha > 0$. The right-sided Riemann-Liouville fractional integral, denoted by $I_a^\alpha f(t)$ and the left-sided one by $I_b^\alpha f(t)$, for a given function f, are defined as:*

$$I_a^\alpha f(t) = \frac{1}{\Gamma(\alpha)} \int_a^t (t-u)^{\alpha-1} f(u)\, du, \quad \forall t \in [a,b]. \tag{1.7}$$

$$I_b^\alpha f(t) = \frac{1}{\Gamma(\alpha)} \int_t^b (u-t)^{\alpha-1} f(u)\, du, \quad \forall t \in [a,b]. \tag{1.8}$$

By convention, if $\alpha = 0$, we define $I_a^0 f(t) = I_b^0 f(t) = f(t)$.

Definition 1.5. *[51, 72] Let $\alpha > 0$ and $n = [\alpha] + 1$, where $[\alpha]$ means the integer part of α. The Riemann-Liouville fractional derivatives $D_{a+}^\alpha f$ and $D_{b-}^\alpha f$ of order α are defined by*

$$\begin{aligned} \left(D_{a+}^\alpha f\right)(t) &:= \left(\frac{d}{dt}\right)^n \left(I_a^{n-\alpha} f\right)(t) \\ &= \frac{1}{\Gamma(n-\alpha)} \left(\frac{d}{dt}\right)^n \int_a^t \frac{f(t)dt}{(t-t)^{\alpha-n+1}} \quad (t > a) \end{aligned} \tag{1.9}$$

and

$$\begin{aligned} \left(D_{b-}^\alpha f\right)(t) &:= \left(-\frac{d}{dt}\right)^n \left(I_{b-}^{n-\alpha} f\right)(t) \\ &= \frac{1}{\Gamma(n-\alpha)} \left(-\frac{d}{dt}\right)^n \int_t^b \frac{f(t)dt}{(t-t)^{\alpha-n+1}} \quad (t < b) \end{aligned} \tag{1.10}$$

In particular, when $\alpha = 0$***, then*** $\left(D_{a+}^0 f\right)(t) = \left(D_{b-}^0 f\right)(t) = f(t)$ ***; and or*** $\alpha = n \in \mathbb{N}$ $\left(D_a^n f\right)(t) = f^{(n)}(t)$

The Riemann-Liouville fractional derivative has played a crucial role in the development of fractional calculus, but it has certain limitations, especially in applications to physical or real-world problems [25]. In biological models, it results in initial conditions that are often challenging to interpret and does not assign a zero derivative to constants, which poses issues for consistency. Therefore, a revision of this approach is necessary to bridge the gap between theoretical mathematics and practical applications.

1.2.2 Caputo derivative

In this section, we focus on the Caputo fractional derivative, which was first introduced by Michele Caputo in 1967 [22]. This derivative has several advantages over the traditional Riemann-Liouville approach, particularly for modeling real-world phenomena.

One key benefit is its treatment of initial conditions, which are more intuitively applicable in physical or biological contexts. Unlike the Riemann-Liouville operator, the Caputo-type operator sets the derivative of a constant function to zero, making it more suitable for physical models where this property is expected. This feature simplifies the formulation of initial value problems, which is especially important in epidemiological models, as it allows the direct application of classical initial conditions (e.g., population size).

Definition 1.6. *([22, 72, 76]). Let $\alpha > 0$ and $n = \lfloor \alpha \rfloor + 1$, where $\lfloor \alpha \rfloor$ denotes the integer part of α. If $f(x) \in C^n[a,b]$, the Caputo fractional derivatives, denoted by $\left({}^C D^{\alpha}_{a+} f\right)(x)$ and $\left({}^C D^{\alpha}_{b-} f\right)(x)$, are expressed as follows:*

$$\left({}^C D^{\alpha}_{a+} f\right)(x) = \frac{1}{\Gamma(n-\alpha)} \int_a^x \frac{f^{(n)}(t)}{(x-t)^{\alpha-n+1}}\, dt = \left(I^{n-\alpha}_{a+} D^n f\right)(x), \tag{1.11}$$

and

$$\left({}^C D^{\alpha}_{b-} f\right)(x) = \frac{(-1)^n}{\Gamma(n-\alpha)} \int_x^b \frac{f^{(n)}(t)}{(t-x)^{\alpha-n+1}}\, dt = (-1)^n \left(I^{n-\alpha}_{b-} D^n f\right)(x), \tag{1.12}$$

where $D = \frac{d}{dx}$.

Specifically, for $0 < \alpha < 1$, we have the following result

$$\left({}^C D^{\alpha}_{a+} f\right)(x) = \frac{1}{\Gamma(1-\alpha)} \int_a^x \frac{f'(t)dt}{(x-t)^{\alpha}} =: \left(I^{1-\alpha}_{a+} Df\right)(x), \tag{1.13}$$

$$\left({}^C D^{\alpha}_{b-} f\right)(x) = -\frac{1}{\Gamma(1-\alpha)} \int_x^b \frac{f'(t)dt}{(t-x)^{\alpha}} =: -\left(I^{1-\alpha}_{b-} Df\right)(x). \tag{1.14}$$

We observe that most studies in this field predominantly employ the *left-sided* definitions, whereas the *right-sided* definitions are rarely used due to their anti-causal nature (they depend on the future values of the function when x exceeds t). For simplicity, throughout this thesis, we will adopt the left-sided Caputo derivative, denoted by ${}^C D^{\alpha}_{a+} = {}^C D^{\alpha}_t$. In the following sections, we will introduce several key properties of the Caputo fractional derivative that will be fundamental for the subsequent chapters, particularly for values of α between 0 and 1.

Properties 1.1. *([51, 72]).*

- ***Derivative of a constant**: The Caputo fractional derivative of a constant function $f(t) = C$ equals zero, i.e.,*

$$ {}^C D^{\alpha}_t C = 0.$$

- ***Linearity property***: *The Caputo derivative preserves linearity, meaning that the derivative of a linear combination of functions is equal to the linear combination of their respective derivatives. For any constants a and b, and functions $f(x)$ and $g(x)$, the following holds:*

$$^{C}D_{t}^{\alpha}(af(x)+bg(x)) = a\,^{C}D_{t}^{\alpha}f(x)+b\,^{C}D_{t}^{\alpha}g(x).$$

Having established the key properties of the Caputo fractional derivative, we now introduce the following lemmas and corollary, which further elucidate its behavior under specific conditions.

Lemma 1.1. *([4, 88]). Let $f(t)\in\mathbb{R}^{+}$ be a differentiable function and let $\bar{x}\geq 0$. Then, for all $t\geq 0$ and $0<\alpha<1$, the following inequalities hold:*

$$^{C}D_{a}^{\alpha}\left[f(t)-\bar{x}-\bar{x}\ln\frac{f(t)}{\bar{x}}\right]\leq\left(1-\frac{\bar{x}}{f(t)}\right)^{C}D_{a}^{\alpha}f(t), \tag{1.15}$$

$$^{C}D_{a}^{\alpha}f^{2}(t)\ \leq 2f(t)^{C}D_{a}^{\alpha}f(t). \tag{1.16}$$

Lemma 1.2. ***(Generalized Mean Value Theorem [70])*** *Suppose that $f\in\mathscr{C}[a,b]$ and $^{C}D_{t}^{\alpha}f(t)\in\mathscr{C}(a,b]$, for $0<\alpha\leq 1$. Then,*

$$f(t)=f(0)+\frac{1}{\Gamma(\alpha)}\left(^{C}D_{t}^{\alpha}f\right)(\xi)(t-a)^{\alpha},$$

where $0\leq\xi\leq t, \forall t\in(a,b]$.

Corollary 1.1. *[70] Suppose that $f\in\mathscr{C}[a,b]$, and $^{C}D_{t}^{\alpha}f(t)\in\mathscr{C}(a,b]$ for $0<\alpha\leq 1$.*

1. *If $^{C}D_{t}^{\alpha}f(t)\geq 0, \forall t\in(a,b]$, then $f(t)$ is non-decreasing.*
2. *If $^{C}D_{t}^{\alpha}f(t)\leq 0, \forall t\in(a,b]$, then $f(t)$ is non-increasing.*

The fractional Caputo derivative has a singular kernel. This singularity appears in the formulation of the Caputo derivative, which can make it difficult to accurately model certain physical phenomena, particularly in cases where the behavior of the function at the boundary is crucial or when the domain extends to singular points. The Atangana-Baleanu-Caputo (ABC) fractional derivative was introduced specifically to mitigate or eliminate this singularity.

1.2.3 Atangana–Baleanu Fractional Derivative and Integral

The ABC fractional derivative, introduced by Atangana and Baleanu in 2016 [14], extends the classical Caputo derivative by using a generalized kernel that allows for a broader range of applications. This extension facilitates the modeling of systems with memory, offering a more accurate representation of dynamic processes.

Definition 1.7. *([14]). Let $f \in H^1(a,b), b > a, \alpha \in (0,1)$ then, the definition of the Atangana-Baleanu fractional derivative in the sense of Caputo is given as follows:*

$$ {}^{ABC}_{b}D^{\alpha}_{t}(f(t)) = \frac{M(\alpha)}{1-\alpha}\int_{b}^{t} f'(x)E_{\alpha}\left[-\alpha\frac{(t-x)^{\alpha}}{1-\alpha}\right]dx. \tag{1.17}$$

where $M(\alpha)$ represents a normalization function that satisfies $M(0) = M(1) = 1$.

Following the definition of the Atangana-Baleanu fractional derivative in the sense of Caputo, we now extend our discussion to its formulation in the Riemann-Liouville framework, which allows for a broader understanding of fractional calculus applications.

Definition 1.8. *([14]). Let $f \in H^1(a,b), b > a, \alpha \in (0,1)$ then, the definition of Atangana-Baleanu fractional derivative in the sense of Riemann-Liouville is given as follows:*

$$ {}^{ABR}_{b}D^{\alpha}_{t}(f(t)) = \frac{M(\alpha)}{1-\alpha}\frac{d}{dt}\int_{b}^{t} f(x)E_{\alpha}\left[-\alpha\frac{(t-x)^{\alpha}}{1-\alpha}\right]dx. \tag{1.18}$$

where $M(\alpha)$ denotes a normalization function obeying $M(0) = M(1) = 1$.

Remark 1. *The Atangana-Baleanu derivative in the sense of Caputo satisfies the property that the derivative of a constant is equal to zero. Additionally, the two definitions described in equations (1.18) and (1.17) feature a non-local kernel.*

Definition 1.9. *([14]). The fractional integral corresponding to the ABC fractional derivative with a non-local kernel is expressed as*

$$ {}^{ABC}_{b}I^{\alpha}_{t}\{f(t)\} = \frac{1-\alpha}{M(\alpha)}f(t) + \frac{\alpha}{M(\alpha)\Gamma(\alpha)}\int_{b}^{t} f(y)(t-y)^{\alpha-1}dy, \tag{1.19}$$

when $\alpha = 0$, the original function is restored, and when $\alpha = 1$, we obtain the ordinary integral.

1.3 Fractional Laplace transform

The Laplace transform is a powerful tool in fractional calculus, offering a method to convert complex fractional differential equations into algebraic forms, making them

easier to solve and analyze. This approach is particularly useful in various fields like control theory, physics, and epidemiology. In this section, we will discuss the Laplace transforms of key fractional operators, including the Riemann–Liouville, Caputo, Mittag-Leffler functions, and the Atangana–Baleanu–Caputo (ABC) derivative. Understanding these transforms is essential for applying fractional calculus in both theoretical and practical problem-solving contexts.

Definition 1.10. *([51, 71]). Consider a function $f(t)$ dependent on the variable t, where the product $e^{-st}f(t)$ is integrable over the interval $[0,\infty)$ for a certain range of values of s. The Laplace transform of $f(t)$ is defined within this range of s, and is represented as*

$$\mathscr{L}\{f(t)\} = \int_0^\infty e^{-st} f(t)\,dt. \tag{1.20}$$

For the specific case where $f(t) = t^\alpha$, and α is a non-integer such that $n-1 < \alpha \le n$, the Laplace transform is given by:

$$\mathscr{L}\left\{t^\alpha\right\} = \frac{\Gamma(\alpha+1)}{s^{\alpha+1}}. \tag{1.21}$$

Now, we present the Laplace transform for some basic fractional operators (for more details on the Laplace transform, please refer to [72]). Suppose s > 0 and F(s) is the Laplace transform of $f(t)$, then the following statements hold:

- **Laplace transform of the two-parameter Mittag-Leffler function**: The Laplace transform of the function $t^{b-1}E_{a,b}\left(\pm\mu t^b\right)$ is given by

$$\mathscr{L}\left(t^{b-1}E_{a,b}(\pm\mu t^a)\right) = \frac{s^{a-b}}{s^a \mp \mu}, \quad \text{for } \mu \in \mathbb{R} \quad \text{and } a,b>0. \tag{1.22}$$

- **Laplace transform of the Riemann–Liouville fractional derivative** of order α is expressed as:

$$\mathscr{L}\left\{{}_0^{RL}D_t^\alpha f(t)\right\}(s) = s^\alpha F(s) - \sum_{k=0}^{n-1} s^k \left[{}_0^{RL}D^{\alpha-k-1} f(t)\right]_{t=0}, \quad n-1 \le \alpha < n, n \in \mathbb{N}.$$

- **Laplace transform of the Caputo fractional derivative** is written as:

$$\mathscr{L}\left\{{}_0^{C}D_t^\alpha f(t)\right\}(s) = s^\alpha F(s) - \sum_{k=0}^{n-1} s^{\alpha-k-1} f^{(k)}(0), \quad n-1 < \alpha \le n, n \in \mathbb{N}.$$

- **Laplace transform of the Atangana–Baleanu (ABC) fractional derivatives** are as follows[14]:

$$\mathscr{L}\left\{{}_0^{ABR}D_t^{\alpha}(f(t))\right\}(s)=\frac{B(\alpha)}{1-\alpha}\frac{s^{\alpha}\mathscr{L}\{f(t)\}(s)}{s^{\alpha}+\frac{\alpha}{1-\alpha}}, \tag{1.23}$$

and

$$\mathscr{L}\left\{{}_0^{ABC}D_t^{\alpha}(f(t))\right\}(s)=\frac{B(\alpha)}{1-\alpha}\frac{s^{\alpha}\mathscr{L}\{f(t)\}(s)-s^{\alpha-1}f(0)}{s^{\alpha}+\frac{\alpha}{1-\alpha}}. \tag{1.24}$$

1.4 Analysis of existence, uniqueness, and stability for fractional differential systems

This section discusses specific findings related to the behavior of dynamical systems with fractional order. We will examine the stability of fractional systems in a way that parallels the theory of ordinary differential equations.

1.4.1 Temporal System Equilibria

Consider the following system of fractional differential equations (FDEs):

$$\begin{cases} D_t^{\alpha}X(t) &= f(X(t)), \quad \text{for all } t\geq 0\\ X(0) &= X_0. \end{cases} \tag{1.25}$$

where $0<\alpha\leq 1$, $f:\mathbb{R}^+\times D\to\mathbb{R}^n$ with $D\subseteq\mathbb{R}^n$, and D_t^{α} denotes the fractional derivative.

Definition 1.11. *([32]). The constant e^* is an equilibrium point of the fractional dynamical system (1.25) when $f(e^*(t))=0$.*

Remark 2. *Note that when the fractional order is between 0 and 1, the fractional system shares the same equilibrium points as the integer-order system.*

1.4.2 Existence and uniqueness of solution

Theorem 1.1. *([57]). Assume that $f(X(t))$ satisfies the following:*

1. *f is a continuous function with respect to t for all $X(t)\in\mathbb{R}^n$,*
2. *f and $\frac{\partial f}{\partial X}$ are continuous functions with respect to $X(t)\in\mathbb{R}^n$,*
3. *$\|f\|\leq c_1+c_2\|X\|$ for all $X\in\mathbb{R}^n$, and all $c_1,c_2>0$.*

Then, the system (1.25) with the Caputo fractional derivative has a unique solution on $[0,+\infty)$.

1.4.3 Stability of equilibrium points

Consider $e(t)$ as any solution of the general system (1.25). The solution $e(t)$ is called stable if any solution that begins "near" $e(t)$ at a certain time stays near $e(t)$ for all subsequent times. Furthermore, $e(t)$ is asymptotically stable if nearby solutions approach $e(t)$ as $t \to \infty$. If a solution does not meet the stability criterion, it is referred to as unstable [63].

Theorem 1.2. *([56, 63]). If all the eigenvalues λ_k of the Jacobian matrix $f(X(t))$ at equilibrium point satisfy*

$$|\arg(\lambda_k)| > \frac{\alpha\pi}{2}, \tag{1.26}$$

then the equilibrium point of system (1.25) is locally asymptotically stable.

The subsequent result by [44] extends the classical findings for ordinary differential equations to the fractional-order context, offering sufficient conditions for the global asymptotic stability of fractional-order dynamical systems.

Definition 1.12. *[44] A set M is said to be an invariant set with respect to (1.25) if $x(0) \in M$ implies $x(t) \in M$, for all $t \in \mathbb{R}$. A set M is said to be a positively invariant set if $x(0) \in D$ implies $x(t) \in M$, for all $t \geq 0$.*

We will now present the Fractional version of LaSalle's invariance principle.

Lemma 1.3. *[44] Suppose D is a bounded closed set. Every solution of (1.25) starts from a point in D and remains in D for all time. If $\exists V(x) : D \to R$ with continuous first partial derivatives satisfies following condition:*

$$D^{\alpha}V\big|_{(1.25)} \leq 0.$$

Let $E = \{x \,|D^{\alpha}V|_{(1.25)} = 0\}$ and M be the largest invariant set of E. Then every solution $x(t)$ originating in D tends to M as $t \to \infty$. Particularly, when $M = \{0\}$, then $x \to 0, t \to \infty$.

1.4.4 Sensitivity analysis

Sensitivity indices measure how sensitively a state variable responds to variations in a given parameter. Specifically, the normalized forward sensitivity index of a variable with respect to a parameter is defined as the ratio of the relative change in the variable to that in the parameter. When the variable depends smoothly on the parameter, this index can also be expressed in terms of partial derivatives. To reduce disease prevalence, we apply this sensitivity index as defined in [26].

Definition 1.13. *[26] The normalized forward sensitivity index of a variable, V, that depends differentiably on a parameter p is defined as:*

$$\Upsilon_p^V := \frac{\partial V}{\partial p} \times \frac{p}{V}. \tag{1.27}$$

Highly sensitive parameters should be estimated with precision, as small changes in these parameters can lead to significant variations in key outcomes. Conversely, less sensitive parameters require less exact estimation, as minor adjustments in these values have minimal impact on the variables of interest.

1.5 Numerical approximation of FDEs

Finding an exact solution for fractional differential equation systems with initial conditions is complex and challenging. Therefore, numerical simulation is the preferred approach for understanding the dynamic behavior of these systems. The literature has introduced and developed several numerical schemes, including the fractional Euler method, Adams-Bashforth-Moulton method, and the Laplace-Adomian decomposition method [15, 33, 69, 82]. This section presents the various numerical schemes that will be utilized throughout the thesis.

1.5.1 Adams-Bashforth-Moulton fractional technique

In this part, we focus on the Adams-Bashforth-Moulton fractional numerical technique, which we will use to simulate fractional-order equations of the Caputo type. This technique was introduced and discussed by K.Diethelm and A. D. Freed [33].

To be specific, we first consider the fractional differential equation.

$$\begin{cases} {}^{C}D_t^{\alpha}(y(x)) = f(x, y(x)), \quad 0 < \alpha < 1, \\ y^{(0)}(0) = y_0. \end{cases} \tag{1.28}$$

Equation (1.28) is equivalent to the Volterra integral equation in the Caputo sense.

$$y(x) = \sum_{k=0}^{\lceil \alpha \rceil - 1} y_0^{(k)} \frac{x^k}{k!} + \frac{1}{\Gamma(\alpha)} \int_0^x (x-t)^{\alpha-1} f(t, y(t)) \mathrm{d}t. \tag{1.29}$$

Note that in the case of the classic one-step Adams-Bashforth-Moulton algorithm ($\alpha = 1$), to obtain the approximation of y_{n+1}, the integration range starts at x_n. In the case of the Volterra integral equation, on the other hand, it starts at 0, demonstrating the non-local structure of fractional differential equations.

The method is explained in the following manner.
Let $x \in [0,T], x_k = jh, j = 0,1,2,\ldots,n+1,$ and $h = \frac{T}{m}$.

To obtain the corrector formula for Adams Bashforth's fractional method, approximate the right-hand side of (1.29) by Lagrange's method and we find

$$y_{n+1} = \sum_{k=0}^{\lceil\alpha\rceil-1} \frac{t_{n+1}^k}{k!} y_0^{(k)} + \frac{h^\alpha}{\Gamma(\alpha+2)} \sum_{j=0}^{n} a_{j,k+1} f\left(x_j, y_j\right) + \frac{h^\alpha}{\Gamma(\alpha+2)} f\left(x_{k+1}, y_{k+1}^p\right), \tag{1.30}$$

where

$$a_{j,n+1} = \begin{cases} n^{\alpha+1} - (n-\alpha)(n+1)^\alpha, & \text{if } j = 0, \\ (n-j+2)^{\alpha+1} + (n-j)^{\alpha+1} - 2(n-j+1)^{\alpha+1}, & \text{if } 0 < j \le n, \\ 1, & \text{if } j = n+1. \end{cases} \tag{1.31}$$

Predictor formulae for $y_h^{\mathrm{P}}(t_{n+1})$ is given by the Adams Bashforth fractional method

$$y_{n+1}^{\mathrm{P}} = \sum_{k=0}^{\lceil\alpha\rceil-1} \frac{t_{n+1}^k}{k!} y_0^{(k)} + \frac{1}{\Gamma(\alpha)} \sum_{j=0}^{n} b_{j,n+1} f\left(x_j, y_j\right), \tag{1.32}$$

where

$$b_{j,n+1} = \frac{h^\alpha}{\alpha}\left[(n+1-j)^\alpha - (n-j)^\alpha\right], \quad 0 \le j \le n. \tag{1.33}$$

Based on the analysis presented in [46], the order of convergence of the Adams method is found to be $1+\alpha$, where α represents the fractional order of the derivative. Consequently, the error can be expressed as

Based on the analysis presented in [46], the order of convergence of the Adams method is found to be $1+\alpha$, where α represents the fractional order of the derivative. Consequently, the error can be expressed as

$$|y(x_n) - y_n| = \mathcal{O}\left(h^{1+\alpha}\right).$$

This method allows for accurate numerical solutions and has been widely used in various applications of fractional calculus due to its stability and efficiency.

1.5.2 Taoufik–Atangana scheme: two-step Lagrange polynomial approximation

We will now provide a brief overview of the scheme employed for the ABC fractional derivative.

Let us start by considering the fractional differential equation

$$\begin{cases} {}^{ABC}D_t^{\alpha}(y(t)) = f(t, y(t)), 0 < \alpha < 1, \\ y^{(0)}(0) = y_0. \end{cases} \tag{1.34}$$

We first apply the ABC integral to both sides of Equation (1.34) to obtain:

$$y(t) - y(0) = \frac{1-\alpha}{M(\alpha)} f(t, y(t)) + \frac{\alpha}{M(\alpha)\Gamma(\alpha)} \int_0^t f(x, y(x))(t-x)^{\alpha-1} dx. \tag{1.35}$$

At a specific point t_{n+1}, this becomes:

$$\begin{aligned} y(t_{n+1}) - y(0) &= \frac{1-\alpha}{M(\alpha)} f(t_n, y(t_n)) \\ &\quad + \frac{\alpha}{M(\alpha)\Gamma(\alpha)} \left[\int_0^{t_{n+1}} f(x, y(x))(t_{n+1}-x)^{\alpha-1} dx \right], \\ &= \frac{1-\alpha}{M(\alpha)} f(t_n, y(t_n)) \\ &\quad + \frac{\alpha}{M(\alpha)\Gamma(\alpha)} \left[\sum_{k=0}^{n} \int_{t_k}^{t_{k+1}} f(x, y(x))(t_{n+1}-x)^{\alpha-1} dx \right]. \end{aligned} \tag{1.36}$$

We approximate $f(x, y(x))$ using a two-step Lagrange polynomial:

$$f(x, y(x)) \approx \mathscr{P}_k(x) = \frac{f(t_k, y(t_k))}{h}(x - t_{k-1}) - \frac{f(t_{k-1}, y(t_{k-1}))}{h}(x - t_k). \tag{1.37}$$

Substituting this approximation into Equation (1.36) yields:

$$\begin{aligned} y_{n+1} &= y_0 + \frac{1-\alpha}{M(\alpha)} f(t_n, y_n) \\ &\quad + \frac{\alpha}{M(\alpha)\Gamma(\alpha)} \sum_{k=0}^{n} \left[\frac{f(t_k, y_k)}{h} \int_{t_k}^{t_{k+1}} (x - t_{k-1})(t_{n+1} - x)^{\alpha-1} dx \right. \\ &\quad \left. - \frac{f(t_{k-1}, y_{k-1})}{h} \int_{t_k}^{t_{k+1}} (x - t_k)(t_{n+1} - x)^{\alpha-1} dx \right]. \end{aligned} \tag{1.38}$$

Simplifying the integral expressions, we obtain:

$$\begin{aligned} y_{n+1} &= y_0 + \frac{1-\alpha}{M(\alpha)} f(t_n, y(t_n)) \\ &\quad + \frac{\alpha}{M(\alpha)} \sum_{k=0}^{n} \left[\frac{h^{\alpha} f(t_k, y_k)}{\Gamma(\alpha+2)} \left((n+1-k)^{\alpha}(n-k+2+\alpha) - (n-k)^{\alpha}(n-k+2+2\alpha) \right) \right. \\ &\quad \left. - \frac{h^{\alpha} f(t_{k-1}, y_{k-1})}{\Gamma(\alpha+2)} \left((n+1-k)^{\alpha+1} - (n-k)^{\alpha}(n-k+1+\alpha) \right) \right]. \end{aligned} \tag{1.39}$$

CHAPTER 2

THE EFFECT OF MIGRATION ON THE TRANSMISSION OF HIV/AIDS USING A FRACTIONAL MODEL: LOCAL AND GLOBAL DYNAMICS AND NUMERICAL SIMULATIONS

AIDS, caused by the human immunodeficiency virus (HIV), leads to a progressive decline in the immune system's functionality [66, 67]. This deterioration renders the body susceptible to opportunistic infections, and without intervention, often results in death.

The first reported cases of HIV were identified in 1981 among five young men in California who were diagnosed with Pneumocystis carinii pneumonia [38]. Since then, the virus has spread globally, becoming a major public health crisis. According to the World Health Organization (WHO), approximately 20 million people have died due to acquired immunodeficiency syndrome (AIDS), with an estimated 38.4 million individuals living with the virus as of 2021. Of these, 25.6 million are in Africa. HIV primarily attacks CD4+ T cells, weakening the immune system and leaving it vulnerable to cancer and other infections. Importantly, not all individuals with HIV will develop AIDS immediately; it may take years before the virus severely compromises the immune system. Over the years, a variety of mathematical models have been created to analyze and forecast the spread of HIV/AIDS, aiming to provide insights for effective responses([1, 44, 65, 78, 81]).

Several studies have examined the evolution of the HIV/AIDS pandemic and strategies for its prevention. For instance, [43] explored the impact of treatment on HIV progression by incorporating a compartment for treated individuals in their epidemiological

model. Hsieh and Sheu [42] proposed a model that examines HIV transmission through heterosexual relationships, incorporating community-based testing and care. In another study, Joshi et al. [45] developed a model to analyze the effect of awareness and education campaigns on the spread of HIV.

Migration is another significant factor in the global spread of HIV. Several studies have explored the link between migration and HIV transmission [29, 34, 86]. In this chapter, we introduce a fractional-order system to model HIV/AIDS progression, both with and without population movement (migration).

Building on the work of [12], where the authors developed a classical model incorporating population migration and concluded that migration plays a crucial role in the spread of HIV/AIDS, we extend this model by employing fractional derivatives to highlight the advantages of fractional differential equations. Initially, we utilized the Caputo derivative due to its well-established mathematical properties and its suitability for initial value problems, which are commonly encountered in epidemiological modeling. The Caputo derivative is widely favored for its capacity to generalize the classical derivative while preserving a straightforward physical interpretation, making it more straightforward to implement in many applications.

On the other hand, we opted for the ABC derivative due to its distinct features, including non-locality and non-singularity, which are particularly advantageous for modeling the memory effects intrinsic to biological systems.

This comparative analysis examines the effectiveness of both derivatives in modeling the dynamics of HIV and AIDS, especially in the context of migration. The goal is to provide deeper insights into infectious disease modeling, enhancing our understanding of transmission patterns and informing effective control strategies.

This chapter is organized as follows: Section 2.1 covers the fundamental properties of the fractional models with and without migration, employing the Caputo derivative and highlighting the key characteristics of both approaches. In Section 2.2, we present the HIV and AIDS model developed with the ABC fractional derivative and discuss its key mathematical properties. Section 2.3 features a comparative numerical analysis of the Caputo and ABC fractional derivatives, focusing on their influence on HIV transmission dynamics. Finally, the chapter concludes with a summary of the main findings and explores their implications for future research in fractional HIV modeling.

2.1 Caputo fractional model of HIV and AIDS: with and without migration

In this section, we investigate the dynamics of HIV and AIDS using the Caputo fractional derivative, examining both models with and without migration.

2.1.1 Formulation of a fractional model of HIV/AIDS without migration

In this model, we divide the host population $N(t)$ into three compartments: susceptible individuals (S), those infected with HIV (I), and those with AIDS (A), such that $N(t) = S + I + A$. Susceptible individuals can be infected at a rate of βIS, where β is the transmission rate of HIV. Individuals infected with HIV develop AIDS at a rate of γ.

Additionally, μ represents the natural mortality rate, Λ is the recruitment birth rate, and δ_1 and δ_2 denote the HIV-related and AIDS-related mortality rates, respectively.

The flow diagram of HIV transmission without migration is shown in Figure 2.1.

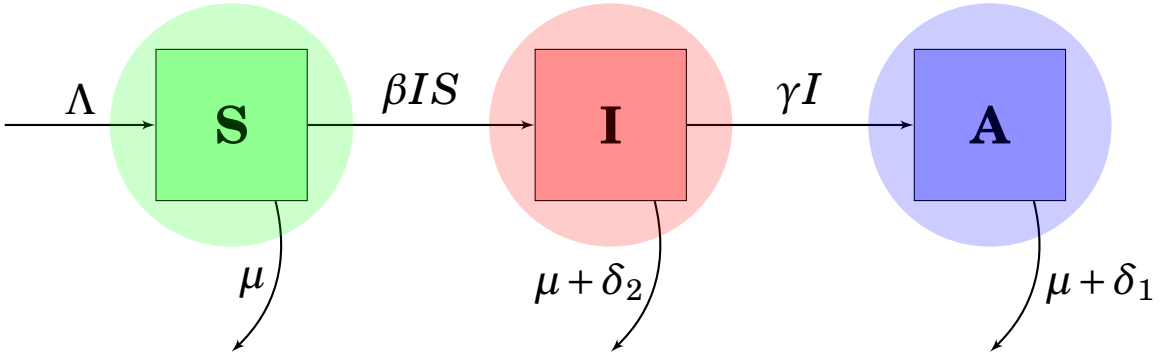


Figure 2.1: Schematic diagram of HIV and AIDS transmission.

Based on the assumptions outlined above, we can express the classical formula (the ordinary differential equations) for this model as follows:

$$\begin{cases} \frac{dS}{dt} = \Lambda - \beta IS - \mu S, \\ \frac{dI}{dt} = \beta IS - (\mu + \delta_1 + \gamma)I, \\ \frac{dA}{dt} = \gamma I - (\mu + \delta_2)A. \end{cases} \tag{2.1}$$

Fractional Model

Now, by changing the classical derivative in model (2.1) to the fractional derivative in the sense of Caputo, we obtain the following system of fractional ODEs.

$$\begin{cases} {}^{C}D_t^{\rho} S = \Lambda - \beta IS - \mu S, \\ {}^{C}D_t^{\rho} I = \beta IS - (\mu + \delta_1 + \gamma) I, \\ {}^{C}D_t^{\rho} A = \gamma I - (\mu + \delta_2) A, \end{cases} \tag{2.2}$$

with non-negative initial conditions $S(0) = S_0 \geq 0, I(0) = I_0 \geq 0, A(0) = A_0 \geq 0$ and the operator ${}^{C}D_t^{\rho}$ is the Caputo fractional derivatives of order $\rho \in (0,1]$. We assume that the functions $S(t), I(t), A(t)$ and their fractional Caputo derivatives of order $0 < \rho \leq 1$ are continuous functions. The parameters $\Lambda, \beta, \mu, \delta_1, \delta_2$, and γ of the fractional-order SIA epidemic model (2.2) are taken as positive values, as shown in Table 2.1.

Parameters	Value	Source
β	9.7847e-08	Assumed
γ	7.7416e-02	[12]
μ	3.9060e-01	[12]
Λ	4.2249e-10	[12]
δ_1	1.7396e-12	[12]
δ_2	4.8233e-07	[12]

Table 2.1: The parameter values used in the SIA model without migration.

2.1.1.1 Positivity and boundedness of solution

In this subsection, we establish the non-negativity and boundedness of the solutions to the system (2.2). To accomplish this, we utilize lemma 1.2 and corollary 1.1 presented in Chapter 1.

Theorem 2.1. *The region* $\Theta_+ = \{(S, I, A) \in \mathbb{R}^3; S \geq 0, I \geq 0, A \geq 0\}$ *is positively invariant for the Caputo fractional system* (2.2).

Proof. Now, we demonstrate the positivity of the solution.

$$
\begin{aligned}
{}^{C}D_t^{\rho} S\setminus_{S=0} &= \Lambda \geq 0,\\
{}^{C}D_t^{\rho} I\setminus_{I=0} &= 0,\\
{}^{C}D_t^{\rho} A\setminus_{A=0} &= \gamma I \geq 0.
\end{aligned}
$$

By using Corollary 1.1, we conclude that the solution will stay in $\mathbb{R}_+^4$ and hence, $\Theta_+ = \{(S,I,A) \in \mathbb{R}^+; S \geq 0, I \geq 0, A \geq 0\}$ is positivity invariant set for the system (2.2). ■

Next, we study the boundedness of the solution using the following theorem.

Theorem 2.2. *The region* $\Theta = \{(S,I,A) \in \mathbb{R}^3; S \geq 0, I \geq 0, A \geq 0,$ $0 \leq N(t) \leq \dfrac{\Lambda}{\mu}$, *where* $N(t) = S(t) + I(t) + A(t)\}$ *is a positivity invariant set for the system* (2.2).

Proof. Summing all the equations of system (2.2), we have

$$
\begin{aligned}
{}^{C}D_t^{\rho} N(t) = &\quad \Lambda - \mu N(t) - \delta_1 I(t) - \delta_2 A(t),\\
\leq &\quad \Lambda - \mu N(t). \qquad (2.3)
\end{aligned}
$$

By applying the Laplace transform to equation (2.3), we obtain

$$
s^{\rho}\mathscr{L}(N(t)) - s^{\rho-1}N(0) \leqslant \frac{\lambda}{s} - \mu\mathscr{L}(N(t)). \qquad (2.4)
$$

It can be written as follows

$$
\mathscr{L}(N(t)) \leq \Lambda\frac{s^{\rho-(1+\rho)}}{s^{\rho}+\mu} + \frac{s^{\rho-1}}{s^{\rho}+\mu}N(0). \qquad (2.5)
$$

Utilizing formula (1.22) on the preceding inequality, followed by the application of the inverse Laplace transform, results in

$$
N(t) \leq \Lambda t^{\rho} E_{\rho,\rho+1}\left(-\mu t^{\rho}\right) + E_{\rho,1}\left(-\mu t^{\rho}\right)N(0). \qquad (2.6)
$$

We can deduce from Equation (1.4) that if $0 \leq N(0) \leq \dfrac{\Lambda}{\mu}$, then

$$
N(t) \leq \frac{\Lambda}{\mu}\left[E_{\rho,1}(-\mu t^{\rho}) + \mu t^{\rho} E_{\rho,\rho+1}(-\mu t^{\rho})\right] = \frac{\Lambda}{\mu}. \qquad (2.7)
$$

Then, the feasible region Θ is positively invariant. This implies the boundedness of the solution. ■

2.1.1.2 Existence and uniqueness

The study of the existence and uniqueness of solutions for fractional differential equations or systems requires the application of various mathematical methods, such as the successive iterative technique and limit points [48], as well as fixed point theory [8, 18, 49]. In our model, we adopt the following approach based on Theorem 1.1 presented in Chapter 1.

Theorem 2.3. *The fractional system* (2.2) *attains an unique solution in* Θ*, for any given initial conditions satisfying* $S(0) = S_0 \geq 0, I(0) = I_0 \geq 0, A(0) = A_0 \geq 0$.

Proof. We verify the existence and uniqueness of the solution by reformulating the model (2.2) as follows.

$$^{C}D_t^{\rho} X(t) = f(X(t)), \text{ for } t \geq 0, \text{ with } X(0) = X_0 \in \mathbb{R}_+^3,$$

with

$$X(t) = \begin{pmatrix} S(t) \\ I(t) \\ A(t) \end{pmatrix}, \quad f(X(t)) = \begin{pmatrix} \Lambda - \beta SI - \mu S \\ \beta SI - (\mu + \delta_1 + \gamma) I \\ \gamma I - (\mu + \delta_2) A \end{pmatrix}, X_0 = \begin{pmatrix} S_0 \\ I_0 \\ A_0 \end{pmatrix}.$$

The vector function f clearly satisfies the first and second assertions of Theorem 1.1, and now we need to demonstrate that f also meets the third requirement. We have

$$\|f(X(t))\| \leq \|\nu\| + (\|A\| + \|B\| \, \|S(t)\|) \|X(t)\|,$$

where

$$\nu = \begin{pmatrix} \Lambda \\ 0 \\ 0 \end{pmatrix}, A = \begin{pmatrix} -\mu & 0 & 0 \\ 0 & -(\mu + \delta_1 + \gamma) & 0 \\ 0 & \gamma & -(\mu + \delta_2) \end{pmatrix}, B = \begin{pmatrix} 0 & -\beta & 0 \\ 0 & \beta & 0 \\ 0 & 0 & 0 \end{pmatrix}$$

From Theorem 1.1, the solution of system (2.2) exist and is unique. ■

2.1.1.3 Equilibrium and basic reproduction number

To calculate the equilibrium points of model (2.2), we solve the following equations

$$^{C}D_t^{\rho} S(t) = {}^{C}D_t^{\rho} I(t) = {}^{C}D_t^{\rho} A(t) = 0. \tag{2.8}$$

Then, we obtain the disease-free equilibrium (DFE) where $I \equiv 0$ and $A \equiv 0$, given by

(2.9) $$\mathscr{E}_0 = (S_0, I_0, A_0),$$

where $S_0 = \dfrac{\Lambda}{\mu}$, $I_0 = 0$, and $A_0 = 0$.

If $I \neq 0$ and $A \neq 0$, we can identify the endemic equilibrium $\mathscr{E}_1$ of model (2.2). To determine the existence and uniqueness of this equilibrium point, we first compute the basic reproduction number $\mathscr{R}_0$. This value serves as a critical threshold for evaluating the potential spread of the disease: when $\mathscr{R}_0 > 1$, the infection is likely to become widespread; whereas if $\mathscr{R}_0 < 1$, the disease is expected to decline and eventually disappear. In our model, $\mathscr{R}_0$ is derived using the next-generation matrix method, which utilizes the transmission matrix T and the transition matrices Σ as defined below:

$$T = \begin{pmatrix} \beta S_0 & 0 \\ 0 & 0 \end{pmatrix}, \quad \Sigma = \begin{pmatrix} -(\mu+\delta_1+\gamma) & 0 \\ \gamma & -(\mu+\delta_2) \end{pmatrix}.$$

Ultimately, the basic reproduction number for the SIA model (2.2) is obtained from the spectral radius of the matrix $-T\Sigma^{-1}$ and can be expressed as follows:

(2.10) $$\mathscr{R}_0 = \varrho\left(-T\Sigma^{-1}\right) = \frac{\beta S_0}{(\mu+\delta_1+\gamma)} = \frac{\beta\Lambda}{\mu(\mu+\delta_1+\gamma)}.$$

Hence, if $\mathscr{R}_0 > 1$, the model (2.2) has a unique endemic equilibrium (positive endemic), denoted by $\mathscr{E}_1 = (S^*, I^*, A^*)$ with

(2.11) $$S^* = \frac{\mu+\delta_1+\gamma}{\beta}, \qquad I^* = \frac{\mu}{\beta}(\mathscr{R}_0 - 1), \qquad A^* = \frac{\gamma I^*}{\mu+\delta_2}.$$

2.1.1.4 Stability analysis

First, we establish the local asymptotic stability of system (2.2) by applying Theorem 1.2. In order to achieve this, we linearize system (2.2) around each equilibrium point.

Theorem 2.4. *If $\mathscr{R}_0 < 1$, then the disease free equilibrium $\mathscr{E}_0$ of system (2.2) is locally asymptotically stable. If $\mathscr{R}_0 > 1$, then $\mathscr{E}_0$ is unstable.*

Proof. The Jacobian matrix of system (2.2) at $\mathscr{E}_0$ is

$$\mathscr{J}(\mathscr{E}_0) = \begin{bmatrix} -\mu & -\beta & 0 \\ 0 & \beta S_0 - (\mu+\delta_1+\gamma) & 0 \\ 0 & \gamma & -(\mu+\delta_2) \end{bmatrix}.$$

Through certain calculations, we determine that the characteristic roots of $\mathscr{J}(\mathscr{E}_0)$ are

$$\lambda_1 = -\mu, \qquad \lambda_2 = -(\mu+\delta_2), \qquad \lambda_3 = \beta\frac{\Lambda}{\mu} - (\mu+\delta_1+\gamma).$$

It is evident that $\lambda_1 < 0$ and $\lambda_2 < 0$. If $\mathscr{R}_0 < 1$, then $\lambda_3 < 0$. Thus, we have $|\arg(\lambda_i)| = \pi > \frac{\rho\pi}{2}$ for $i = 1,2,3$. Therefore, according to Theorem 1.2, the disease-free equilibrium $\mathscr{E}_0$ is locally asymptotically stable. ■

Theorem 2.5. *If $\mathscr{R}_0 > 1$, then the endemic equilibrium $\mathscr{E}_1$ of system (2.2) is locally asymptotically stable. If $\mathscr{R}_0 < 1$, then $\mathscr{E}_1$ is unstable.*

Proof. The Jacobian matrix of system (2.2) at $\mathscr{E}_1$ is

$$\mathscr{J}(\mathscr{E}_1) = \begin{bmatrix} -\beta I^* - \mu & -\beta S^* & 0 \\ \beta I^* & \beta S^* - (\mu+\delta_1+\gamma) & 0 \\ 0 & \gamma & -(\mu+\delta_2) \end{bmatrix}.$$

When we replace I^* and S^* with their respective values, we obtain

$$\mathscr{J}(\mathscr{E}_1) = \begin{bmatrix} -\mu\mathscr{R}_0 & -(\mu+\delta_1+\gamma) & 0 \\ \mu(\mathscr{R}_0-1) & 0 & 0 \\ 0 & \gamma & -(\mu+\delta_2) \end{bmatrix}.$$

To determine the eigenvalues, we solve the equation

$$\det(\mathscr{J}(\mathscr{E}_1) - \lambda I_3) = 0,$$

which implies,

$$(\mu+\delta_2+\lambda)\left(\lambda^2 + \mu\mathscr{R}_0\lambda + \mu(\mu+\delta_1+\gamma)(\mathscr{R}_0-1)\right) = 0. \tag{2.12}$$

It's easy to see that the equation (2.12) has a real root $\lambda_1 = -(\mu+\delta_2)$. To solve the solutions of equation $\left(\lambda^2 + \mu\mathscr{R}_0\lambda + \mu(\mu+\delta_1+\gamma)(\mathscr{R}_0-1)\right) = 0$, consider the following cases. We will set $\Delta = (\mu\mathscr{R}_0)^2 - 4\mu(\mu+\delta 1+\gamma)(\mathscr{R}_0-1)$.

1. If $\Delta > 0$, the equation has two distinct real roots

$$\lambda_2 = \frac{-(\mu\mathscr{R}_0) - \sqrt{\Delta}}{2}, \qquad \lambda_3 = \frac{-(\mu\mathscr{R}_0) + \sqrt{\Delta}}{2}.$$

Then, $\lambda_2 < 0$, and if $\mathscr{R}_0 > 1$, $\lambda_3 < 0$.

2. If $\Delta < 0$, the equation has two complex roots (where $j^2 = -1$).

$$\lambda_2 = \frac{-(\mu\mathscr{R}_0) - j\sqrt{|\Delta|}}{2}, \qquad \lambda_3 = \frac{-(\mu\mathscr{R}_0) + j\sqrt{|\Delta|}}{2}$$

Clearly, the eigenvalues λ_2 and λ_3 have negative real parts.

Since $\lambda_1 < 0$, all eigenvalues have negative real parts(all cases). This implies that $|\arg(\lambda_i)| = \pi > \frac{\rho\pi}{2}$ for $i = 1,2,3$. Hence the endemic equilibrium of system (2.2) is locally asymptotically stable for all $\rho \in (0,1]$. ■

Next, we will present the global equilibrium stability results in the following theorems, utilizing the generalized LaSalle Invariance Principle, as indicated in Lemma 1.3.

As A does not appear in the first two equations, we can express system (2.2) as follows:

$$\begin{cases} {}^{C}D_t^{\rho} S = \Lambda - \beta IS - \mu S, \\ {}^{C}D_t^{\rho} I = \beta IS - (\mu + \delta_1 + \gamma) I. \end{cases} \tag{2.13}$$

Theorem 2.6. *The disease-free equilibrium $\mathscr{E}_0 = (S_0, I_0)$, of the fractional model (2.13) is globally asymptotically stable when $\mathscr{R}_0 < 1$.*

Proof. Consider the Lyapunov function $\mathscr{L}_0(t)$ defined as follows

$$\mathscr{L}_0(t) = \left(S(t) - S_0 + S_0 \ln \frac{S(t)}{S_0}\right) + I(t).$$

The function $\mathscr{L}_0(t)$ is continous and positive for all $t \geq 0$.
Now, according to the linearity property of the fractional derivative in the sense of Caputo, we can calculate the derivative of $\mathscr{L}_0$ along the solution of model (2.13). We find that

$${}^{C}D_t^{\rho}\mathscr{L}_0(t) = {}^{C}D_t^{\rho}\left(S(t) - S_0 + S_0 \ln \frac{S(t)}{S_0}\right) + {}^{C}D_t^{\rho} I(t).$$

Using Lemma 1.1, we obtain the following inequality

$$\begin{aligned} {}^{C}D_t^{\rho}\mathscr{L}_0(t) &\leq \left(1 - \frac{S_0}{S(t)}\right) {}^{C}D_t^{\rho} S(t) + {}^{C}D_t^{\rho} I(t), \\ &= \left(1 - \frac{S_0}{S(t)}\right)\left(\Lambda - \mu S(t) - \beta S(t) I(t)\right) \\ &\quad + \left(\beta S(t) I(t) - \left(\mu + \delta_1 + \gamma\right) I(t)\right). \end{aligned}$$

By using the endemic condition $\Lambda = \mu S_0$ and considering the expressions for $\mathscr{R}_0$ and S_0, we obtain

$$^{C}D_t^{\rho}\mathscr{L}_0(t) = -\mu\frac{(S(t)-S_0)^2}{S(t)} + (\mu+\delta_1+\gamma)(\mathscr{R}_0-1)I(t).$$

If $\mathscr{R}_0 < 1$, then we get

$$^{C}D_t^{\rho}\mathscr{L}_0(t) \le 0, \quad \forall t \ge 0.$$

Moreover, it easy to see that $^{C}D_t^{\rho}\mathscr{L}_0(t) = 0$ if and only if $S(t) = S_0$ and $I(t) = 0$. Then, the largest invariant set for

$$E = \left\{(S(t), I(t)) \in \Theta_+^{'} : {}^{C}D_t^{\rho}\mathscr{L}_0(t) = 0\right\}$$

is $\{\mathscr{E}_0\}$, where $\Theta_+^{'} = \{(S,I) \in \mathbb{R}^2; S \ge 0, I \ge 0\}$. However, Lyapunov's stability Lemma 1.3 implies that all solutions in $\Theta_+^{'}$ converge to $\mathscr{E}_0$. Therefore, if $\mathscr{R}_0 < 1$, the disease-free equilibrium of model (2.13) is globally asymptotically stable. This completes the proof. ■

Theorem 2.7. *The endemic equilibrium $\mathscr{E}_1 = (S^*, I^*)$ of the fractional model (2.13) is globally asymptotically stable when $\mathscr{R}_0 > 1$.*

Proof. We define the Lyapunov function as follows

$$\mathscr{L}_1(t) = \left(S - S^* - S^*\ln\frac{S}{S^*}\right) + \left(I - I^* - I^*\ln\frac{I}{I^*}\right)$$

It's clear that the function $\mathscr{L}_1(t)$ is continous and positive for all $t \ge 0$. In addition, $\mathscr{L}_1(t) = 0$, if and only if $S(t) = S^*, I(t) = I^*$, and $A(t) = A^*$.

Using Lemma 1.1, we find

$$\begin{aligned}
^{C}D_t^{\rho}\mathscr{L}_1(t) &\le \left(1-\frac{S^*}{S(t)}\right){}^{C}D_t^{\rho}S(t) + \left(1-\frac{I^*}{I(t)}\right){}^{C}D_t^{\rho}I(t),\\
&= \left(1-\frac{S^*}{S(t)}\right)\left(\Lambda - \mu S(t) - \beta S(t)I(t)\right)\\
&\quad + \left(1-\frac{I^*}{I(t)}\right)\left(\beta S(t)I(t) - \left(\mu+\delta_1+\gamma\right)I(t)\right).
\end{aligned}$$

We have $\Lambda = \mu S^* + \beta S^* I^*$ and $\beta S^* I^* = \left(\mu+\delta_1+\gamma\right)I^*$, we get

$$\begin{aligned}
^{C}D_t^{\rho}\mathscr{L}_1(t) &\le -\mu\frac{(S(t)-S^*)^2}{S(t)} + \beta(S(t)-S^*)\left(\frac{S^*I^*}{S(t)} - I(t)\right)\\
&\quad + \beta(S-S^*)(I(t)-I^*)\\
&\le -\frac{(S(t)-S^*)^2}{S(t)}\left(\mu+\beta I^*\right).
\end{aligned}$$

Then,

$$^{C}D_{t}^{\rho}\mathscr{L}_1(t) \leq 0, \quad \text{for all} \quad t \geq 0.$$

In addition, we can see that $^{C}D_{t}^{\rho}\mathscr{L}_1(t) = 0$ if and only if $S(t) = S^*$ and $I(t) = I^*$. Thus, the largest invariant set of $E = \left\{(S(t), I(t)) \in \Theta_+' : {}^{C}D_{t}^{\rho}\mathscr{L}_1(t) = 0\right\}$ is $\{\mathscr{E}_1\}$. By LaSalle's invariance principle Lemma 1.3, $\mathscr{E}_1$ is globally asymptotically stable on Θ_+' when $\mathscr{R}_0 > 1$. ■

2.1.1.5 Sensitivity analysis

In this section, we perform a sensitivity analysis of $\mathscr{R}_0$ with respect to the parameters of model (2.2), using the definition provided in Equation (1.27). The sensitivity indices for the parameters β, Λ, μ, δ_1, and γ are given as follows:

$$\begin{aligned}
\Upsilon_{\beta}^{\mathscr{R}_0} &:= \frac{\partial \mathscr{R}_0}{\partial \beta} \times \frac{\beta}{\mathscr{R}_0} = \frac{\Lambda\beta}{\mu(\mu+\delta_1+\gamma)} \times \frac{1}{\mathscr{R}_0} = 1,\\
\Upsilon_{\lambda}^{\mathscr{R}_0} &:= \frac{\partial \mathscr{R}_0}{\partial \Lambda} \times \frac{\Lambda}{\mathscr{R}_0} = \frac{\Lambda\beta}{\mu(\mu+\delta_1+\gamma)} \times \frac{1}{\mathscr{R}_0} = 1,\\
\Upsilon_{\mu}^{\mathscr{R}_0} &:= \frac{\partial \mathscr{R}_0}{\partial \mu} \times \frac{\mu}{\mathscr{R}_0} = -\frac{2\mu+\delta_1+\gamma}{\mu+\delta_1+\gamma},\\
\Upsilon_{\delta_1}^{\mathscr{R}_0} &:= \frac{\partial \mathscr{R}_0}{\partial \delta_1} \times \frac{\delta_1}{\mathscr{R}_0} = -\frac{\delta_1}{\mu+\delta_1+\gamma},\\
\Upsilon_{\gamma}^{\mathscr{R}_0} &:= \frac{\partial \mathscr{R}_0}{\partial \gamma} \times \frac{\gamma}{\mathscr{R}_0} = -\frac{\gamma}{\mu+\delta_1+\gamma}.
\end{aligned}$$

Parameters	Sensitivity index
β	+1
γ	-0.9182
μ	-1.0818
Λ	+1
δ_1	-2.0632e-11
δ_2	0

Table 2.2: Sensitivity analysis of $\mathscr{R}_0$ concerning the parameters of model SIA

Based on the information presented in Table 2.2, the most sensitive parameters are the HIV transmission rate β, and the birth rate Λ. Specifically, since $\Upsilon_{\beta}^{\mathscr{R}0} = 1$, a slight increase in β or Λ will lead to a decrease of 10% in $\mathscr{R}_0$. Similarly, a small decrease in β or Λ will result in an increase of 10% in $\mathscr{R}_0$. The situation is the same when the HIV

mortality rate δ_1, the rate at which HIV progresses to AIDS γ, or the rate at which people die naturally μ are high; consequently, the reproduction rate is low. Our analysis shows that the γ, δ_2, δ_1 and μ parameters do not affect the transmission of HIV, whereas the β and Λ parameters have a more significant effect.

2.1.2 Formulation of a fractional model of HIV/AIDS with migration

In many regions around the world, a significant portion of the population has relocated from various areas. While some regions conduct health screenings, this practice is not universal. Consequently, some migrating individuals may unknowingly carry infectious diseases. In this section, we explore the impact of migration on infectious diseases such as HIV and AIDS, utilizing the SIA model. To reflect this impact, the HIV/AIDS model is extended in this part to account for migration, as shown in the following Figure 2.2.

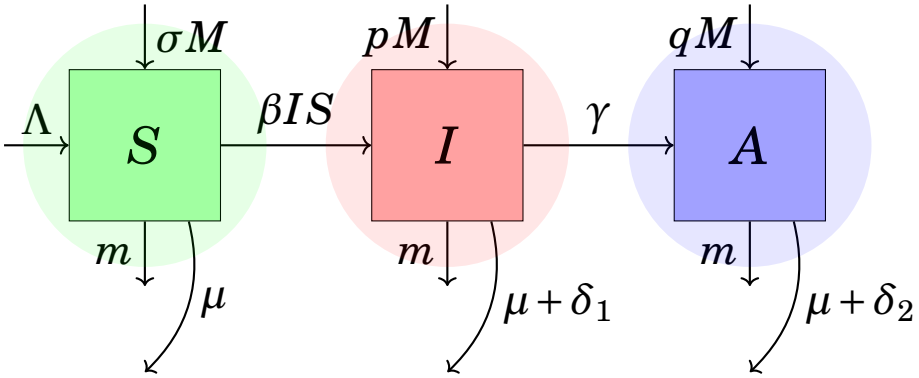


Figure 2.2: HIV/AIDS transmission pattern with migration.

We use the same parameters as in the previous model and add the following:

- M: immigration of people into the host country,
- σ: rate of migrants engaged in S,
- p: rate of migrants enrolled in I,
- q: rate of migrants enrolled in A,
- m: migration rate at which the population leaves.

We assume that the proportions σ, p, and q are recruited from the populations $S(t)$, $I(t)$, and $A(t)$, respectively, where $p+q+\sigma=1$. Additionally, we assume that immigrants in populations $S(t)$, $I(t)$, and $A(t)$ leave the host country at a rate of m.

Under these assumptions, we present the model described below.

$$\begin{cases} {}^{C}D_t^{\rho} S = \sigma M + \Lambda - \beta IS - (\mu+m)S, \\ {}^{C}D_t^{\rho} I = pM + \beta IS - (\mu+m+\delta_1+\gamma)I, \\ {}^{C}D_t^{\rho} A = qM + \gamma I - (\mu+m+\delta_2)A, \end{cases} \tag{2.14}$$

where $S(0)=S_0\geq 0, I(0)=I_0\geq 0, A(0)=A_0\geq 0$.

Parameters	Value	Source
ρ	6.0792e-08	Assumed
γ	7.4165e-02	[12]
μ	3.0475e-01	[12]
Λ	4.2249e-10	Assumed
δ_1	3.9684e-05	[12]
δ_2	4.3603e-05	[12]
σ	1.5572e-01	[12]
p	6.3773e-04	[12]
q	1.6611e-08	[12]
m	2.5e-01	Assumed

Table 2.3: The parameter values used in the SIA model with migration.

2.1.2.1 Positivity and boundedness of solution

Theorem 2.8. *The region* $\Theta_2=\{(S,I,A)\in\mathbb{R}^3; S\geq 0, I\geq 0, A\geq 0,$ $0\leq N(t)\leq \dfrac{\Lambda+M}{\mu+m}$, *where* $N(t)=S(t)+I(t)+A(t)\}$ *is positivity invariant set for the system* (2.14).

Proof. Firstly, we verify the existence and uniqueness of the solution to system (2.14) using Theorem 1.1. We find that

$$ {}^{C}D_t^{\rho} X(t) = f_2(X(t)), \text{ for } t\geq 0, \text{ with } X(0)=X_0\in\mathbb{R}^3_+, \tag{2.15}$$

with

$$X(t)=\begin{pmatrix} S(t)\\ I(t)\\ A(t)\end{pmatrix},\quad f_2(X(t))=\begin{pmatrix} \sigma M+\Lambda-\beta SI-(\mu+m)S\\ pM+\beta SI-(\mu+m+\delta_1+\gamma)I\\ qM+\gamma I-(\mu+m+\delta_2)A\end{pmatrix},\ X_0=\begin{pmatrix} S_0\\ I_0\\ A_0\end{pmatrix}.$$

The vector function f_2 clearly fulfills the initial and second conditions outlined in Theorem 1.1. Our next task is to demonstrate that f also satisfies the third criterion. We have

$$\|f_2(X(t))\|\le\|v\|+(\|A\|+\|B\|\,\|S(t)\|)\|X(t)\|,$$

where

$$v=\begin{pmatrix}\sigma M+\Lambda\\ pM\\ qM\end{pmatrix},\quad A=\begin{pmatrix}-(\mu+m) & 0 & 0\\ 0 & -(\mu+m+\delta_1+\gamma) & 0\\ 0 & \gamma & -(\mu+m+\delta_2)\end{pmatrix},$$

$$B=\begin{pmatrix}0 & -\beta & 0\\ 0 & \beta & 0\\ 0 & 0 & 0\end{pmatrix}.$$

Hence, the fractional SIA system (2.14) has a unique solution in $\mathbb{R}^3_+$.

Secondly, we prove the nonnegative of solution. Since, ${}^{C}D_t^{\rho}S\setminus_{S=0}=\sigma M+\Lambda\ge 0$, ${}^{C}D_t^{\rho}I\setminus_{I=0}=pM\ge 0$, and ${}^{C}D_t^{\rho}A\setminus_{A=0}=qM+\gamma I\ge 0$. By using Corollary (1.1), we conclude that the solution will remain in $\mathbb{R}^3_+$.

Next, we show that the solutions are bounded

$$\begin{aligned}{}^{C}D_t^{\rho}N(t)&=\Lambda+(p+q+\sigma)M-(\mu+m)N(t)-\delta_1 I(t)-\delta_2 A(t),\\ &\le \Lambda+M-(\mu+m)N(t).\end{aligned}\tag{2.16}$$

By applying the Laplace transform to inequality (2.16) using formula (1.22), we obtain:

$$N(t)\le\Lambda t^{\rho}E_{\rho,\rho+1}\left(-\mu t^{\rho}\right)+E_{\rho,1}\left(-\mu t^{\rho}\right)N(0).\tag{2.17}$$

According to the formula (1.4), and if $0\le N(0)\le\dfrac{\Lambda+M}{\mu}$, then

$$N(t)\le\frac{\Lambda+M}{\mu}\left[E_{\rho,1}(-\mu t^{\rho})+\mu t^{\rho}E_{\rho,\rho+1}(-\mu t^{\rho})\right]=\frac{\Lambda}{\mu+M}.$$

As a result, the solutions are bounded within specific limits. ■

2.1.2.2 The steady states

Theorem 2.9. *When $p \neq 0$, $q \neq 0$ and if $\beta(\Lambda+\sigma M)-(\mu+\delta_1+m+\gamma)(\mu+m)>0$, the model (2.14) admits a unique endemic equilibrium, denoted by $E^*=(S^*,I^*,A^*)$, where*

$$\begin{cases} S^* = \dfrac{(p+\sigma)M+\Lambda-(\mu+\delta_1+m+\gamma)I^*}{\mu+m}, \\ I^* = \dfrac{(\mu+\delta_1+m+\gamma)(\mu+m)(B-1)+\beta p m+\sqrt{C}}{2\beta(\mu+\delta_1+m+\gamma)}, \\ A^* = \dfrac{qM+\gamma I^*}{\mu+m+\delta_2}. \end{cases} \tag{2.18}$$

with

$$B = \frac{\beta(\Lambda+\sigma M)}{(\mu+\delta_1+m+\gamma)(\mu+m)},$$
$$C = (\beta(\Lambda+(p+\sigma)m)-(\mu+\delta_1+m+\gamma)(\mu+m))^2+4\beta p m(\mu+\delta_1+m+\gamma)(\mu+m).$$

Proof. To determine the equilibrium points of the model in equation (2.14), the following procedure can be applied:

$$\begin{aligned} \sigma M+\Lambda-\beta I^*S^*-(\mu+m)S^* &= 0, \\ pM+\beta I^*S^*-(\mu+m+\delta_1+\gamma)I^* &= 0, \\ qM+\gamma I^*-(\mu+m+\delta_2)A^* &= 0. \end{aligned} \tag{2.19}$$

It is evident that none of the solutions to the equation (2.19) can have $I=0$ and $A=0$ due to the conditions $p \neq 0$ and $q \neq 0$. This implies that the model (2.14) lacks a disease-free equilibrium but does admit an endemic equilibrium, denoted by $E^*=(S^*,I^*,A^*)$.

We add the first two equations from system (2.19) and determine the value of S^* in the following manner

$$S^* = \frac{(p+\sigma)M+\Lambda-(\mu+\delta_1+m+\gamma)I^*}{\mu+m}.$$

After some calculations, we find

$$a{I^*}^2+bI^*+c=0, \tag{2.20}$$

where

$$\begin{aligned} a &= -\beta(\mu+\delta_1+m+\gamma), \\ b &= (\beta(\Lambda+(\sigma+p)m)-(\mu+\delta_1+m+\gamma)(\mu+m)), \\ c &= 4\beta p\, m(\mu+\delta_1+m+\gamma)(\mu+m). \end{aligned}$$

If $\beta(\Lambda+\sigma M)-(\mu+\delta_1+m+\gamma)(\mu+m)>0$, the equation (4.18) admits one positive solution I^*. ■

2.1.2.3 The local stability analysis of the equilibrium points

The following theorem allows to study the local stability of the endemic equilibrium of model (2.14) in the case when $p\neq 0$ and $q\neq 0$.

Theorem 2.10. *When $p\neq 0$, $q\neq 0$, and if $\beta(\Lambda+\sigma M)-(\mu+\delta_1+m+\gamma)(\mu+m)>0$, the endemic equilibrium $E^*=(S^*,I^*,A^*)$ of model (2.14) is locally asymptotically stable.*

Proof. The Jacobian matrix at the endemic equilibrium E^* of model (2.14) is given by

$$\mathscr{J}(E^*)=\begin{pmatrix} -\beta I^*-(\mu+m) & -\beta S^* & 0 \\ \beta I^* & \beta S^*-(\mu+\delta_1+m+\gamma) & 0 \\ 0 & \gamma & -(\mu+m+\delta_2) \end{pmatrix}.$$

We find the eigenvalues of the Jacobian matrix $\mathscr{J}(E^*)$ as follows

$$\det(\lambda-\mathscr{J}(E^{**}))=0. \tag{2.21}$$

Morever, the equation (2.21) is expressed as follows

$$(\lambda+\mu+m+\delta_2)(\lambda^2+a_1\lambda+a_2)=0,$$

where,

$$a_1=\beta I^*+\mu+m+(\mu+\delta_1+m+\gamma)-\beta S^*,$$
$$a_2=(\beta I^*+\mu+m)(\mu+\delta_1+m+\gamma-\beta S^*)+\beta^2 S^* I^*.$$

It is evident that $\lambda_1=-(\mu+m+\delta_2)<0$, and we will now calculate the other eigenvalues. Let $\Delta_1=a_1^2-4a_2$,

Case 1. If $\Delta_1>0$, then we have

$$\lambda_2=\frac{-a_1-\sqrt{\Delta_1}}{2},\quad \lambda_3=\frac{-a_1+\sqrt{\Delta_1}}{2}.$$

If $\beta(\Lambda+\sigma M)-(\mu+\delta_1+m+\gamma)(\mu+m)>0$, then $\lambda_2<0$ and $\lambda_3<0$.

Case 2. If $\Delta_1<0$, then we have two roots complex ($j^2=-1$)

$$\lambda_2=\frac{-a_1-j\sqrt{|\Delta_1|}}{2},\quad \lambda_3=\frac{-a_1+j\sqrt{|\Delta_1|}}{2}.$$

If $\beta(\Lambda+\sigma M)-(\mu+\delta_1+m+\gamma)(\mu+m)>0$, then $a_1>0$. So, the real parts of the eigenvalues λ_1 and λ_2 are negative.

Hence, we have $|\arg(\lambda_i)|>\frac{\rho\pi}{2}$ for $i=1,2,3$ in both previous cases. Consequently, the local stability of the endemic equilibrium E^* is established. ■

2.1.2.4 The global stability analysis of the equilibrium point

We will follow the same procedure as in Section 2.1.1.4, where we focused the study on the following system

$$\begin{cases} {}^{C}D_t^{\rho} S = \sigma M + \Lambda - \beta IS - (\mu + m)S, \\ {}^{C}D_t^{\rho} I = pM + \beta IS - (\mu + m + \delta_1 + \gamma)I. \end{cases} \tag{2.22}$$

Theorem 2.11. *When $p \neq , q \neq 0$, and if $\beta(\Lambda+\sigma M)-(\mu+\delta_1+m+\gamma)(\mu+m) > 0$, the endemic equilibrium $E^* = (S^*, I^*)$ of model (2.22) is globally asymptotically stable.*

Proof. We define the Lyapunov function as follows

$$\mathscr{L}_2(t) = \left(S - S^* - S^* \ln \frac{S}{S^*}\right) + \left(I - I^* - I^* \ln \frac{I}{I^*}\right).$$

Using Lemma 1.1, we have

$$\begin{aligned} {}^{C}D_t^{\rho} \mathscr{L}_2(t) &\leq \left(1 - \frac{S^*}{S(t)}\right) {}^{C}D_t^{\rho} S(t) + \left(1 - \frac{I^*}{I(t)}\right) {}^{C}D_t^{\rho} I(t), \\ &= \left(1 - \frac{S^*}{S(t)}\right)\left(\sigma M + \Lambda - (\mu + m)S - \beta S(t)I(t)\right) \\ &\quad + \left(1 - \frac{I^*}{I(t)}\right)\left[pM + \beta S(t)I(t) - (\mu + m + \delta_1 + \gamma)I(t)\right], \\ &= -(\mu + m)\frac{(S(t) - S^*)^2}{S(t)} + \beta S^* I^* \left(\frac{S(t)I(t)}{S^* I^*} - \frac{I}{I^*}\right) + pM\left(1 - \frac{I^*}{I(t)}\right)\left(1 - \frac{I(t)}{I^*}\right) \\ &\quad + \beta S^* I^* \left(1 - \frac{I^*}{I(t)}\right)\left(\frac{S(t)I(t)}{S^* I^*} - \frac{I(t)}{I^*}\right), \\ &= -(\mu + m)\frac{(S(t) - S^*)^2}{S(t)} - pM\frac{(I(t) - I^*)^2}{I^* I(t)} + \beta S^* I^* \left(2 - \frac{S^*}{S(t)} - \frac{S(t)}{S^*}\right). \end{aligned}$$

It is clear that $\left(2 - \frac{S^*}{S(t)} - \frac{S(t)}{S^*}\right) \leq 0$, hence

$${}^{C}D_t^{\rho} \mathscr{L}_2(t) \leq 0, \quad \text{for all} \quad t \geq 0.$$

Therefore, $E^* = (S^*, I^*)$ is globally asymptotically stable . ■

Remark 3. *Crucially, when p=q=0, system (2.14) has two equilibrium points: disease-free equilibrium $E_0 = \left(\frac{\Lambda+\sigma M}{\mu+m}, 0, 0\right)$, and the endemic equilibrium $E_1 = (S^{**}, I^{**}, A^{**})$, with the values of S^*, I^*, and A^* given as follows.*

$$S^{**} = \frac{\mu + m + \delta_1 + \gamma}{\beta}, \qquad I^{**} = \frac{(\mu + m)(\mathscr{R}_0 - 1)}{\beta(\mu + m + \delta_1 + \gamma)}, \qquad A^{**} = \frac{\gamma I^{**}}{\mu + m + \delta_2},$$

with $\mathscr{R}_0 = \dfrac{\beta(\Lambda+\sigma M)}{(\mu+m)(\mu+m+\delta_1+\gamma)}$, *is the basic reproduction number obtained by the next generation matrix [87].*

As a result, we obtain the following theorems.

Theorem 2.12. *When* $p = q = 0$, *we have*

1. *If* $\mathscr{R}_0 < 1$, *then the fractional SIA model* (2.14) *has a unique disease-free equilibrium* E_0.
2. *If* $\mathscr{R}_0 > 1$, *then the fractional SIA model* (2.14) *also has a unique endemic equilibrium* $E_1 = (S^*, I^*, A^*)$.

Theorem 2.13. *For model SIA fractional with* $p = 0$ *and* $q = 0$, *we get*

1. *The disease-free equilibrium* E_0 *is locally asymptotically stable when* $\mathscr{R}_0 < 1$, *and it is unstable when* $\mathscr{R}_0 > 1$.
2. *The unique endemic equilibrium* $E_1 = (S^*, I^*, A^*)$ *is locally asymptotically stable when* $\mathscr{R}_0 > 1$.

Proof. 1. **Analysis for Disease-Free Equilibrium** E_0

The Jacobian matrix at equilibrium E_0 of fractional model (2.14) can be presented as

$$\mathscr{J}(E_0) = \begin{pmatrix} -(\mu+m) & -\beta & 0 \\ 0 & (\mathscr{R}_0-1)(\mu+m+\delta_1+\gamma) & 0 \\ 0 & \gamma & -(\mu+m+\delta_2) \end{pmatrix}.$$

The eigenvalues of the matrix can be easily obtained

$$\lambda_1 = -(\mu+m+\delta_2), \quad \lambda_2 = -(\mu+m), \quad \lambda_3 = (\mathscr{R}_0-1)(\mu+m+\delta_1+\gamma).$$

Since, $\mathscr{R}_0 < 1$, the eigenvalues are all less than zero. This suggests that $|\arg(\lambda_i)| = \pi > \frac{\rho\pi}{2} (i = 1,2,3)$. We can conclude, in accordance with Theorem 1.2, that E_0 is locally asymptotically stable.

2. **Analysis for Endemic Equilibrium** E_1**.**

For the endemic equilibrium E_1, the Jacobian matrix is given by

$$\mathscr{J}(E_1) = \begin{pmatrix} -(\mu+m)\mathscr{R}_0 & -(\mu+m+\delta_1+\gamma) & 0 \\ (\mu+m)(\mathscr{R}_0-1) & 0 & 0 \\ 0 & \gamma & -(\mu+m+\delta_2) \end{pmatrix}.$$

The eigenvalues are found by solving the following characteristic equation

$$\det\left(\mathscr{J}(E_1)-\lambda I_3\right)=0.$$

Two cases are examined based on the value of the discriminant. $\Delta=((\mu+m)\mathscr{R}_0)^2-4(\mu+m)(\mu+m+\delta_1+\gamma)(\mathscr{R}_0-1)$

- If $\Delta>0$, we have obtained real solutions

  $$\lambda_1=\frac{-((\mu+m)\mathscr{R}_0)-\sqrt{\Delta}}{2},\quad \lambda_2=\frac{-((\mu+m)\mathscr{R}_0)+\sqrt{\Delta}}{2},\quad \lambda_3=-(\mu+m+\delta_2).$$

  We have $\lambda_3<0$, and if $\mathscr{R}_0>1$, then $\lambda 1<0$ and $\lambda_2<0$ as well.

- If $\Delta<0$, we obtained complex conjugate solutions

  $$\lambda_1=\frac{-((\mu+m)\mathscr{R}_0)-j\sqrt{\Delta}}{2};\quad \lambda_2=\frac{-((\mu+m)\mathscr{R}_0)+j\sqrt{\Delta}}{2};\quad \lambda_3=-(\mu+m+\delta_2).$$

  Evident, Thus all eigenvalues have negative real parts.

Therefore, in both cases the eigenvalues verify condition 1.26, confirming the local stability of the endemic equilibrium of system (2.14) when $p=q=0$.

■

Theorem 2.14. *when $p=q=0$, we have*

1. *If $\mathscr{R}_0<1$, the disease-free equilibrium $E_0=\left(\frac{\sigma M+\Lambda}{\mu+m},0\right)$, of the model (2.22) is globally asymptotically stable.*
2. *if $\mathscr{R}_0>1$, the endemic equilibrium $E^1=(S^{**},I^{**})$ of the model (2.22) exhibits global asymptotic stability.*

Proof. 1. Consider the following Lyapunov function:

$$L_0(t)=\left(S(t)-S_0+S_0\ln\frac{S(t)}{S_0}\right)+I(t).$$

where $S_0=\frac{\sigma M+\Lambda}{\mu+m}$

Following a series of calculations, we find

$$\begin{aligned}
{}^{C}D_t^{\rho}L_0(t)&\leq\left(1-\frac{S_0}{S(t)}\right){}^{C}D_t^{\rho}S(t)+{}^{C}D_t^{\rho}I(t),\\
&=\left(1-\frac{S_0}{S(t)}\right)\left(\sigma M+\Lambda-\mu S(t)-\beta S(t)I(t)\right)\\
&\quad+\left(\beta S(t)I(t)-\left(\mu+\delta_1+\gamma\right)I(t)\right),\\
&\leq-\mu\frac{(S(t)-S_0)^2}{S(t)}+(\mu+\delta_1+\gamma)(\mathscr{R}_0-1)I(t).
\end{aligned}$$

We have $\mathscr{R}_0 < 1$, then ${}^{C}D_t^{\rho} L_0(t) < 0 \qquad \forall t \geq 0.$

Consequently, the disease-free equilibrium is globally asymptotically stable.

2. We use the Lyapunov function mentioned in Theorem 2.1.2.4 and follow the same procedures to obtain our results.

$$L_2(t) = \left(S - S^{**} - S^{**} \ln \frac{S}{S^{**}}\right) + \left(I - I^{**} - I^{**} \ln \frac{I}{I^{**}}\right).$$

$$\begin{aligned}
{}^{C}D_t^{\rho} L_2(t) &\leq \left(1 - \frac{S^{**}}{S(t)}\right) {}^{C}D_t^{\rho} S(t) + \left(1 - \frac{I^{**}}{I(t)}\right) {}^{C}D_t^{\rho} I(t), \\
&= \left(1 - \frac{S^{**}}{S(t)}\right) \left(\sigma M + \Lambda - (\mu + m)S - \beta S(t) I(t)\right) \\
&\quad + \left(1 - \frac{I^{**}}{I(t)}\right) \left[\beta S(t) I(t) - (\mu + m + \delta_1 + \gamma) I(t)\right], \\
&= -(\mu + m) \frac{(S(t) - S^{**})^2}{S(t)} + \beta S^* I^* \left(2 - \frac{S^{**}}{S(t)} - \frac{S}{S^{**}}\right).
\end{aligned}$$

We have $\left(2 - \frac{S}{S(t)} - \frac{S}{S^{**}}\right) \leq 0$, which gives

$${}^{C}D_t^{\rho} L_2(t) < 0, \quad \text{for all} \quad t \geq 0.$$

Therefore, $E_1 = (S^{**}, I^{**})$ is globally asymptotically stable .

■

2.1.3 Numerical Solutions of FDEs using the Adams-Bashforth-Moulton fractional Technique

In this section, we outline the numerical approach used to solve the fractional differential equations (FDEs) governing the dynamics of the HIV and AIDS models. Specifically, we employ the Adams-Bashforth-Moulton fractional technique, which is well-regarded for its accuracy and efficiency in capturing the non-local behaviors of fractional derivatives. The general formulation of this method was discussed in the previous chapter. We begin by presenting the specific numerical schemes used for our models, highlighting the advantages of this approach, followed by a discussion of the numerical results.

2.1.3.1 Numerical schemes for the model without migration

In this subsection, we discuss the algorithm used to obtain the numerical solution of the fractional-order SIA model without migration. We employ the Adams-Bashforth-Moulton predictor-corrector scheme outlined in Section 1.5.1, which is applied to our

model (2.2). The details of the algorithm are presented as follows.

(2.23)

$$
\begin{aligned}
S_{n+1} &= S_0 + \frac{h^\rho}{\Gamma(\rho+2)}\left(\Lambda - \beta S_{n+1}^p I_{n+1}^p - \mu S_{n+1}^p\right) + \frac{h^\rho}{\Gamma(\rho+2)}\sum_{j=0}^{n} a_{j,n+1}\left(\Lambda - \beta S_j I_j - \mu S_j\right),\\
I_{n+1} &= I_0 + \frac{h^\rho}{\Gamma(\rho+2)}\left(\beta S_{n+1}^p I_{n+1}^p - (\mu+\delta_1+\gamma) I_{n+1}^p\right) + \frac{h^\rho}{\Gamma(\rho+2)}\sum_{j=0}^{n} a_{j,n+1}\left(\beta S_j I_j - (\mu+\delta_1+\gamma) I_j\right),\\
A_{n+1} &= A_0 + \frac{h^\rho}{\Gamma(\rho+2)}\left(\gamma I_{n+1}^p - (\mu+\delta_2) A_{n+1}^p\right) + \frac{h^\rho}{\Gamma(\rho+2)}\sum_{j=0}^{n} a_{j,n+1}\left(\gamma I_j - (\mu+\delta_2) A_j\right),
\end{aligned}
$$

where

(2.24)

$$
\begin{aligned}
S_{n+1}^p &= S_0 + \frac{1}{\Gamma(\rho)}\sum_{j=0}^{n} b_{j,n+1}\left(\Lambda - \beta S_j I_j - \mu S_j\right),\\
I_{n+1}^p &= I_0 + \frac{1}{\Gamma(\rho)}\sum_{j=0}^{n} b_{j,n+1}\left(\beta S_j I_j - (\mu+\delta_1+\gamma) I_j\right),\\
A_{n+1}^p &= A_0 + \frac{1}{\Gamma(\rho)}\sum_{j=0}^{n} b_{j,n+1}\left(\gamma I_j - (\mu+\delta_2) A_j\right),
\end{aligned}
$$

and $a_{j,n+1}$ and $b_{j,n+1}$ are described in 1.31 and 1.33.

2.1.3.2 Numerical schemes for the model with migration dynamics

We use the Adams-Bashforth-Moulton predictor-corrector scheme, and with the same notations from the previous section, we derive the numerical schemes for the SIA model with migration.

(2.25)

$$
\begin{aligned}
S_{n+1} &= S_0 + \frac{h^\rho}{\Gamma(\rho+2)}\left(\Lambda + \sigma M - \beta S_{n+1}^p I_{n+1}^p - (\mu+m) S_{n+1}^p\right)\\
&\quad + \frac{h^\rho}{\Gamma(\rho+2)}\sum_{j=0}^{n}\left(\Lambda + \sigma M - \beta S_j I_j - (\mu+m) S_j\right),\\
I_{n+1} &= I_0 + \frac{h^\rho}{\Gamma(\rho+2)}\left(pM + \beta S_{n+1}^p I_{n+1}^p - (\mu+m+\delta_1+\gamma) I_{n+1}^p\right)\\
&\quad + \frac{h^\rho}{\Gamma(\rho+2)}\sum_{j=0}^{n} a_{j,n+1}\left(pM + \beta S_j I_j - (\mu+m+\delta_1+\gamma) I_j\right),\\
A_{n+1} &= A_0 + \frac{h^\rho}{\Gamma(\rho+2)}\left(qM + \gamma I_{n+1}^p - (\mu+m+\delta_2) A_{n+1}^p\right)\\
&\quad + \frac{h^\rho}{\Gamma(\rho+2)}\sum_{j=0}^{n} a_{j,n+1}\left(qM + \gamma I_j - (\mu+m+\delta_2) A_j\right),
\end{aligned}
$$

with

$$
\begin{aligned}
S^p_{n+1} &= S_0 + \frac{1}{\Gamma(\rho)} \sum_{j=0}^{n} b_{j,n+1} \left(\Lambda + \sigma M - \beta S_j I_j - (\mu + m) S_j\right), \\
I^p_{n+1} &= I_0 + \frac{1}{\Gamma(\rho)} \sum_{j=0}^{n} b_{j,n+1} \left(pM + \beta S_j I_j - \left(\mu + m + \delta_1 + \gamma\right) I_j\right), \\
A^p_{n+1} &= A_0 + \frac{1}{\Gamma(\rho)} \sum_{j=0}^{n} b_{j,n+1} \left(qM + \gamma I_j - \left(\mu + m + \delta_2\right) A_j\right),
\end{aligned}
\tag{2.26}
$$

and $a_{j,n+1}$ and $b_{j,n+1}$ are described in 1.31 and 1.33.

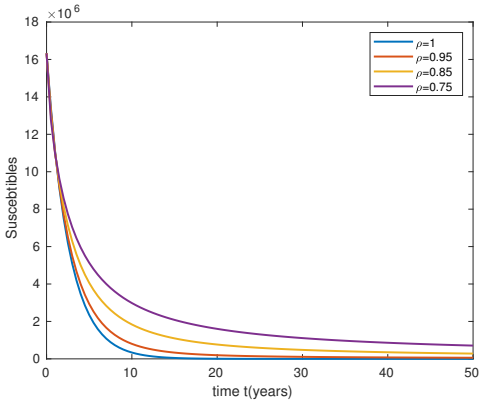
2.1.3.3 Numerical simulations and discussions

In this part, we perform numerical simulations to evaluate and validate the theoretical results of the two models presented in (2.2) and (2.14). Using the schemes outlined in (2.25) and (2.23), we demonstrate the influence of the fractional order. The initial values are taken as $N = 16{,}329{,}400$, $S(0) = 16{,}329{,}396$, $I(0) = 3$, $A(0) = 1$, and $M = 435{,}408$ [12], with the parameter values provided in Tables 2.1 and 2.3. The graphs in Figures 2.3(a), 2.3(b), and 2.3(c) display the solution curves for $S(t)$, $I(t)$, and $A(t)$ for different values of the fractional order ρ.

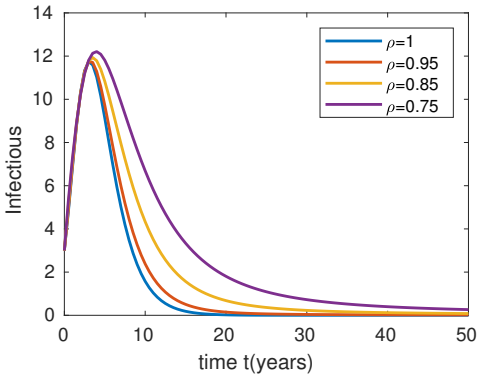
As illustrated in Figures 2.3(a) and 2.3(c), when ρ is near 1, both the number of susceptible individuals and those infected with AIDS increase. Figure 2.3(c) reveals that higher values of the fractional order result in a larger disease peak, with a maximum value higher than cases where ρ is less than 1. These graphical representations indicate that fractional derivatives are crucial for capturing the dynamics of the model. Specifically, for $\rho = 0.99, 0.85, 0.75$, convergence is faster compared to classical derivatives ($\rho = 1$).

Therefore, differential equations with fractional-order derivatives capture richer dynamics and more accurately reflect the behavior of biological systems compared to conventional integer-order models. The fractional derivative is particularly suitable for modeling the dynamics of HIV and AIDS, as it accounts for long-term interactions, latency periods, and recovery times. This approach aligns well with the reality of the progression from HIV to AIDS, as it more accurately represents the time required for this transition.

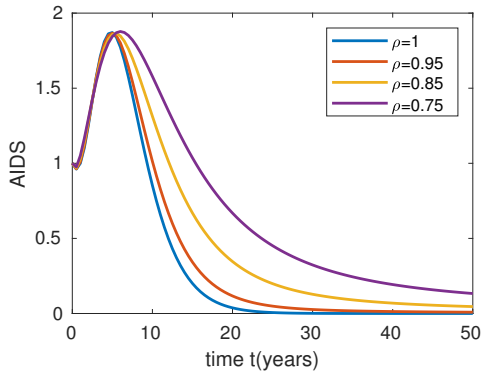
In model (2.2), we have $\mathscr{R}_0 < 1$, and the equilibrium point is $\mathscr{E}_0 = (1.0816 \times 10^{-9}, 0, 0)$. Figure 2.3 shows that the solution of model (2.2) converges to its equilibrium point for all fractional-order derivative. Moreover, the disease-free equilibrium $\mathscr{E}_0$ is globally asymptotically stable, which confirms the theoretical results.



(a) Susceptible population



(b) HIV-affected population



(c) Population affected by AIDS

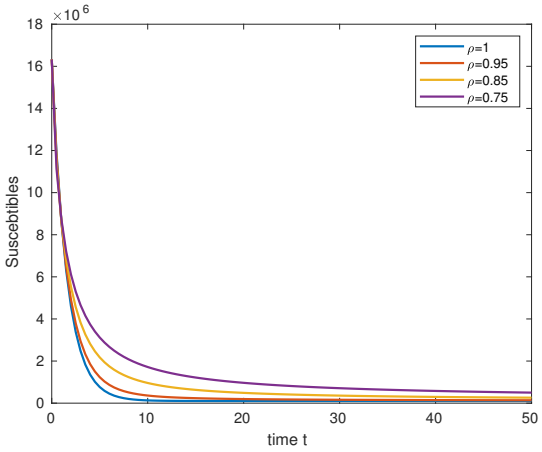
Figure 2.3: Dynamic behavior of the SIA model without migration as a function of Time (years) for different ρ values using the Adams-Bashforth-Moulton fractional method

In Figure 2.4, the subplots illustrate the populations of susceptible individuals, HIV-infected individuals, and individuals with AIDS in the presence of migration. As the value of ρ decreases (i.e., $\rho < 1$), the populations of HIV-infected and AIDS-infected individuals increase, while the susceptible population decreases.

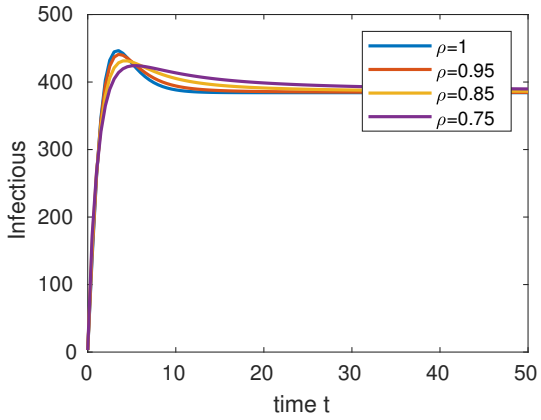
We computed the stability condition as specified in Theorem 2.10 for the model with migration. The result, $\beta(\Lambda + \sigma M) - (\mu + \delta_1 + m + \gamma)(\mu + m) = -0.0867 < 0$, indicates that the endemic equilibrium is unstable. As shown in Figures 2.4(a), 2.4(c), and 2.4(b), model (2.14) does not converge to the expected equilibrium, validating the theoretical predictions.

The illustrations demonstrate that, for different values of ρ, the solution curves converge to distinct points, denoted as $E_m = (1.0355 \times 10^5, 384.2372, 43.5316)$, rather than the equilibrium point. This observation is consistent with and supports our analytical findings.

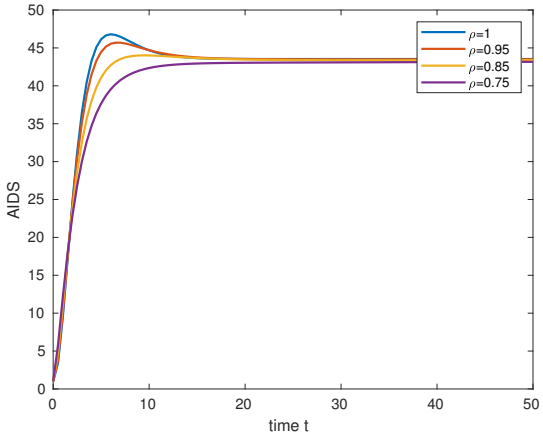
In our analysis of the system dynamics, we specifically examined the effects of the



(a) Susceptible population



(b) HIV-affected population

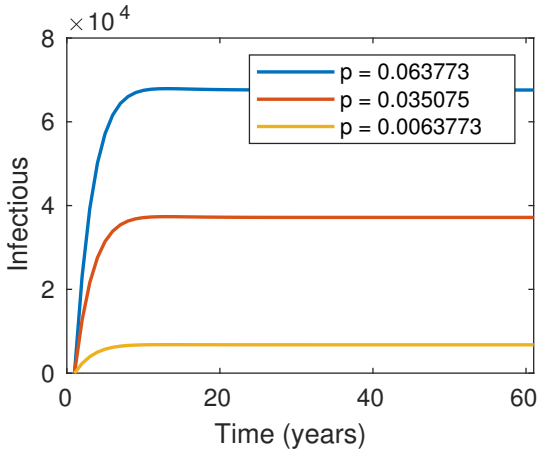


(c) Population affected by AIDS

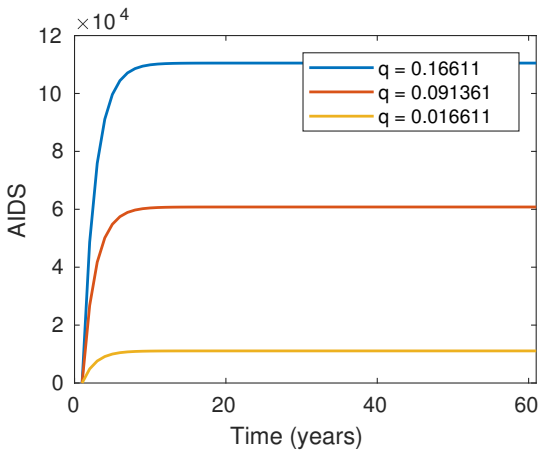
Figure 2.4: Dynamic Behavior of the SIP model with migration as a function of time (Years) for different ρ values using the Adams-Bashforth-Moulton fractional method

migration rates of infectious individuals (p) and AIDS-infected individuals (q). Figures 2.5(a) and 2.5(b) illustrate the system's behavior for various values of these parameters. We observed significant changes in the dynamics, highlighting the influence of migration rates on the system. For instance, varying the migration rate of infectious individuals, with values of $p = 0.0063773$, $p = 0.035075$, and $p = 0.063773$, led to a notable increase in the number of infectious individuals. This suggests a positive correlation between the number of infectious individuals and the migration rate (p).

These findings highlight the critical role that migration rates play in shaping the overall dynamics of the system. The graphs clearly illustrate how migration influences the spread of infectious diseases within the studied population.



(a) Influence of migration rates p on HIV-affected population.



(b) Influence of migration rates q on population affected by AIDS

Figure 2.5: System behavior with migration for different values of p and q.

2.2 Dynamic analysis of the ABC fractional approach to HIV and AIDS with migration

In the previous section, we employed the Caputo fractional derivative to analyze the impact of migration on the dynamics of the epidemic. In this section, we explore the advantages of using the ABC fractional derivative to investigate the model's behavior specifically in the context of migration, as this aspect provides valuable insights. The system is defined as follows:

$$\begin{cases} {}^{ABC}D_t^{\rho} S = \sigma M + \Lambda - \beta IS - (\mu + m)S, \\ {}^{ABC}D_t^{\rho} I = pM + \beta IS - (\mu + m + \delta_1 + \gamma)I, \\ {}^{ABC}D_t^{\rho} A = qM + \gamma I - (\mu + m + \delta_2)A, \end{cases} \tag{2.27}$$

with initial conditions $S(0) = S_0 \geq 0$, $I(0) = I_0 \geq 0$, and $A(0) = A_0 \geq 0$, where ${}^{ABC}D_t^{\rho}$ denotes the Atangana-Baleanu-Caputo fractional derivative of order $\rho \in (0,1]$.

2.2.1 ABC-Fractional equations: existence and uniqueness

In this section, we demonstrate the existence and uniqueness of solutions using the fixed point theorem and the Picard operator. Consider $C\left([0,T],\mathbb{R}^3\right)$ as a Banach space

consisting of continuous functions on $[0,T]$ with the norm defined by

$$\|(S,I,A)\| = \|S\|_\infty + \|I\|_\infty + \|A\|_\infty,$$

where $\|\cdot\|_\infty$ represents the supremum norm over $\mathbb{R}$.
We put

$$\begin{cases} \varphi_1(t,S(t)) = \sigma M + \Lambda - \beta IS - (\mu+m)S, \\ \varphi_2(t,I(t)) = pM + \beta IS - (\mu+m+\delta_1+\gamma)I, \\ \varphi_3(t,A(t)) = qM + \gamma I - (\mu+m+\delta_2)A. \end{cases} \tag{2.28}$$

Thus, the fractional model (2.27) can be reformulated as follows

$$\begin{cases} {}^{\mathrm{ABC}}D_t^\rho(S(t)) = \varphi_1(t,S(t)), \\ {}^{\mathrm{ABC}}D_t^\rho(I(t)) = \varphi_2(t,I(t)), \\ {}^{\mathrm{ABC}}D_t^\rho(A(t)) = \varphi_3(t,A(t)). \end{cases} \tag{2.29}$$

Using the fractional ABC integral over each equation in the system (2.29), we derive

$$\begin{aligned} S(t) - S(0) &= \frac{1-\rho}{M(\rho)} + \frac{\rho}{M(\rho)\Gamma(\rho)}\int_0^t (t-z)^{\rho-1}\varphi_1(z,S)dz, \\ I(t) - I(0) &= \frac{1-\rho}{M(\rho)} + \frac{\rho}{M(\rho)\Gamma(\rho)}\int_0^t (t-z)^{\rho-1}\varphi_2(z,I)dz, \\ A(t) - A(0) &= \frac{1-\rho}{M(\rho)} + \frac{\rho}{M(\rho)\Gamma(\rho)}\int_0^t (t-z)^{\rho-1}\varphi_3(z,P)dz. \end{aligned}$$

The following theorems will be established under the assumptions that $\|S(t)\| \le C_1$, $\|I(t)\| \le C_2$, and $\|A(t)\| \le C_3$, where the constants C_i are positive for all $i = 1,\ldots,3$.
we set

$$\begin{aligned} &K_1 = \beta C_2 + \mu + m, \quad K_2 = \mu + m + \delta_1 + \gamma + \beta C_1, \\ &K_3 = \mu + m + \delta_2. \end{aligned} \tag{2.30}$$

Theorem 2.15. *Assume the following condition holds:*

$$0 < \max\{K_i\} < 1, \quad i \in \{1,\ldots,3\} \tag{2.31}$$

Under this condition, the kernels φ_1, φ_2, and φ_3 are contraction mappings.

Proof. Let S_1 and S_2 be two functions,

$$\begin{aligned} \|\varphi_1(t,S_1) - \varphi_1(t,S_2)\| &\le \|(\beta I + (\mu+m))(S_1 - S_2)\|, \\ &\le \|(\beta C_2 + \mu + m)(S_1 - S_2)\|, \\ &\le K_1 \|S_1 - S_2\|. \end{aligned}$$

Using the same process for φ_2 and φ_3, we find that

$$\left\|\varphi_2(t,I_1)-\varphi_2(t,I_2)\right\| \leq K_2 \left\|I_1-I_2\right\|,$$
$$\left\|\varphi_3(t,A_1)-\varphi_3(t,A_2)\right\| \leq K_3 \left\|A_1-A_2\right\|.$$

Then, according to condition (2.31), φ_1, φ_2, and φ_3 are contraction mappings. ■

Theorem 2.16. *Suppose the following condition holds:*

$$0 < \Gamma = \left(\frac{1-\rho}{M(\rho)} + \frac{t^\rho}{M(\rho)\Gamma(\rho)}\right) \max_{i=1,\ldots,3}\{K_i\} < 1, \tag{2.32}$$

under which the HIV/AIDS model with the fractional ABC derivative has a unique solution.

Proof. We consider

$$X(t)=\begin{pmatrix} S(t) \\ I(t) \\ A(t) \end{pmatrix}, \qquad X_0=\begin{pmatrix} S_0 \\ I_0 \\ A_0 \end{pmatrix}, \qquad \mathscr{F}(t,X(t))=\begin{pmatrix} \varphi_1(t,S) \\ \varphi_2(t,I) \\ \varphi_3(t,A) \end{pmatrix}.$$

$\mathbb{J}=[-T,T]$ and $B=\prod_{i=1}^{3}\left[{X_0}^i-\epsilon,{X_0}^i+\epsilon\right]$.

Consider $\mathscr{C}(\mathbb{J},B)$ as a metric space, equipped with the norm:

$$\|\Phi_1-\Phi_2\|_\infty = \sup_{t\in\mathbb{J}}|\Phi_1(t)-\Phi_2(t)|. \tag{2.33}$$

We now introduce the following Picard operator:

$$\begin{aligned} f:\mathscr{C}(\mathbb{J},B) &\to \mathscr{C}(\mathbb{J},B) \\ f(X(t)) &= X_0(t)+\frac{1-\rho}{M(\rho)}\mathscr{F}(t,X(t)) \\ &\quad + \frac{\rho}{M(\rho)\Gamma(\rho)}\int_0^t (t-z)^{\rho-1}\mathscr{F}(z,X(z))dz. \end{aligned}$$

To complete the proof of this theorem, we will demonstrate that the operator f defined above is a contraction mapping. Given $(X_1,X_2)\in\mathscr{C}(\mathbb{J},B)$, we have the following:

$$\begin{aligned} \|f(X_1(t))-f(X_2(t))\| &\leqslant \frac{1-\rho}{M(\rho)}\|\mathscr{F}(t,X_1(t))-\mathscr{F}(t,X_2(t))\| \\ &\quad + \frac{\rho}{M(\rho)\Gamma(\rho)}\int_0^t (t-z)^{\rho-1}\|\mathscr{F}(z,X_1(z))-\mathscr{F}(z,X_2(z))\|dz. \end{aligned}$$

Since the function $\mathscr{F}$ is a contraction mapping (as established in Theorem 2.15), we obtain:

$$\|f(X_1(t))-f(X_2(t))\| \leqslant \Gamma\|X_1(t)-X_2(t)\|.$$

If the condition given in (2.32) is met, then f acts as a contraction on $\mathscr{C}(\mathbb{J},B)$. As a result, the Banach fixed-point theorem ensures the existence and uniqueness of a fixed point for the operator f. Thus, the SIA model with the ABC fractional derivative (2.27) has a unique solution. ■

2.2.2 Non-negativity and boundedness of solutions

In this section, we establish the positivity and boundedness of the fractional model (2.27), starting with a proof of the non-negativity of its solutions.

Consider the following set:

$$\Theta_1 = \left\{(S,I,A) \in \mathbb{R}^3; S(t) \geq 0, I(t) \geq 0, A(t) \geq 0\right\}.$$

Theorem 2.17. *The solutions* (S,I,A) *of the model* (2.27) *are all positive for all* $t \geq 0$ *and belong to* Θ_1.

Proof. We begin with the first equation in the system (2.27), which is expressed as follows:

$$\begin{aligned} {}^{ABC}D_t^{\rho} S(t) &= \sigma M + \Lambda - \beta IS - (\mu + m)S, \\ &\geq -\left(\beta + \mu + m\right) S(t). \end{aligned}$$

Then,

$$ {}^{ABC}D_t^{\rho} S(t) \geq -\left(\beta + \mu + m\right) S(t). \tag{2.34}$$

By employing the Laplace transform of the ABC operator on the inequality (2.34), we obtain

$$\mathscr{L}\{S(t)\}(s) \geq \frac{M(\rho)S(0)}{M(\rho) + \left(\rho + \mu + m\right)(1-\rho)} \cdot \frac{s^{\rho-1}}{s^{\rho} + \frac{(\rho+\mu+m)\rho}{M(\rho)+(\rho+\mu+m)(1-\rho)}}.$$

By utilizing the inverse Laplace transform and referring to formula (1.22), we derive

$$S(t) \geq \frac{M(\rho)S(0)}{M(\rho) + \left(\beta + \mu\right)(1-\rho)} E_{\rho,1}\left(-t^{\rho} \frac{\left(\beta + \mu + m\right)\rho}{M(\rho) + \left(\beta + \mu + m\right)(1-\rho)}\right).$$

Given that $S(0) \geq 0$ and $0 < E_{\rho,1}\left(-t^{\rho} \frac{(\beta+\mu+m)\rho}{M(\rho)+(\beta+\mu+m)(1-\rho)}\right) \leq 1$, it follows that $S(t) \geq 0$.

Similarly, by proving that $S(t) \geq 0$, $I(t) \geq 0$, and $A(t) \geq 0$, we can conclude that the solution remains within $\mathbb{R}^3_+$. ■

Next, we demonstrate that the solutions are bounded.

Theorem 2.18. *The biologically relevant region for the ABC fractional model* (2.27) *is defined as follows*

$$\Theta := \left\{ (S(t), I(t), A(t)) \in \mathbb{R}^3_+ \mid 0 \le N(t) \le \frac{M+\Lambda}{\mu+m} \right\},$$

where $N(t) = S(t) + I(t) + A(t)$.

Proof. By adding all the equations of the model (2.27), we obtain

$$^{ABC}D_t^{\rho} N(t) = M + \Lambda - (\mu+m)N(t) - (\delta_1+\gamma)I(t) - \delta_2 A(t). \tag{2.35}$$

When there are no infections $I = 0$ and $A = 0$, we find

$$^{ABC}D_t^{\rho} N(t) \le M + \Lambda - (\mu+m)N(t). \tag{2.36}$$

Applying the Laplace transform of the ABC fractional derivative to inequality (2.36) gives:

$$\frac{M(\rho)s^{\rho}\mathscr{L}\{N(t)\}(s)}{\rho+(1-\rho)s^{\rho}} + (\mu+m)\,\mathscr{L}\{N(t)\}(s) \le (M+\Lambda)\,s^{\rho-(\rho+1)} + \frac{M(\rho)N(0)s^{\rho-1}}{\rho+(1-\rho)s^{\rho}}.$$

This simplifies to:

$$\mathscr{L}\{N(t)\}(s) \le \frac{1}{M(\rho)+(\mu+m)(1-\rho)} \times \frac{(M+\Lambda)(1-\rho)s^{\rho-1} + (M+\Lambda)\rho\, s^{\rho-(\rho+1)} + N(0)M(\rho)s^{\rho-1}}{s^{\rho} + \frac{\rho(\mu+m)}{M(\rho)+(\mu+m)(1-\rho)}}.$$

From here, using formula (1.22), we arrive at the following expression:

$$N(t) \le \frac{(M+\Lambda)\,\rho\, t^{\rho}}{(1-\rho)(\mu+m)+M(\rho)} E_{\rho,\rho+1}\left(-\xi t^{\rho}\right) + \left[\frac{(M+\Lambda)(1-\rho)}{(1-\rho)(\mu+m)+M(\rho)} + \frac{M(\rho)N(0)}{M(\rho)+(1-\rho)(\mu+m)}\right] E_{\rho,1}\left(-\xi t^{\rho}\right),$$

where $\xi = \frac{(\mu+m)\rho}{M(\rho)+(\mu+m)(1-\rho)}$. We find that $\lim_{t\to\infty} N \le \frac{M+\Lambda}{\mu+m}$. This indicates that $N(t)$, $S(t)$, $I(t)$, and $A(t)$ are constrained within Θ. ■

2.2.3 Numerical schemes for FDEs using the Atangana–Taoufik fractional method

In this subsection, we analyze the behavior of the SIA fractional epidemiological model (2.27) using the ABC derivative to illustrate how the memory index affects disease incidence. This analysis is conducted through the application of the two-step Lagrange

polynomial approximation, as detailed in Section 1.5.2. We then apply the scheme described in equation (1.5.1) to our model (2.27).

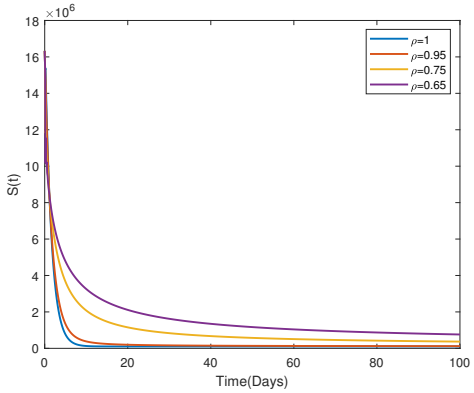
$$
\begin{aligned}
S(t_{n+1}) =& S(0) + \frac{1-\rho}{M(\rho)}\phi_1(t_n, S(t_n)) + \frac{\rho}{M(\rho)}\sum_{j=0}^{n}\left[\frac{h^\rho \phi_1(t_k, z(t_k))}{\Gamma(\rho+2)}\times\right.\\
&\{(n-k+2+\rho)(n+1-k)^\rho(n-k+2+2\rho)(n-k)^\rho\}\\
&\left.-\frac{h^\rho \phi_1(t_{k-1}, z(t_{k-1}))}{\Gamma(\rho+2)}\{(n+1-k)^{\rho+1}-(n-k+1+\rho)(n-k)^\rho\}\right],\\
I(t_{n+1}) =& I(0) + \frac{1-\rho}{M(\rho)}\phi_2(t_n, z(t_n)) + \frac{\rho}{M(\rho)}\sum_{k=0}^{n}\left[\frac{h^\rho \phi_2(t_k, z(t_k))}{\Gamma(\rho+2)}\times\right.\\
&\{(n-k+2+\rho)(n+1-k)^\rho(n-k+2+2\rho)(n-k)^\rho\}\\
&\left.-\frac{h^\rho \phi_1(t_{k-1}, z(t_{k-1}))}{\Gamma(\rho+2)}\{(n+1-k)^{\rho+1}-(n-k+1+\rho)(n-k)^\rho\}\right],\\
A(t_{n+1}) =& A(0) + \frac{1-\rho}{M(\rho)}\phi_3(t_n, z(t_n)) + \frac{\rho}{M(\rho)}\sum_{k=0}^{n}\left[\frac{h^\rho \phi_3(t_k, z(t_k))}{\Gamma(\rho+2)}\times\right.\\
&\left.\{(n-k+2+\rho)(n+1-k)^\rho(n-k+2+2\rho)(n-k)^\rho\}\right],
\end{aligned}
\tag{2.37}
$$

where φ_1,φ_2 and φ_3 are desribed in 2.28.

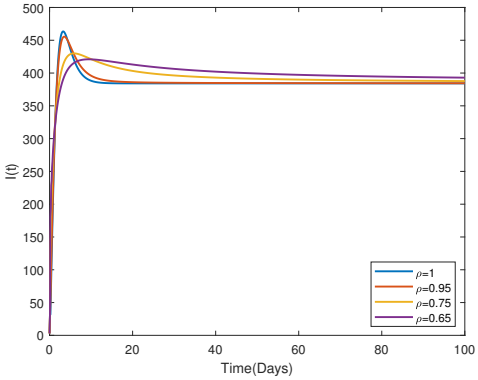
2.2.4 Numerical sumulations and discussions

This section examines the behavior of the SIA fractional model using the Taoufik–Atangana numerical scheme, as detailed in Section 1.5.2. The parameters and initial values for the numerical simulations are consistent with those used for the Caputo fractional derivatives (see Table 2.3). We apply the ABC fractional derivative with varying values of the order ρ to assess its impact on the model's dynamics, as shown in Figure 2.6. From this figure, we observe that as ρ decreases, the infection peak of the disease decline, emphasizing the role of fractional derivatives particularly the ABC fractional derivative in shaping disease transmission and management.

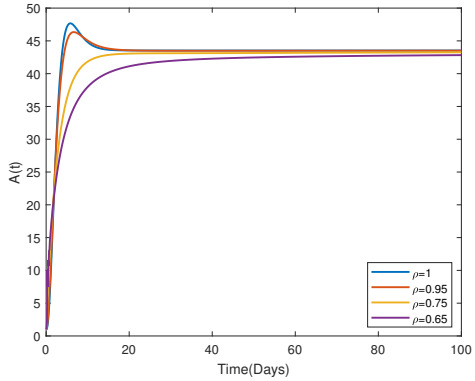
The fractional parameter ρ is key to capturing the long-term behavior of HIV, including its slow progression and chronic nature. Compared to the integer-order case ($\rho = 1$), the fractional model introduces a "memory effect," which better reflects HIV's prolonged latency period and slows the spread of infection. This indicates that fractional derivatives offer a more nuanced approach to controlling HIV transmission, providing potential advantages over traditional integer-order models in epidemic management.



(a) Susceptible population



(b) HIV-infected population



(c) Individuals impacted by AIDS

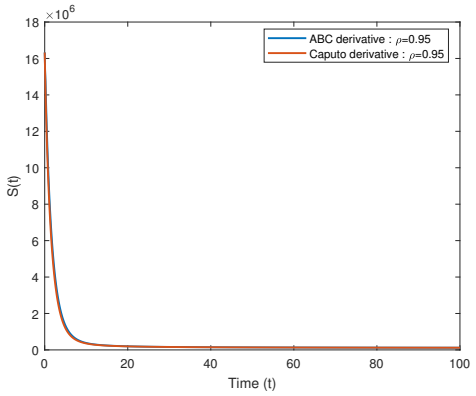
Figure 2.6: Dynamics of the SIA model over time (in years) for various values of ρ using the Taoufik–Atangana scheme

2.3 Comparison of ABC and Caputo fractional derivatives in HIV and AIDS dynamics

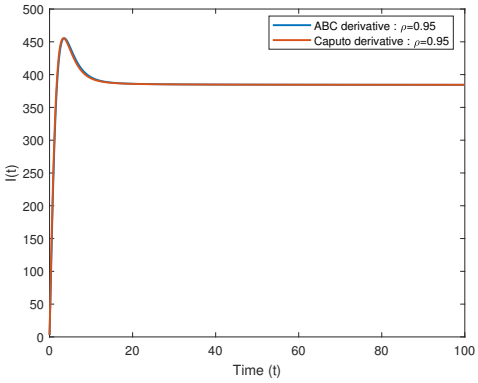
To tackle the persistent challenge of selecting the appropriate fractional derivative, this section presents a comparative analysis between the Atangana–Baleanu-Caputo (ABC) and Caputo derivatives within the context of HIV and AIDS models, particularly in cases involving migration. The Caputo derivative is approximated using the Adams-Bashforth method, as shown in equation (2.25), while the ABC derivative is approximated using the Taoufik-Atangana scheme, as detailed in equation (2.37).

Figures 2.7 to 2.9 illustrate the trajectories of the susceptible population, the infected population with HIV $I(t)$, and the AIDS population for both the fractional ABC and Caputo derivatives, with values of $\rho = 0.95$, 0.75, and 0.60. Our objective is to determine which derivative more accurately models the spread of HIV, considering their distinct

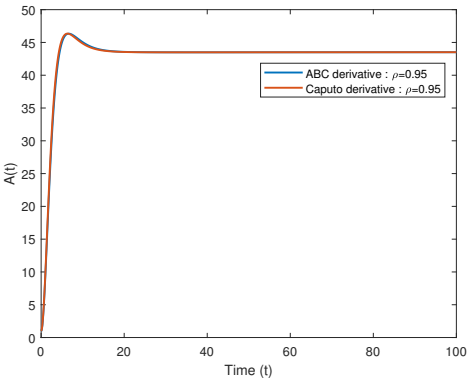
mathematical properties and implications for modeling real-world phenomena. The results reveal that the ABC derivative leads to slower convergence compared to the Caputo derivative, suggesting a more pronounced impact on HIV transmission and highlighting the significance of incorporating memory effects. Furthermore, as ρ deviates further from 1, the differences between the two derivatives become increasingly significant.



(a) Susceptible population

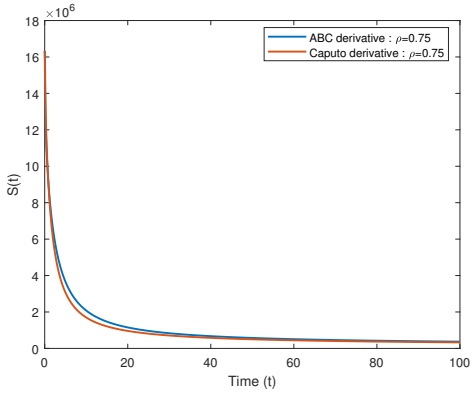


(b) HIV-infected population

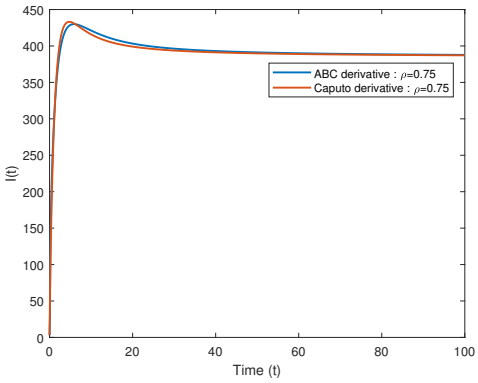


(c) Individuals impacted by AIDS

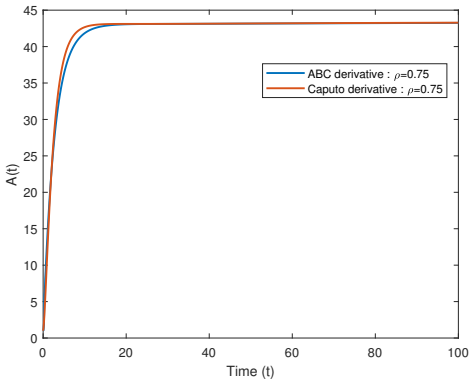
Figure 2.7: Comparison of the ABC and Caputo fractional derivatives in the dynamics of the SIA model with $\rho = 0.95$.



(a) Susceptible population

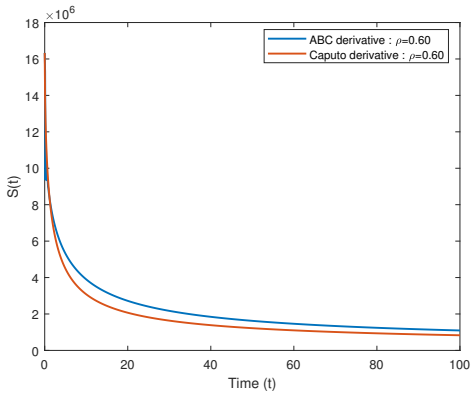


(b) HIV-infected population

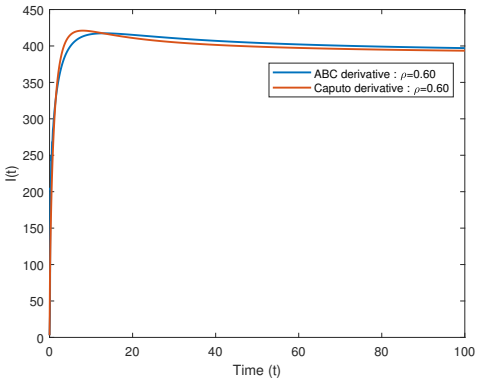


(c) Individuals impacted by AIDS

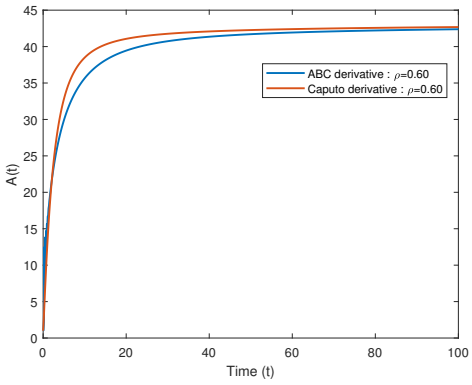
Figure 2.8: Comparison of the ABC and Caputo fractional derivatives in the dynamics of the SIA model with $\rho = 0.75$.



(a) Susceptible population



(b) HIV-infected population



(c) Individuals impacted by AIDS

Figure 2.9: Comparison of the ABC and Caputo fractional derivatives in the dynamics of the SIA model with $\rho = 0.60$.

2.4 Conclusion

In this chapter, we presented two fractional models of HIV/AIDS, one including migration and the other without, and applied two fractional operators: Caputo and ABC. We demonstrated that both models are well-posed, establishing their local stability by analyzing the equilibria. Additionally, we computed the basic reproduction number for both models and proved their global stability using appropriate Lyapunov functions. The theoretical results were corroborated by numerical simulations, which showed that while the fractional order derivative ρ did not affect the stability of the equilibrium, it had a significant impact on the time required to reach a stable state. Specifically, we observed that convergence to stable states was slower with fractional values of ρ, consistent with the slow progression characteristic of HIV. These findings highlight the robustness and consistency of the models, confirming that the results are valid across different fractional derivative approaches.

Furthermore, our comparative analysis of the Caputo and ABC fractional derivatives revealed that the ABC derivative captures more intricate dynamics, offering a richer understanding of the system's behavior. This increased detail enables a more accurate representation of HIV/AIDS transmission dynamics. Based on these findings, we conclude that fractional derivatives, particularly the ABC fractional derivative, provide a more flexible and detailed framework for modeling the disease dynamics. The results emphasize the critical importance of selecting an optimal value for ρ, as it significantly influences the model's predictive capacity and can enhance the effectiveness of disease control strategies.

CHAPTER 3

FRACTIONAL ORDER MODELING OF PARASITE-PRODUCED MARINE DISEASES WITH MEMORY EFFECT

The growing global demand for marine resources, driven by changes in food preferences and technological advances in fisheries and aquaculture, highlights the critical importance of marine ecosystems. These ecosystems play a vital role in human nutrition and economic stability, particularly in developing countries, where marine resources serve as a primary source of dietary protein and livelihoods [36, 59]. However, marine ecosystems face significant challenges, including the rise of parasitic infections that affect both the health of marine organisms and the human populations that rely on them [2, 10].

Despite the importance of addressing marine diseases, the development of mathematical models to understand the dynamics of infectious diseases in marine environments remains limited [21]. This limitation is largely due to the complexity and vastness of marine ecosystems, the diversity of marine life, and the unique challenges of conducting research in these environments [40]. Building on previous research, this chapter explores the application of fractional calculus to model disease dynamics in marine ecosystems. Specifically, it presents the SIP model with a general incidence rate using the Caputo fractional derivative, while also extending the analysis by incorporating the Atangana-Baleanu-Caputo (ABC) derivative to further capture the memory and complexity inherent in marine systems. The Caputo fractional derivative, as highlighted in the introduction, is particularly suited for models with conventional initial conditions,

while the ABC derivative offers a more generalized approach. Together, these fractional derivatives enhance the model's ability to account for non-local effects and memory properties in disease transmission dynamics.

In eco-epidemiological models, the choice of incidence rate is crucial for accurately analyzing disease transmission dynamics, as it defines how infections spread among populations over time. Researchers have investigated various incidence rates to enhance their models, including the bilinear incidence rate [89], the saturated incidence rate [3, 58], the Beddington-DeAngelis incidence rate [30], and specific nonlinear functions [83]. By integrating these incidence rates, models can better reflect the complexities of disease spread in marine ecosystems.

The remainder of this chapter is organized as follows: The classical model is formulated in Section 3.1. In Section 3.2, we analyze the dynamics of diseases caused by marine parasites using the Caputo derivative. In Section 3.3, we conduct a sensitivity analysis of the model parameters. In Section 3.4, we examine the primary findings from the numerical simulations in the context of the Caputo derivative. In Section 3.5, we investigate the dynamics of diseases produced by marine parasites through the ABC fractional derivative. Finally, the chapter concludes with a summary of the results.

3.1 Model formulation

In this section, we consider a compartmental SIP model, proposed by [19], for modeling the transmission of marine parasites. The host population $N(t)$ is divided into two categories ($N(t) = S(t) + I(t)$): the susceptible class (S), representing the uninfected individuals, and the infected class (I), comprising individuals infected with a parasite. This model assumes that both susceptible and infected hosts come into contact with parasite stages (P) present in their local environment. The interaction between hosts and parasites is characterized by the coefficient c, which measures the rate at which hosts contact parasites per unit of time. The parasitic states (P) within the environment interact with the host population, leading to an additional disease-induced mortality rate δ. In the marine environment, susceptible individuals become infected at a rate β (the transmission rate). The parameters of our model include: B, the rate of recruitment of the marine population into the local environment; λ, the rate of parasite multiplication in infected hosts; b, representing local host production; and μ_p, the rate at which parasite stages exit the local environment through inactivation and export. Additionally, μ is the rate of natural mortality, with $\mu > b$. The dynamics of this model can be described by the

following linked differential equations

$$\begin{cases} \frac{dS}{dt} = B + b(S+I) - \mu S - \beta SP, \\ \frac{dI}{dt} = \beta SP - (\mu + \delta)I, \\ \frac{dP}{dt} = \lambda I - \mu_p P - c(S+I)P, \end{cases} \tag{3.1}$$

with the following initial conditions

$$S(0) = S_0 \geq 0, \qquad I(0) = I_0 \geq 0, \qquad P(0) = P_0 \geq 0. \tag{3.2}$$

Parameters	Value	Source
B	2	Assumed
β	$0.02 - 0.009$	[95]
μ	0.1	Assumed
c	0.01	Assumed
b	0.001	Assumed
δ	1	[95]
μ_p	1	[95]
λ	5.252	[95]

Table 3.1: The parameter values used in the fractional order SIP model.

3.2 Analyzing the dynamics of marine parasite diseases using the Caputo derivative

Fractional derivatives offer many advantages over classical derivatives, as integer-order derivatives are limited in accounting for memory effects and complex biological processes. Therefore, in this part, we replace the integer order derivative in (3.1) with fractional Caputo derivative ${}^{C}D^{\alpha}$, where α represents the orde derivative. As P represents the marine parasites, which is the key variable in the SIP model, we have generalized it with a function $\mathscr{F}(P)$ that can take many forms. For all $\beta > 0$ and $k_1 > 0$ we have

$$\mathscr{F}(P) = \beta P, \qquad \mathscr{F}(P) = \frac{\beta P}{1 + k_1 P}. \tag{3.3}$$

These forms will be studied further in this chapter. The SIP fractional model is subsequently defined as follows:

$$\begin{cases} {}^{C}D_t^{\alpha} S = B + b(S+I) - \mu S - S\mathscr{F}(P), \\ {}^{C}D_t^{\alpha} I = S\mathscr{F}(P) - (\mu+\delta)I, \\ {}^{C}D_t^{\alpha} P = \lambda I - \mu_p P - c(S+I)\mathscr{F}(P), \end{cases} \tag{3.4}$$

with the non-negative initial conditions described in (3.2), $\alpha \in (0,1]$, and the parameters in system (3.4) being the same as those of the classical model, the parasite transmission diagram is shown in Figure 3.1.

For the purpose of our study, we assume that the function $\mathscr{F} : \mathbb{R}^+ \to \mathbb{R}^+$, meets the following hypothesis

($\mathscr{H}1$) $\mathscr{F}(0) = 0$,

($\mathscr{H}2$) $\frac{\partial \mathscr{F}(P)}{\partial P} > 0$, for all $P > 0$,

($\mathscr{H}3$) $\frac{\partial (f(P)S)}{\partial P}$ is bounded for all $S > 0$ and $P \geq 0$.

We have made these assumptions for biological reasons. Hypothesis ($\mathscr{H}1$) implies that the disease cannot spread in the absence of parasitic individuals, while hypothesis ($\mathscr{H}2$) indicates that the incidence rate increases as the number of parasites increases. Hypothesis ($\mathscr{H}3$) ensures that the response of the incidence function to changes in the number of parasites remains controlled and does not become unbounded. This reflects a realistic scenario where the rate at which new infections occur cannot increase indefinitely with the number of parasites, which helps in maintaining the stability and feasibility of the model.

3.2.1 Existence and uniqueness of solution and non-negativity

Since model (3.4) represents a total population (specifically, a marine population), it is essential for all variables to remain positive. To guarantee this, we present the following theorem.

Theorem 3.1. *The region* $\mathscr{D}_+ = \{(S,I,P) \in \mathbb{R}^3; S \geq 0, I \geq 0, P \geq 0\}$ *is positively invariant for Caputo's fractional model* (3.4).

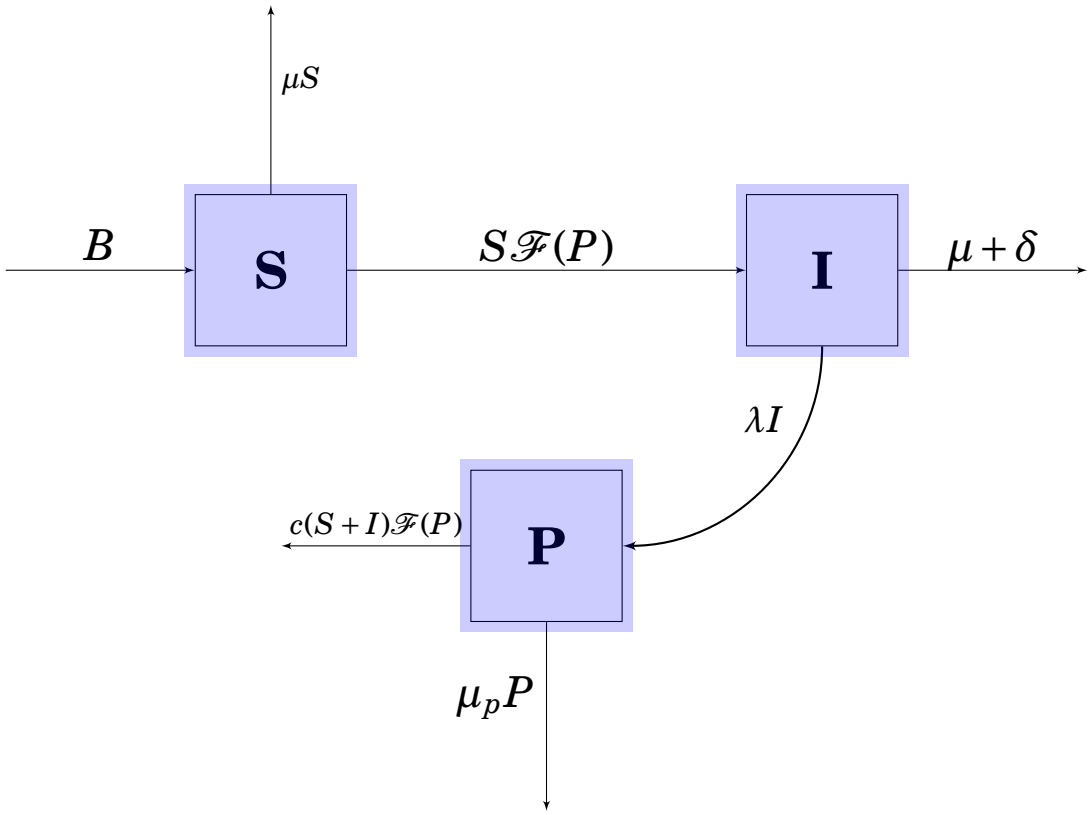


Figure 3.1: Schematic diagram representing the SIP model.

Proof. We first show the existence and uniqueness of the solution to the problem (3.4). The system (3.4) can be rewritten as follows:

$$ {}^{C}D_t^{\alpha} X(t) = f(X(t)), \quad t \geq 0. \tag{3.5} $$

where

$$ f(X(t)) = \begin{pmatrix} B + b(S+I) - \mu S - S\mathscr{F}(P) \\ S\mathscr{F}(P) - (\mu+\delta)I \\ \lambda I - \mu_p P - c(S+I)\mathscr{F}(P) \end{pmatrix}, \quad X(t) = \begin{pmatrix} S(t) \\ I(t) \\ P(t) \end{pmatrix}. \tag{3.6} $$

It's evident that the function f fulfills the initial condition stated in Theorem 1.1. Therefore, our task is to demonstrate that f satisfies the second condition. According to hypothesis ($\mathscr{H}3$), therefore, there exists a positive constant a_1 such that $\mathscr{F}(P)S \leq a_1 S$. Then, we have

$$ \|f(t, S(t))\| \leq \|\epsilon\| + (\|M_0\| + \|M_1\|)\|X(t)\|, \tag{3.7} $$

where

$$\epsilon = \begin{pmatrix} B \\ 0 \\ 0 \end{pmatrix}, M_0 = \begin{pmatrix} b-\mu & b & 0 \\ 0 & -(\mu+\delta) & 0 \\ 0 & \lambda & -\mu_p \end{pmatrix}, M_1 = \begin{pmatrix} 0 & 0 & -a_1 \\ 0 & 0 & a_1 \\ 0 & 0 & -c\,a_1 \end{pmatrix}. \tag{3.8}$$

Theorem 1.1 ensures that there is a unique solution to system (3.4) within the interval $[0, +\infty)$. Now, we prove that the solutions are non-negative.
We have

$$\begin{aligned} {}^{C}D_t^{\alpha} S/_{S=0} &= B + b\,I \geq 0, \\ {}^{C}D_t^{\alpha} I/_{I=0} &= S\mathscr{F}(P) \geq 0, \\ {}^{C}D_t^{\alpha} P/_{P=0} &= \lambda\, I \geq 0. \end{aligned} \tag{3.9}$$

Applying Lemma 1.2 and Corollary 1.1, we conclude that the solution remains in $\mathbb{R}^3_+$. ■

3.2.2 Biologically feasible region of the solution

Next, we establish that the solutions are bounded by constructing the biologically feasible region. The comprehension and control of disease transmission in marine population can be facilitated by applying the concept of a biologically viable area. It helps us pinpoint the circumstances under which a disease can endure and proliferate and create efficient countermeasures to stop its spread.

Theorem 3.2. *The feasible domain for solutions of the fractional model* (3.4) *is given by*

$$\Theta = \left\{ (S,I,P) \in \mathbb{R}^3_+ : N(t) \leq \max\left(\tfrac{B}{\mu-b}, N(0)\right), and\ P(t) \leq \lambda \max\left(\frac{B}{\mu-b}, N(0)\right) \right\},$$

where, $N(t) = S(t) + I(t)$.

Proof. By adding the two equations of the system (3.4), we obtain

$${}^{C}D_t^{\alpha} N(t) \leq B - (\mu-b)N(t). \tag{3.10}$$

Applying the Laplace transform to the inequality (3.10), we obtain

$$s^{\alpha}\mathscr{L}(N(t)) - s^{\alpha-1}N(0) \leqslant \frac{B}{s} - (\mu-b)\mathscr{L}(N(t)). \tag{3.11}$$

Then

$$\mathscr{L}(N(t)) \leq B\frac{s^{\alpha-(1+\alpha)}}{s^{\alpha}+(\mu-b)} + \frac{s^{\alpha-1}}{s^{\alpha}+(\mu-b)}N(0). \tag{3.12}$$

The expression in formula (1.22) provides the inequality

$$N(t) \leq B\,t^{\alpha} E_{\alpha,\alpha+1}\left(-(\mu-b)t^{\alpha}\right) + E_{\alpha,1}\left(-(\mu-b)t^{\alpha}\right)N(0). \tag{3.13}$$

According to the property of the Mittag Leffer function (1.4), we obtain

$$\begin{aligned} N(t) &\leq \max\left(\frac{B}{\mu-b}, N(0)\right)\left(E_{\alpha,1}(-(\mu-b)t^{\alpha}) + (\mu-b)t^{\alpha}E_{\alpha,\alpha+1}(-(\mu-b)t^{\alpha})\right) \\ &\leq \max\left(\frac{B}{\mu-b}, N(0)\right). \end{aligned} \tag{3.14}$$

This suggests that $S(t)$ and $I(t)$ are bounded. ■

3.2.3 Basic reproduction number and equilibrium

In this section, we focus on a crucial concept in epidemiology essential for understanding the transmission dynamics of infectious diseases: the basic reproduction rate, $\mathscr{R}_0$. As indicated in the introduction, $\mathscr{R}_0$ represents the expected number of secondary infections when an infected marine host, along with its associated parasitic stages, encounters a population of fully susceptible marine hosts. This rate is derived using the next-generation method [87], which involves calculating the transmission matrix T for newly infected cases and the transition infection matrix Σ related to the model (3.4).

$$T = \begin{pmatrix} 0 & S_0\mathscr{F}'(0) \\ \lambda & 0 \end{pmatrix}, \quad \Sigma = \begin{pmatrix} -(\mu+\delta) & 0 \\ 0 & -\left(\mu_P + \frac{cB}{\mu-b}\mathscr{F}'(0)\right) \end{pmatrix}.$$

Then, the basic reproduction number for the SIP model is given by

$$\mathscr{R}_0 = \rho\left(-T\Sigma^{-1}\right) = \sqrt{\frac{\lambda B F'(0)}{(\mu_p(\mu-b) + cBF'(0))(\mu+\delta)}}, \tag{3.15}$$

where ρ represents the spectral radius.

Disease-Free and Endemic Equilibria

To calculate the equilibrium of the proposed model (3.4), we need to solve the following equations

$$\begin{cases} 0 = B + b(S^* + I^*) - \mu S^* - S^*\mathscr{F}(P^*), \\ 0 = S\mathscr{F}(P^*) - (\mu+\delta)I^*, \\ 0 = \lambda I^* - \mu_p P^* - c(S^* + I^*)\mathscr{F}(P^*). \end{cases} \tag{3.16}$$

First, we determine the disease-free equilibrium, which represents the absence of infection within the marine population, where all individuals are susceptible to the disease. This equilibrium is expressed as:

$$\mathscr{E}_0 = (S_0, I_0, P_0) = \left(\frac{B}{\mu - b}, \quad 0, \quad 0\right). \tag{3.17}$$

Next, we determine the endemic equilibrium of fractional model (3.4).

If ($I \neq 0$ and $P \neq 0$), then we have

$$S^* = \frac{B - (\mu - b + \delta)I^*}{\mu - b}, \quad I^* = \frac{B\mathscr{F}(P^*)}{(\mu - b + \delta)\mathscr{F}(P^*) + (\mu - b)(\mu + \delta)}. \tag{3.18}$$

We replace in the third equation of system (3.16) the values of I^* and S^* found in (3.18), we get

$$\begin{aligned} &-Bc(\mu - b)\left(\mathscr{F}(P^*)\right)^2 + (\mu - b)\left(\lambda B - cB(\mu + \delta)\right)\mathscr{F}(P^*) \\ &\qquad -\mu_p(\mu - b)(\mu - b + \delta)\mathscr{F}(P^*)P^* - \mu_p(\mu - b)^2(\mu + \delta)P^* = 0. \end{aligned} \tag{3.19}$$

Since $P^* \neq 0$, then

$$\begin{aligned} &-Bc(\mu - b)P^*\left(\frac{\mathscr{F}(P^*)}{P^*}\right)^2 + (\mu - b)\left(\lambda B - cB(\mu + \delta)\right)\left(\frac{\mathscr{F}(P^*)}{P^*}\right) \\ &\qquad -\mu_p(\mu - b)(\mu - b + \delta)\mathscr{F}(P^*) - \mu_p(\mu - b)^2(\mu + \delta) = 0. \end{aligned} \tag{3.20}$$

To establish the existence and uniqueness of the solution to equation (3.20), we consider the specific cases of incidence rates given in equation (3.3).

1. If $\mathscr{F}(P) = \beta P$ and $\mathscr{R}_0 > 1$, then there exists a unique positive solution to equation (3.20)

   $$P^* = \frac{\lambda B\beta - (\mu_p(\mu - b) + \beta Bc)(\mu + \delta)}{\beta(Bc\beta + \mu_p)(\mu - b + \delta)}. \tag{3.21}$$

   Consequently, there is only one endemic equilibrium point for model (3.4).

2. If $\mathscr{F}(P) = \frac{\beta P}{1 + k_1 P}$, and $\mathscr{R}_0 = \sqrt{\dfrac{\lambda\beta B}{(\mu_p(\mu - b) + cB\beta)(\mu + \delta)}}$

   Equation (3.20) becomes

   $$-A_1P^2 + A_2P + A_3 = 0, \tag{3.22}$$

where,

$$
\begin{aligned}
A_1 &= \mu_p(\mu-b)^2k_1\beta+\mu_p(\mu-b)\delta k_1\beta+\mu_p(\mu-b)^2(\mu+\delta)k_1^2,\\
A_2 &= \beta B\lambda(\mu-b)k_1-\mu_p(\mu-b)(\mu-b+\delta)\beta\\
&\quad -2\mu_p(\mu-b)^2(\mu+\delta)k_1-cB\beta^2(\mu-b)-cB\beta(\mu+\delta)(\mu-b)k_1,\\
&= \beta B\lambda(\mu-b)k_1-\mu_p(\mu-b)^2\beta-\mu_p(\mu-b)\delta\beta-\mu_p(\mu-b)^2(\mu+\delta)k_1\\
&\quad -(\mu+\delta)(\mu-b)k_1(\mu_p(\mu-b)+cB\beta)-cB\beta^2(\mu-b),\\
&= (\mu-b)k_1\left(\frac{\beta B\lambda}{(\mu+\delta)(\mu_p(\mu-b)+cB\beta)}-1\right)-\mu_p(\mu-b)^2\beta-\mu_p(\mu-b)\delta\beta \qquad (3.23)\\
&\quad -\mu_p(\mu-b)^2(\mu+\delta)k_1-cB\beta^2(\mu-b),\\
&= (\mu-b)k_1\left(\mathscr{R}_0^2-1\right)-\mu_p(\mu-b)^2\beta-\mu_p(\mu-b)\delta\beta-\mu_p(\mu-b)^2(\mu+\delta)k_1-cB\beta^2(\mu-b)\\
A_3 &= (\mu-b)\left[\beta B\lambda-\mu_p(\mu-b)(\mu+\delta)-cB\beta(\mu+\delta)\right],\\
&= (\mu_p(\mu-b)+cB\beta)(\mu+\delta)(\mu-b)\left(\frac{\beta B\lambda}{(\mu_p(\mu-b)+cB\beta)(\mu+\delta)}-1\right),\\
&= (\mu_p(\mu-b)+cB\beta)(\mu+\delta)(\mu-b)\left(\mathscr{R}_0^2-1\right).
\end{aligned}
$$

We have $A_1>0$, and if $\mathscr{R}_0>1$ and $A_3>0$, then $A_2^2+4A_1A_3>0$. Therefore, there exists a unique positive solution for equation (3.20) depending on the sign of A_2.

❶ If $A_2>0$, then $A_2^2+4A_1A_3>A_2^2\Longrightarrow -A_2+\sqrt{A_2^2+4A_1A_3}>0$. This shows the existence of two roots of equation (3.20)

$$P_1=\frac{-A_2+\sqrt{A_2^2+4A_1A_3}}{-2A_1}<0,\quad P_2=\frac{-A_2-\sqrt{A_2^2+4A_1A_3}}{-2A_1}>0.$$

Then, we choose the positive root:

$$P^*=\frac{A_2+\sqrt{A_2^2+4A_1A_3}}{2A_1}. \qquad (3.24)$$

❷ If $A_2<0$, then $\sqrt{A_2^2+4A_1A_3}>A_2^2\Longrightarrow\sqrt{A_2^2+4A_1A_3}>-A_2$.
This implies that the roots of the equation (3.20) are:

$$P_1=\frac{-A_2+\sqrt{A_2^2+4A_1A_3}}{-2A_1}<0,\quad P_2=\frac{-A_2-\sqrt{A_2^2+4A_1A_3}}{-2A_1}>0.$$

Therefore, we choose the positive root:

$$P^*=\frac{A_2+\sqrt{A_2^2+4A_1A_3}}{2A_1}. \qquad (3.25)$$

Based on the above results, we establish the following theorem.

Theorem 3.3. *The disease produced by the marine parasites transmission model* (3.4) *admits a unique endemic equilibrium when* $\mathscr{R}_0 > 1$, *given by* $\mathscr{E}_1 = (S^*, I^*, P^*)$, *where,*

$$\begin{cases} S^* = \dfrac{B - (\mu - b + \delta) I^*}{\mu - b}, \\ I^* = \dfrac{B \mathscr{F}(P^*)}{(\mu - b + \delta)\mathscr{F}(P^*) + (\mu - b)(\mu + \delta)}, \end{cases}$$

and P^* *is defined depending on the form of the incidence rate:*

- *In the case of bilinear incidence rate, we have*

$$P^* = \frac{\lambda B \beta - (\mu_p(\mu - b) + \beta B c)(\mu + \delta)}{\beta(B c \beta + \mu_p)(\mu - b + \delta)}.$$

- *In the case of saturated incidence rate, we have*

$$P^* = \frac{A_2 + \sqrt{A_2^2 + 4 A_1 A_3}}{2 A_1},$$

  where A_1, A_2 *and* A_3 *are defined in equation* (3.23).

3.2.4 Analysis of local stability for the fractional model

In this subsection, we prove the local stability of disease-free and endemic equilibrium by linearizing the model (3.4) around each equilibrium point.

Theorem 3.4. *If* $\mathscr{R}_0 < 1$, *then the disease free equilibrium* $\mathscr{E}_0 = (S_0, I_0, P_0)$ *of system* (3.4) *is locally asymptotically stable. If* $\mathscr{R}_0 > 1$, *then* $\mathscr{E}_0$ *is unstable.*

Proof. The Jacobian matrix of system (3.4) at $\mathscr{E}_0$ is

$$\mathscr{J}(\mathscr{E}_0) = \begin{pmatrix} b - \mu & b & -S_0 \mathscr{F}'(0) \\ 0 & -(\mu + \delta) & S_0 \mathscr{F}'(0) \\ 0 & \lambda & -(\mu_p + c\, S_0 \mathscr{F}'(0)) \end{pmatrix}.$$

By some calculations, we obtain the characteristic roots are:

$$\lambda_1 = b - \mu, \quad \lambda_{2,3} = \frac{-(\mu + \delta + \mu_p + c S_0 \mathscr{F}'(0)) \mp \sqrt{(\mu_p + c S_0 \mathscr{F}'(0) - (\mu + \delta))^2 + 4 \lambda S_0 \mathscr{F}'(0)}}{2}.$$

Evident, $\lambda_1 < 0$ and $\lambda_3 < 0$. If $\mathscr{R}_0 < 1$, then $\lambda_2 < 0$. Thus, we have $|\arg(\lambda_i)| > \frac{\alpha \pi}{2} (i = 1, 2, 3)$, for any $\alpha \in (0, 1]$. According to Theorem 1.2, the disease-free equilibrium $\mathscr{E}_0$ is locally asymptotically stable. ■

Theorem 3.5. *If $\mathscr{R}_0 > 1$, then the endemic equilibrium $\mathscr{E}_1 = (S^*, I^*, P^*)$ of system (3.4) is locally asymptotically stable.*

Proof. The Jacobian matrix of system (3.4) at $\mathscr{E}_1$ is

$$\mathscr{J}(\mathscr{E}_1) = \begin{pmatrix} b-\mu-\mathscr{F}(P^*) & b & -S^*\mathscr{F}'(P^*) \\ \mathscr{F}(P^*) & -(\mu+\delta) & S^*\mathscr{F}'(P^*) \\ -c\mathscr{F}(P^*) & \lambda - c\mathscr{F}(P^*) & -(\mu_p + c(S^*+I^*)\mathscr{F}'(P^*)) \end{pmatrix}.$$

Then the characteristic equation of $\mathscr{J}(\mathscr{E}_1)$ is

$$\lambda^3 + a_1\lambda^2 + a_2\lambda + a_3 = 0. \tag{3.26}$$

Where

$$\begin{aligned}
a_1 &= \mu_p + c(S^* + I^*)\mathscr{F}'(P^*) + \mu + \delta + (\mu - b) + \mathscr{F}'(P^*) > 0, \\
a_2 &= (\mu-b)(\mu+\delta) + (\mu - b + \delta)\mathscr{F}(P^*) + \left(\mu_p + c(S^*+I^*)\mathscr{F}'(P^*)\right)(\mu - b) \\
&\quad + (\mu+\delta)\left(\mu_p + c(S^*+I^*)\mathscr{F}'(P^*)\right) + \left(\mu_p + c(S^*+I^*)\mathscr{F}'(P^*)\right)\mathscr{F}(P^*) - \lambda S^*\mathscr{F}'(P^*), \\
a_3 &= (\mu - b + \delta)cS^*\mathscr{F}'(P^*)\mathscr{F}(P^*) + (\mu-b)(\mu+\delta)\left(\mu_p + c(S^*+I^*)\mathscr{F}'(P^*)\right) \\
&\quad + cS^*(\mu-b)\mathscr{F}'(P^*)\mathscr{F}(P^*) + (\mu - b + \delta)\left(\mu_p + c(S^*+I^*)\mathscr{F}'(P^*)\right) - \lambda(\mu-b)S^*\mathscr{F}'(P^*).
\end{aligned}$$

From the hypothesis ($\mathscr{H}2$), we have $a_1 > 0, a_2 > 0, a_3 > 0$, and $a_1a_2 > a_3$. According to the Routh-Hurwitz stability criterion [90], the $\mathscr{E}_1$ endemic equilibrium will be locally asymptotically stable if a_1, a_2, a_3, and $a_1a_2 > a_3$ are positive.

■

3.3 Sensitivity analysis

To mitigate the spread of disease, we identify the parameters that influence the increase and decrease of the basic reproduction number, $\mathscr{R}_0$, and perform a parameter sensitivity analysis. The sensitivity indices of $\mathscr{R}_0$ with respect to the SIP model parameters were

computed using the values provided in Table 3.1 and are summarized in Table 3.2.

$$
\begin{aligned}
\zeta_B^{\mathscr{R}_0} &:= \frac{\partial \mathscr{R}_0}{\partial B} \times \frac{B}{\mathscr{R}_0} = \frac{1}{2} \times \frac{\mu_p(\mu-b)}{\mu_p(\mu-b)+c\beta B}, \\
\zeta_\beta^{\mathscr{R}_0} &:= \frac{\partial \mathscr{R}_0}{\partial \beta} \times \frac{\beta}{\mathscr{R}_0} = \frac{1}{2} \times \frac{\mu_p(\mu-b)}{\mu_p(\mu-b)+c\beta B}, \\
\zeta_\mu^{\mathscr{R}_0} &:= \frac{\partial \mathscr{R}_0}{\partial \mu} \times \frac{\mu}{\mathscr{R}_0} = -\frac{1}{2} \times \frac{\mu\mu_p(\mu-b+\delta)}{(\mu+\delta)(\mu_p(\mu-b)+c\beta B)}, \\
\zeta_c^{\mathscr{R}_0} &:= \frac{\partial \mathscr{R}_0}{\partial c} \times \frac{c}{\mathscr{R}_0} = -\frac{1}{2} \times \frac{c\beta B}{\mu_p(\mu-b)+c\beta B}, \\
\zeta_b^{\mathscr{R}_0} &:= \frac{\partial \mathscr{R}_0}{\partial b} \times \frac{b}{\mathscr{R}_0} = \frac{1}{2} \times \frac{b\mu_p}{\mu_p(\mu-b)+c\beta B}, \\
\zeta_\delta^{\mathscr{R}_0} &:= \frac{\partial \mathscr{R}_0}{\partial \delta} \times \frac{\delta}{\mathscr{R}_0} = -\frac{1}{2} \times \frac{\delta}{\mu+\delta}, \\
\zeta_{\mu_p}^{\mathscr{R}_0} &:= \frac{\partial \mathscr{R}_0}{\partial \mu_p} \times \frac{\mu_p}{\mathscr{R}_0} = -\frac{\mu_p(\mu-b)}{2}, \\
\zeta_\lambda^{\mathscr{R}_0} &:= \frac{\partial \mathscr{R}_0}{\partial \lambda} \times \frac{\lambda}{\mathscr{R}_0} = \frac{1}{2}.
\end{aligned}
\tag{3.27}
$$

In Figure 3.2, the graphical illustration of sensitivity indices for the parameters of the fractional SIP model is presented.

Parameters	Sensitivity index
B	+0.4980
β	+0.4980
μ	-0.5026
c	-0.0020
b	+0.0050
δ	-0.4545
μ_p	-0.0495
λ	+0.5000

Table 3.2: Sensitivity index results for the SIP model parameters.

Considering the information in Table 3.2 and Figure 3.2, the parameters showing high sensitivity are B, δ, β, λ, and μ as $\mathscr{R}_0$ exhibits significant sensitivity indices, either positive or negative. If the value is positive, it means that the parameter positively affects $\mathscr{R}_0$, indicating that an increase in this parameter leads to an increase in $\mathscr{R}_0$, resulting in the spread of the disease. For instance, among the parameters in our model (3.4) that positively affect $\mathscr{R}_0$ are the rate of recruitment of the marine population into

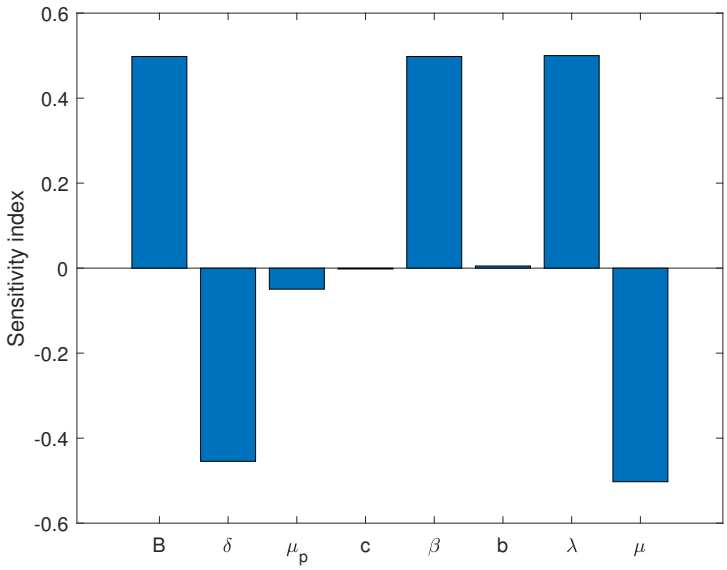


Figure 3.2: Histogram showing sensitivity indices of $\mathscr{R}_0$ with respect to the parameters of the fractional SIP model.

the local environment B, the rate of parasite production from infected hosts λ, and the rate of transmission β. On the other hand, increasing μ, δ, and μ_p reduces $\mathscr{R}_0$, and decreases the degree of infection.

3.4 Numerical simulations and discussion of Caputo fractional derivative

In this section, we validate our theoretical results by applying the Adams-Bashforth-Moulton predictor-corrector scheme to the proposed model (3.4). Furthermore, we examine the impact of fractional derivatives in the Caputo sense on the model and analyze how the parameters influence the system's dynamics.

3.4.1 The impact of memory effect and incidence function on population dynamics

To conduct the numerical simulation and analyze the impact of Caputo-type fractional derivatives and the incidence function on disease dynamics, we apply various incidence rates to the generalized incidence function $\mathscr{F}$ and simulate the model using various values of the fractional order derivative α (specifically, $\alpha = 1, 0.95, 0.90, 0.85$). The values

of the parameters used are presented in Table 3.1. The initial conditions are set as $S(0) = 100$, $I(0) = 1$, and $P(0) = 1$, covering a simulation duration of 100 days.

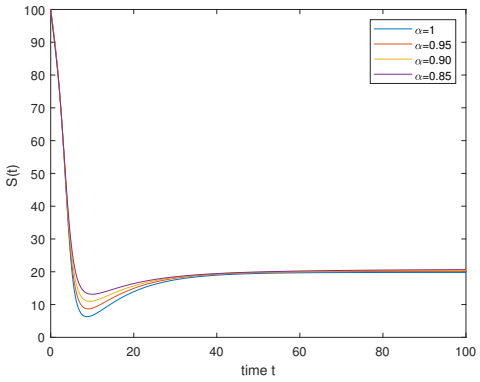
- We begin by examining the incidence function $\mathscr{F}$ defined as a bilinear function, given by $\mathscr{F}(P) = \beta P$. From this formulation, we derive the graphical results presented in Figures 3.3 and 3.4. Additionally, the phase portrait of the SIP model for this case is illustrated in Figure 3.5. In Figure 3.3, with $\beta = 0.009$, we find that the basic reproduction number is $\mathscr{R}_0 = 0.8876 < 1$, indicating the absence of parasites in the marine population. Here, all three compartments $S(t)$, $I(t)$, and $P(t)$ converge toward the disease-free equilibrium point $\mathscr{E}_0 = (20.2020, 0, 0)$ at various fractional order values α, confirming the local stability of this equilibrium.

  Conversely, in Figure 3.4, where $\beta = 0.02$, the basic reproduction number is calculated as $\mathscr{R}_0 = 1.3861 > 1$, indicating that the disease persists. The solution of model (3.4) converges toward the endemic equilibrium $\mathscr{E}_1 = (10.4962, 0.8743, 4.5814)$, which is locally asymptotically stable for $\mathscr{R}_0 > 1$, signifying that the disease becomes endemic.

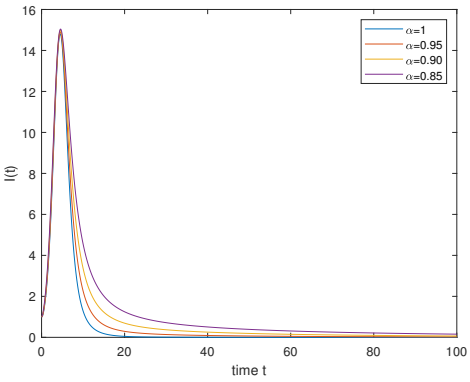
  Moreover, Figure 3.4 shows that varying the value of α results in a decrease in the susceptible population while the infected and parasite populations increase until reaching their maximum values (peaks) before declining. Notably, as α approaches 1, the curves converge more rapidly than when α exceeds one, highlighting the memory effect of the fractional derivative. This behavior indicates that the fractional-order derivative captures more information compared to the classical case ($\alpha = 1$). This aligns with real-world observations, as diseases caused by marine parasites typically take a considerable amount of time to stabilize. Understanding the memory effect enhances our comprehension of the long-term transmission dynamics, since fractional calculus integrates historical data from 0 to t ($t > 0$), providing valuable insights into the disease's trajectory.

- In the second case, we examine the saturated incidence function, expressed as $F(P) = \frac{\beta P}{1+k_1 P}$ with $k_1 = 0.002$, as shown in Figures 3.6 and 3.7. The phase portrait for this scenario is depicted in Figure 3.8. To obtain these graphical representations, we employ the same parameter values used in the bilinear incidence function analysis.

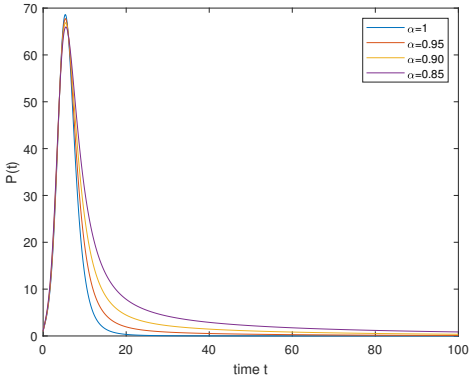
  On the other hand, when $\beta = 0.02$, we find $\mathscr{R}_0 = 1.3861 > 1$, which leads to a unique endemic equilibrium, $\mathscr{E}_1 = (10.1621, 0.9044, 4.8949)$. Figure 3.7 shows that all curves converge to this endemic steady state for various values of the fractional



(a) Dynamics of susceptible hosts.



(b) Dynamics of infected hosts.

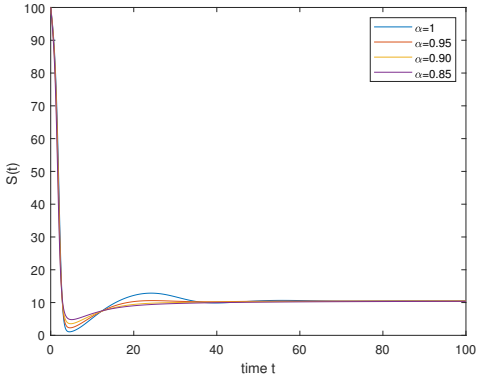


(c) Parasite population dynamics.

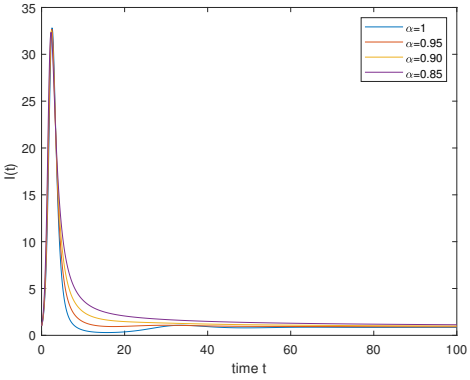
Figure 3.3: The illustration of the numerical solution of the SIP fractional model at different fractional order α, with $\mathscr{F}(P) = \beta P$ and $\mathscr{R}_0 = 0.9309 < 1$.

order α, reinforcing the local stability of the endemic equilibrium and supporting the theoretical findings discussed in the "Analysis of local stability for the fractional model" section. Furthermore, we observe that convergence to the steady state occurs more rapidly as α approaches 1, highlighting the memory effect associated with fractional derivatives.

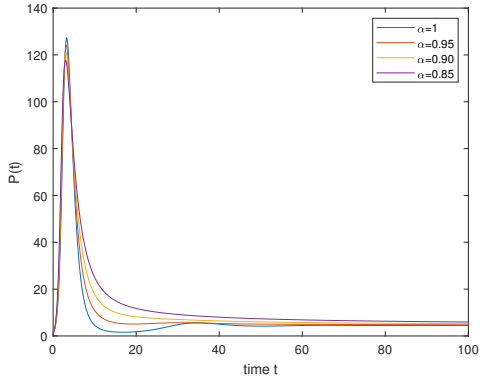
Generally, when there is a high concentration of parasites in the environment, a saturated incidence rate is chosen. However, for our purposes, we set the initial number of marine parasites to $P(0) = 1$ in order to clearly illustrate the differences between bilinear and saturated incidence rates. Figure 3.4(c) shows that the parasite population persists for $\mathscr{R}_0 > 1$ as with $F(P) = \beta P$, but the degree of severity decreases. In the bilinear case, the peak parasite population reaches 127.2925 parasites, whereas in the saturated case, it reaches 121.3573 parasites. This means that the peak of the parasite curve is smaller at the saturated infection rate, indicating that transmission is suppressed at higher



(a) Dynamics of susceptible hosts.

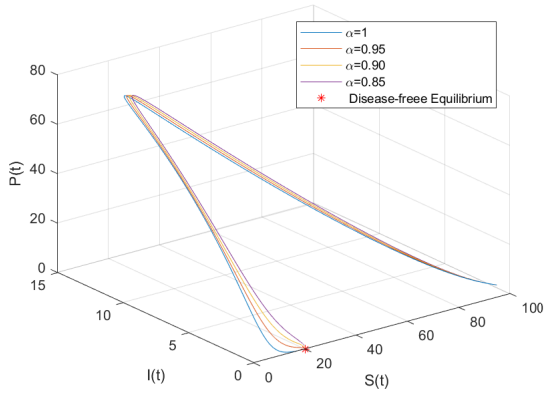


(b) Dynamics of infected hosts.

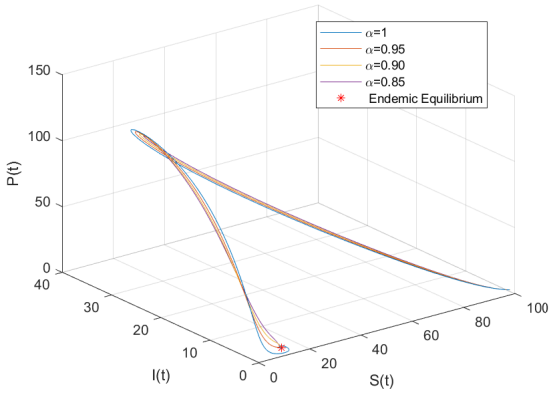


(c) Parasite population dynamics.

Figure 3.4: The illustration of the numerical solution of the SIP fractional model at different fractional order α, with $\mathscr{F}(P) = \beta P$ and $\mathscr{R}_0 = 1.3861 > 1$.



(a) Dynamics of solutions with $\mathscr{R}_0 < 1$.



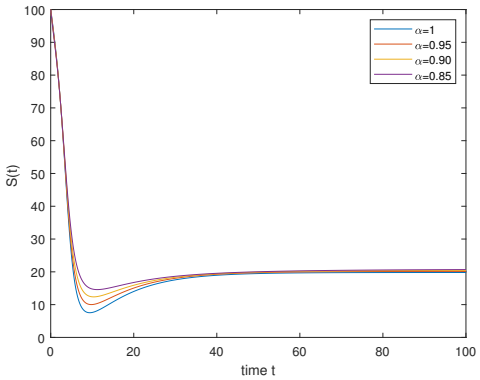
(b) Dynamics of solutions with $\mathscr{R}_0 > 1$.

Figure 3.5: Variations in solution trajectories: three-dimensional model SIP with different α values and $\mathscr{F}(P) = \beta P$.

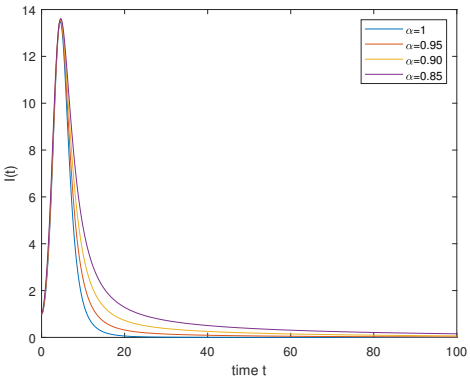
infection levels. This makes sense in biological systems where an epidemic is naturally contained by an immune response, depletion of susceptibility, or limiting environmental interactions.

3.4.2 The influence of the model parameters

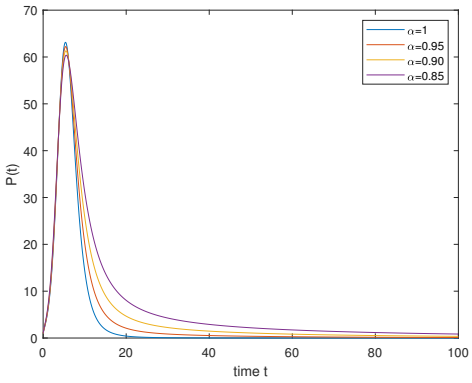
To illustrate the impact of model parameters on the basic reproduction number, $\mathscr{R}_0$, we plot $\mathscr{R}_0$ as a function of two key parameters. From Figure 3.9(a), it is clear that the values of $\mathscr{R}_0(\beta,\lambda)$ exceed 1 as we increase the values of β and λ. This suggests a proportional relationship between the function $\mathscr{R}_0(\beta,\lambda)$ and the parameters β and λ. Figure 3.9(b) shows that the $\mathscr{R}_0(\lambda,\mu_p)$ function is less than 1 as λ increases and μ_p decreases. Finally, in Figure 3.9(c), we have investigated the impact of the disease transmission rate β and the parasite dilution rate μ_p on the behavior of $\mathscr{R}_0$. We observe that $\mathscr{R}_0$ is greater than 1 when μ_p increases and β increases. This implies that β is a more influential parameter than μ_p.



(a) Dynamics of susceptible hosts.

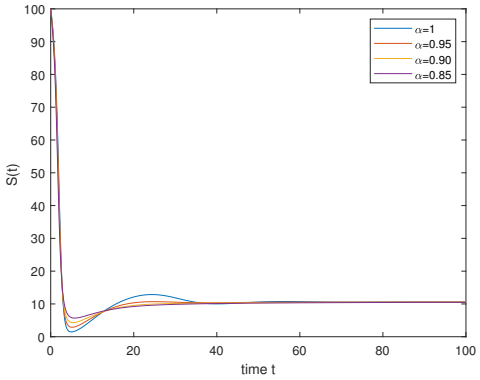


(b) Dynamics of infected hosts.

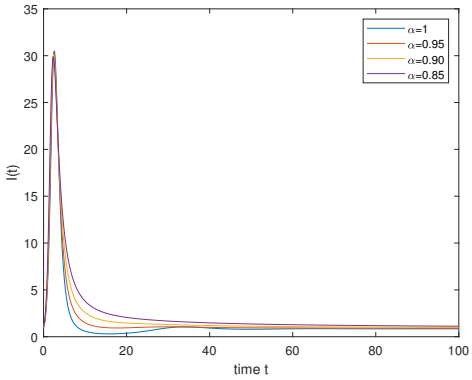


(c) Parasite population dynamics.

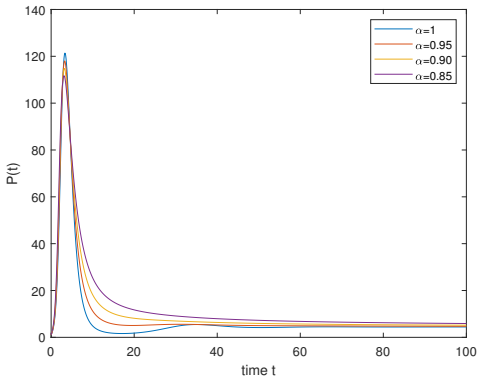
Figure 3.6: The illustration of the numerical solution of the SIP fractional model at different fractional order α, with $\mathscr{F}(P) = \beta P/(1+k_1 P)$ and $\mathscr{R}_0 = 0.9309 < 1$.



(a) Dynamics of susceptible hosts.

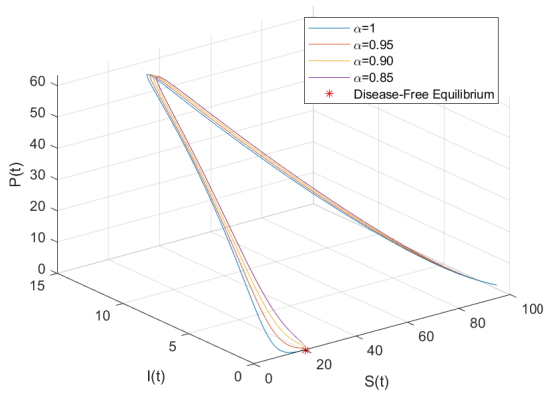


(b) Dynamics of infected hosts.

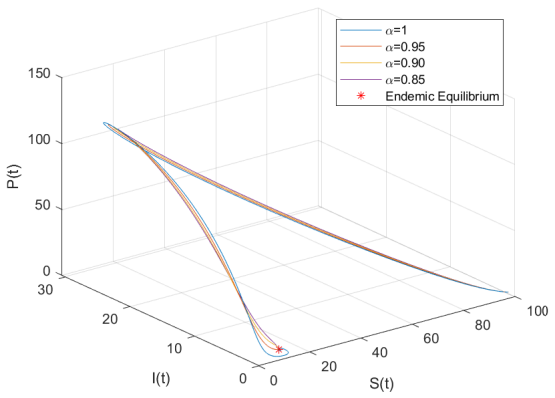


(c) Parasite population dynamics.

Figure 3.7: The illustration of the numerical solution of the SIP fractional model at different fractional orders α, with $\mathscr{F}(P) = \beta P/(1+k_1 P)$ and $\mathscr{R}_0 = 1.3861 > 1$

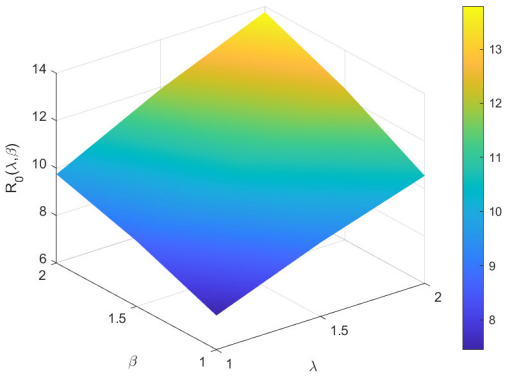


(a) Dynamics of solutions with $\mathscr{R}_0 < 1$.

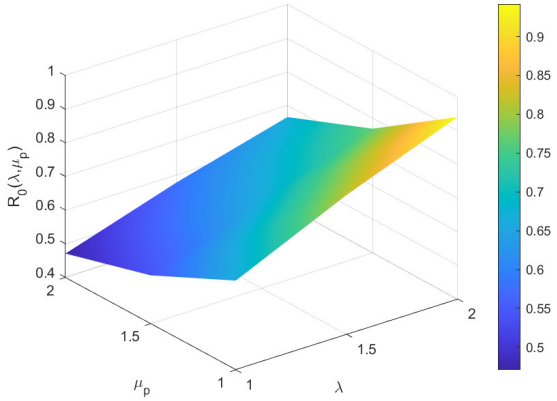


(b) Dynamics of solutions with $\mathscr{R}_0 > 1$.

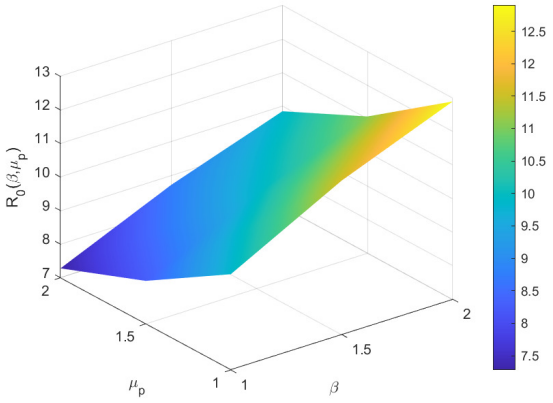
Figure 3.8: Variations in solution trajectories: three-dimensional model SIP with different α values and $\mathscr{F}(P) = \beta P/(1+k_1 P)$.



(a) $\mathscr{R}_0$ versus λ and β.



(b) $\mathscr{R}_0$ versus λ and μ_p.



(c) $\mathscr{R}_0$ versus β and μ_p.

Figure 3.9: Variation of $\mathscr{R}_0$ as a function of the most influential parameters.

3.5 Investigating the SIP model through the ABC derivative

In this section, we explore the dynamics of the model (3.1) using the ABC derivative, highlighting any differences and advancements over the Caputo derivative. The model is defined as follows: we replace the integer-order derivative with the fractional derivative in the sense of the ABC operator. The model we consider, under the ABC operator with fractional order $0 < \alpha < 1$, is as follows:

$$\begin{cases} {}^{ABC}D_t^{\alpha} S = B + b(S+I) - \mu S - \beta SP, \\ {}^{ABC}D_t^{\alpha} I = \beta SP - (\mu + \delta) I, \\ {}^{ABC}D_t^{\alpha} P = \lambda I - \mu_p P - \beta c (S+I) P, \end{cases} \tag{3.28}$$

under initial conditions

$$S(0) = S_0 \geq 0, \qquad I(0) = I_0 \geq 0, \qquad P(0) = P_0 \geq 0. \tag{3.29}$$

Next, we examine some basic properties of the ABC disease model for marine parasites, noting that the stability and equilibrium are similar to those of the model with the Caputo derivative.

3.5.1 Existence and uniqueness of solution

In this section, we establish the existence and uniqueness of the ABC fractional model (3.28) by employing the fixed-point method. Consider $C\left([0,T],\mathbb{R}^3\right)$ as a Banach space comprising continuous functions on $[0,T]$, equipped with the norm defined by

$$\|(S,I,P)\| = \|S\|_{\infty} + \|I\|_{\infty} + \|P\|_{\infty},$$

where $\|\cdot\|_{\infty}$ denotes the supremum norm over $\mathbb{R}$.

The fractional system (3.28)can be reformulated as:

$$\begin{cases} {}^{\mathrm{ABC}}D_t^{\alpha}(S(t)) = \mathscr{F}_1(t, S(t)), \\ {}^{\mathrm{ABC}}D_t^{\alpha}(I(t)) = \mathscr{F}_2(t, I(t)), \\ {}^{\mathrm{ABC}}D_t^{\alpha}(P(t)) = \mathscr{F}_3(t, P(t)). \end{cases} \tag{3.30}$$

Where

$$\begin{cases} \mathscr{F}_1(t,S(t)) = B + b(S+I) - \mu S - \beta SP, \\ \mathscr{F}_2(t,I(t)) = \beta SP - (\mu+\delta)I, \\ \mathscr{F}_3(t,P(t)) = \lambda I - \mu_p P - \beta c(S+I)P. \end{cases} \tag{3.31}$$

By applying the ABC fractional integral to each equation in the system (3.30), we obtain

$$\begin{aligned} S(t) - S(0) &= \frac{1-\alpha}{M(\alpha)} + \frac{\alpha}{M(\alpha)\Gamma(\alpha)} \int_0^t (t-z)^{\alpha-1} \mathscr{F}_1(z,S)dz, \\ I(t) - I(0) &= \frac{1-\alpha}{M(\alpha)} + \frac{\alpha}{M(\alpha)\Gamma(\alpha)} \int_0^t (t-z)^{\alpha-1} \mathscr{F}_2(z,I)dz, \\ P(t) - P(0) &= \frac{1-\alpha}{M(\alpha)} + \frac{\alpha}{M(\alpha)\Gamma(\alpha)} \int_0^t (t-z)^{\alpha-1} \mathscr{F}_3(z,P)dz. \end{aligned}$$

To establish the subsequent theorems, we will assume that $\|S(t)\| \le C_1, \|I(t)\| \le C_2$ and $\|P(t)\| \le C_3$, with $C_i (i = 1,\dots,3)$ representing positive constants. Denote

$$L_1 = (\mu - b) + \beta C_1, \quad L_2 = \mu + \delta, \qquad L_3 = c\,\beta\, C_2 + \mu_p. \tag{3.32}$$

Theorem 3.6. *Suppose the following condition is satisfied:*

$$0 < \max\{L_i\} < 1, \quad i \in \{1,\dots,3\} \tag{3.33}$$

then the kernels $\mathscr{F}_1$, $\mathscr{F}_2$, and $\mathscr{F}_3$ are contraction mappings.

Proof. Let S_1 and S_2 be two functions,

$$\begin{aligned} \|\mathscr{F}_1(t,S_1) - \mathscr{F}_1(t,S_2)\| &= \left\| \left(-\beta P + (\mu - b)\right)(S_1 - S_2) \right\|, \\ &= \left\| \left(\beta C_1 + (\mu - b)\right)(S_1 - S_2) \right\|, \\ &\le L_1 \|S_1 - S_2\|. \end{aligned}$$

We follow the same procedure for $\mathscr{F}_2$ and $\mathscr{F}_3$, we obtain

$$\begin{aligned} \|\mathscr{F}_2(t,I_1) - \mathscr{F}_2(t,I_2)\| &\le L_2 \|I_1 - I_2\|, \\ \|\mathscr{F}_3(t,P_1) - \mathscr{F}_3(t,P_2)\| &\le L_3 \|P_1 - P_2\|. \end{aligned}$$

Then, if the condition in (3.33) is satisfied, $\mathscr{F}_1$, $\mathscr{F}_2$, and $\mathscr{F}_3$ are contraction mappings. ■

Theorem 3.7. *Assume that the following condition is satisfied:*

$$0 < \Gamma = \left(\frac{1-\alpha}{M(\alpha)} + \frac{t^\alpha}{M(\alpha)\Gamma(\alpha)} \right) \max_{i=1,\dots,3} \{L_i\} < 1, \tag{3.34}$$

then the marine parasite model with fractional derivative ABC has a unique solution.

Proof. We consider

$$X(t)=\begin{pmatrix} S(t)\\ I(t)\\ P(t)\end{pmatrix}, X_0=\begin{pmatrix} S_0\\ I_0\\ P_0\end{pmatrix} \text{ and } \mathscr{F}(t,X(t))=\begin{pmatrix} \mathscr{F}_1(t,S)\\ \mathscr{F}_2(t,I)\\ \mathscr{F}_3(t,P)\end{pmatrix}.$$

We define $\mathbb{J}=[-T,T]$, $B=\prod_{i=1}^{3}\left[{X_0}^i-\epsilon,{X_0}^i+\epsilon\right]$.

Let $\mathscr{C}(\mathbb{J},B)$ be a metric space defined by the norm given as:

$$\|\Psi_1-\Psi_2\|_\infty=\sup_{t\in\mathbb{J}}|\Psi_1(t)-\Psi_2(t)| \tag{3.35}$$

We defined the following Picard operator:

$$f:\mathscr{C}(\mathbb{J},B)\to\mathscr{C}(\mathbb{J},B)$$

$$f(X(t))=X_0(t)+\frac{1-\alpha}{M(\alpha)}\mathscr{F}(t,X(t))+\frac{\alpha}{M(\alpha)\Gamma(\alpha)}\int_0^t(t-z)^{\alpha-1}\mathscr{F}(z,X(z))dz.$$

To complete the proof of this theorem, we will show that the operator f defined above is a contraction mapping. Let $(X_1,X_2)\in\mathscr{C}(\mathbb{J},B)$, we have:

$$\begin{aligned}\|f(X_1(t))-f(X_2(t))\|\leqslant&\frac{1-\alpha}{M(\alpha)}\|\mathscr{F}(t,X_1(t))-\mathscr{F}(t,X_2(t))\|\\&+\frac{\alpha}{M(\alpha)\Gamma(\alpha)}\int_0^t(t-z)^{\alpha-1}\|\mathscr{F}(z,X_1(z))-\mathscr{F}(z,X_2(z))\|dz,\end{aligned}$$

since the function $\mathscr{F}$ is a contraction mapping (according to Theorem 3.6), we find:

$$\|f(X_1(t))-f(X_2(t))\|\leqslant\Gamma\|X_1(t)-X_2(t)\|.$$

If the condition described in (3.34) is satisfied, then f is a contraction on $\mathscr{C}(\mathbb{J},B)$. Consequently, the Banach fixed-point Theorem guarantees the existence and uniqueness of a fixed point for the operator f. Therefore, the marine parasite model with ABC fractional derivative (3.28)has a unique solution. ■

3.5.2 Nonnegativity of the solutions

Consider the following set:

$$\Theta_1=\left\{(S,I,P)\in\mathbb{R}^3;S(t)\geq 0,I(t)\geq 0,P(t)\geq 0\right\}.$$

Theorem 3.8. *The solutions (S,I,P) of the model (3.28)are all positive for all $t\geq 0$ and belong to Θ_1.*

Proof. Now, we prove that the solutions are non-negative. We begin with the first equation of the system (3.28), which is as follows:

$$\begin{aligned} {}^{ABC}D_t^{\alpha} S(t) &= B + b(S+I) - \mu S - \beta SP, \\ &\geq -\left(\beta + \mu\right) S(t). \end{aligned}$$

Then,

$$ {}^{ABC}D_t^{\alpha} S(t) \geq -\left(\beta + \mu\right) S(t). \tag{3.36}$$

By applying the Laplace transform to the inequality (3.36), we obtain

$$\mathscr{L}\{S(t)\}(p) \geq \frac{M(\alpha)S(0)}{M(\alpha) + \left(\beta+\mu\right)(1-\alpha)} \cdot \frac{p^{\alpha-1}}{p^{\alpha} + \frac{(\beta+\mu)\alpha}{M(\alpha)+(\beta+\mu)(1-\alpha)}}. \tag{3.37}$$

Applying the inverse Laplace transform and using formula (1.22), we obtain

$$S(t) \geq \frac{M(\alpha)S(0)}{M(\alpha) + \left(\beta+\mu\right)(1-\alpha)} E_{\alpha,1}\left(-t^{\alpha} \frac{\left(\beta+\mu\right)\alpha}{M(\alpha) + \left(\beta+\mu\right)(1-\alpha)}\right). \tag{3.38}$$

As $S(0) \geq 0$ and $0 < E_{\alpha,1}\left(-t^{\alpha} \frac{(\beta+\mu)\alpha}{M(\alpha)+(\beta+\mu)(1-\alpha)}\right) \leq 1$, therefore $S(t) \geq 0$.

Likewise, we prove $S(t) \geq 0, I \geq 0$, and $P(t) \geq 0$, we conclude that the solution will remain in $\mathbb{R}^3_+$.

■

3.5.3 Biologically feasible region of the solution

Next, we establish that the solutions are bounded.

Theorem 3.9. *The biologically feasible domain for the ABC fractional model* (3.28)*is given by*

$$\Theta_2 := \Omega_2 = \left\{(S,I,P) \in \mathbb{R}^3_+ : N(t) \leq \max\left(\tfrac{B}{\mu-b}, N(0)\right), \text{and } P(t) \leq \lambda \max\left(\frac{B}{\mu-b}, N(0)\right)\right\},$$

where $N(t) = S(t) + I(t)$.

Proof. By summing the first two equations of the model (3.28), we find

$$ {}^{ABC}D_t^{\alpha} N(t) = B - (\mu - b)N(t) - \delta I. \tag{3.39}$$

When there are no parasites present in the marine population ($I = 0$), we have

$$ {}^{ABC}D_t^{\alpha} N(t) \leq B - (\mu - b)N(t) \tag{3.40}$$

Applying the Laplace transform to inequality (3.40), we obtain

$$\frac{M(\alpha)p^{\alpha}\mathscr{L}\{N(t)\}(p)}{\alpha+(1-\alpha)p^{\alpha}}+(\mu-b)\mathscr{L}\{N(t)\}(p)\leq B\,p^{\alpha-(\alpha+1)}+\frac{M(\alpha)N(0)p^{\alpha-1}}{\alpha+(1-\alpha)p^{\alpha}}. \tag{3.41}$$

Then

$$\mathscr{L}\{N(t)\}(p)\leq\frac{1}{M(\alpha)+(\mu-b)(1-\alpha)}.\frac{B(1-\alpha)p^{\alpha-1}+B\alpha\,p^{\alpha-(\alpha+1)}+N(0)M(\alpha)p^{\alpha-1}}{p^{\alpha}+\frac{\alpha(\mu-b)}{M(\alpha)+(\mu-b)(1-\alpha)}}.$$

From the Formula (1.22), we find

$$\begin{aligned}N(t)\leq{}&\frac{B\alpha t^{\alpha}}{(1-\alpha)(\mu-b)+M(\alpha)}E_{\alpha,\alpha+1}\left(-\xi t^{\alpha}\right)\\&+\left[\frac{B(1-\alpha)}{(1-\alpha)(\mu-b)+M(\alpha)}+\frac{M(\alpha)N(0)}{M(\alpha)+(1-\alpha)(\mu-b)}\right]E_{\alpha,1}\left(-\xi t^{\alpha}\right),\end{aligned}$$

where $\xi=\frac{(\mu-b)\alpha}{M(\alpha+(\mu-b)(1-\alpha))}$.
We obtain that $\lim_{t\to\infty}N\leq\frac{B}{\mu-b}$. This implies that $N(t),S(t)$ and $I(t)$ are bounded in Θ_2.
■

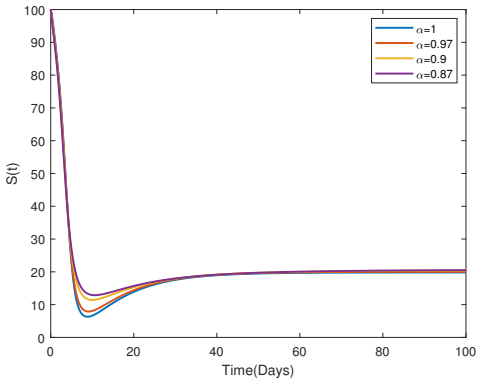
3.5.4 Numerical results and discussion

In this section, we present the numerical results using the Taoufik–Atangana scheme, as described in Chapter 1. The temporal evolution of model (3.28) is illustrated in Figures 3.10 to 3.11, using the initial conditions $S(0)=100$, $I(0)=1$, and $P(0)=1$. The parameter values for these simulations are provided in Table 3.1.

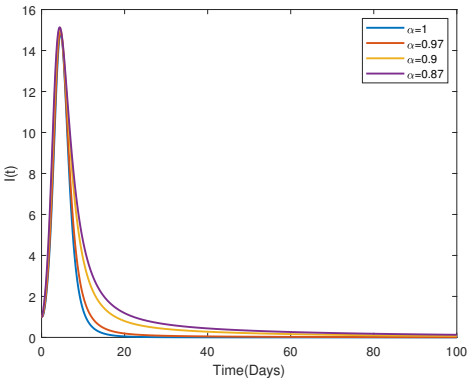
Figure 3.10 shows that the trajectories of $S(t)$, $I(t)$, and $P(t)$ converge to the disease-free equilibrium $\mathscr{E}_0=(20,0,0)$ for various fractional orders α ($\alpha=1,0.97,0.90,0.87$) when $\mathscr{R}_0=0.93087<1$, confirming the local stability of the disease-free equilibrium under the ABC fractional derivative.

As α approaches 1, the number of susceptible hosts decreases, while the infected hosts and parasites initially rise to a peak before declining. This behavior suggests that a lower α value leads to higher populations of both infected hosts and parasites. These results highlight the significant role of α in the system's dynamics, demonstrating the importance of considering different fractional orders when analyzing the behavior of the susceptible and infected populations.

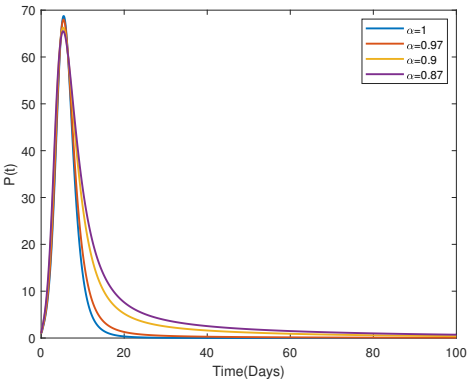
In Figure 3.11, the curves for the three compartments converge to the endemic equilibrium $\mathscr{E}_1=(10.496,0.87432,4.5814)$, confirming its local stability when $\mathscr{R}_0=1.3861>1$. Furthermore, it is observed that for $\alpha=1$ (representing the ordinary derivative), the system converges more rapidly than for $0<\alpha<1$ (under the ABC fractional derivative), illustrating the memory effect inherent to fractional derivatives.



(a) Behavior of susceptible hosts.

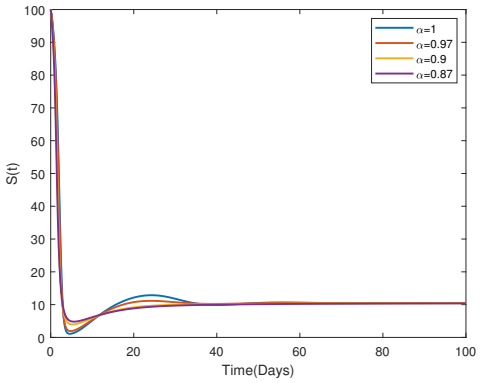


(b) Behavior of infected hosts.

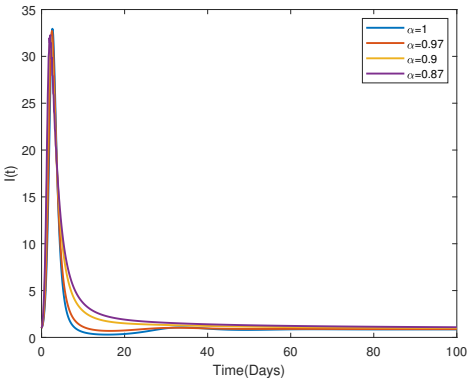


(c) Parasite population behavior.

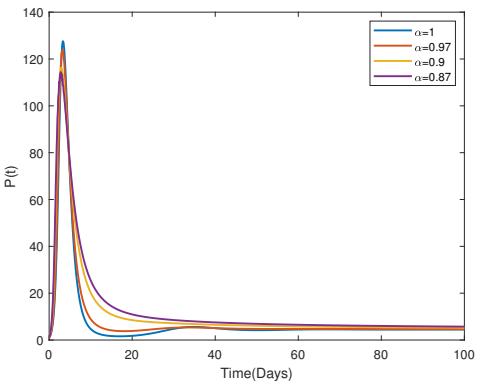
Figure 3.10: Numerical solution of the SIP fractional ABC model at different fractional orders α, with $\mathscr{R}_0 = 0.93087$.



(a) Dynamics of susceptible hosts.



(b) Dynamics of infected hosts.



(c) Parasite population dynamics.

Figure 3.11: Numerical solution of the SIP fractional ABC model at different fractional orders α, with $\mathscr{R}_0 = 1.3861$.

3.6 Conclusion

In this chapter, we investigated the dynamics of the SIP model, which examines a disease caused by marine parasites, using two fractional derivatives: Caputo and Atangana-Baleanu-Caputo (ABC). We analyzed key properties such as positivity, existence, and uniqueness of solutions under both derivatives. However, the local stability was examined only for the Caputo derivative, as the calculations are analogous to those of the ABC case. Similarly, the equilibrium points and sensitivity analysis were also carried out for the Caputo derivative.

For the numerical simulations, the Adams-Bashforth-Moulton method was applied to the Caputo derivative, while the Taoufik-Atangana scheme was used for the ABC derivative. The numerical results demonstrated that the curves for $S(t)$, $I(t)$, and $P(t)$ converge towards the equilibrium points for both $\mathscr{R}_0 > 1$ and $\mathscr{R}_0 < 1$, thereby validating our theoretical findings. Additionally, as observed in the figures, the convergence of fractional derivatives (both Caputo and ABC) is slower compared to the integer-order derivative ($\alpha = 1$), highlighting the memory effect inherent in fractional derivatives, which is absent in the classical case.

In conclusion, both the Caputo and ABC derivatives proved to be suitable tools for studying the dynamics of the SIP model.

CHAPTER 4

FRACTIONAL-ORDER ANALYSIS OF COVID-19 TRANSMISSION: A STUDY USING THE ATANGANA–BALEANU–CAPUTO DERIVATIVE AND OPTIMAL CONTROL

In December 2019, the city of Wuhan in China became the epicenter of an outbreak of COVID-19, a novel coronavirus caused by the SARS-CoV-2 virus, which is related to the SARS epidemic that emerged in 2002 [92]. This outbreak quickly escalated into a global pandemic, officially declared by the World Health Organization on March 11, 2020, severely disrupting the global economy. The pandemic had far-reaching effects, not only on economies worldwide but also on healthcare systems, particularly during the first wave of the disease. It also profoundly impacted health, education, social capital, social vulnerability, relationships, and freedom of movement [7, 27]. Despite the rollout of vaccines in late 2020 and the gradual return to normalcy, including the reopening of airspaces and economic recovery, concerns about the emergence of new variants persisted [85].

Despite the initial emergence of COVID-19 in late 2019, the pandemic's effects continue to resonate globally. New variants of the virus regularly emerge, posing challenges to existing public health measures and vaccination efforts. The persistent nature of the epidemic necessitates further investigation into its dynamics to inform effective control strategies. Numerous studies have utilized ordinary differential equations (ODEs) to research the transmission of this epidemic [9, 11, 84, 93]. However, understanding the

complexities of COVID-19 transmission through innovative mathematical models, such as fractional calculus approaches, provides valuable insights into disease behavior and management. By integrating fractional calculus into our analysis, we aim to provide a more comprehensive understanding of COVID-19 dynamics and contribute to effective control strategies. This study aims to contribute to the existing body of research by applying a fractional SEI^uI^dR model using the Atangana–Baleanu–Caputo derivative, offering a fresh perspective on COVID-19 dynamics that may aid public health responses and improve outcomes.

The structure of this chapter is as follows: Section 4.1 outlines the mathematical formulation of the COVID-19 model. In Section 4.2, we conduct a detailed mathematical analysis of the fractional model. Section 4.3 addresses the sensitivity analysis of the parameters of the model SEI^uI^dR and the formulation of the fractional control problem. Section 4.4 presents the numerical solution of the ABC fractional model for COVID-19 using the Taoufik–Atangana scheme and focuses on the analysis and interpretation of the numerical findings. Finally, the manuscript concludes in Section 4.5 with a summary of the main findings.

4.1 Model formulation

In this section, we present a fractional model utilizing an ABC fractional derivative to depict the transmission of COVID-19 in Morocco. This model is developed based on the research outlined in [39], where the population is divided into five compartments, respectively. Susceptible individuals are denoted by $S(t)$, who have not been infected with COVID-19 and are susceptible to contracting the virus if exposed to it. Exposed individuals are denoted by $E(t)$, who have been exposed to the virus but are not yet infectious. They are in the incubation period, during which they may develop symptoms and become infectious. Infected Detected Individuals are denoted by $I^d(t)$, who have tested positive for COVID-19 and are either isolated or hospitalized, depending on the severity of their symptoms. Infected Undetected Individuals are denoted by $I^u(t)$, who are infected with COVID-19 but have not been detected through testing. They may be asymptomatic or have mild symptoms and thus may not seek testing or medical care. Recovered individuals are denoted by $R(t)$, who have recovered from COVID-19 and are no longer infectious. They may have developed immunity to the virus, at least for a certain period.

The parameters within our model are outlined as follows: Λ signifies the recruitment

rate of the population, while β_u denotes the transmission rate within the community, and β_d represents the transmission rate within hospital settings or any location designated for isolating patients. The parameter $1/\sigma$ indicates the duration of the incubation period for COVID-19, applicable to both detected and undetected cases. τ corresponds to the proportion of individuals exposed to the virus who become infected and undetected. Similarly, the infectious periods for detected and undetected cases are represented by $1/\gamma_{\mathrm{d}}$ and $1/\gamma_{\mathrm{u}}$, respectively. Rates of mortality for detected and undetected cases are denoted by μ_d and μ_u, respectively. Some undetected cases may be confirmed through PCR tests and transition to the detected category at a rate δ. Finally, we indicate the natural mortality rate per d in all compartments.The transmission diagram for covid-19 is shown in Figure 4.1.

To formulate the SEI^dI^uR fractional model, we employ the Atangana-Baleanu-Caputo fractional operator ${}^{ABC}D$. The fractional SEI^dI^uR model is therefore defined as follows

$$
\left\{
\begin{array}{l}
{}^{ABC}D_t^{\alpha} S(t) = \Lambda - \frac{(\beta_{\mathrm{u}} I^{\mathrm{u}} + \beta_{\mathrm{d}} I^{\mathrm{d}})S}{N} - dS, \\
{}^{ABC}D_t^{\alpha} E(t) = \frac{(\beta_{\mathrm{u}} I^{\mathrm{u}} + \beta_{\mathrm{d}} I^{\mathrm{d}})S}{N} - (\sigma + d)E, \\
{}^{ABC}D_t^{\alpha} I^{\mathrm{u}}(t) = \tau\sigma E - \left(\mu_{\mathrm{u}} + \delta + \gamma_{\mathrm{u}} + d\right) I^{\mathrm{u}}, \\
{}^{ABC}D_t^{\alpha} I^{\mathrm{d}}(t) = (1-\tau)\sigma E + \delta I^{\mathrm{u}} - \left(\mu_{\mathrm{d}} + \gamma_{\mathrm{d}} + d\right) I^{\mathrm{d}}, \\
{}^{ABC}D_t^{\alpha} R(t) = \gamma_{\mathrm{u}} I^{\mathrm{u}} + \gamma_{\mathrm{d}} I^{\mathrm{d}} - dR.
\end{array}
\right. \tag{4.1}
$$

with $S(0) = S_0 \geq 0, E(0) = E_0 \geq 0, I^u(0) = I_0^u \geq 0, I^d(0) = I_0^d \geq 0, R(0) = R_0 \geq 0$ and $\alpha \in (0,1]$.

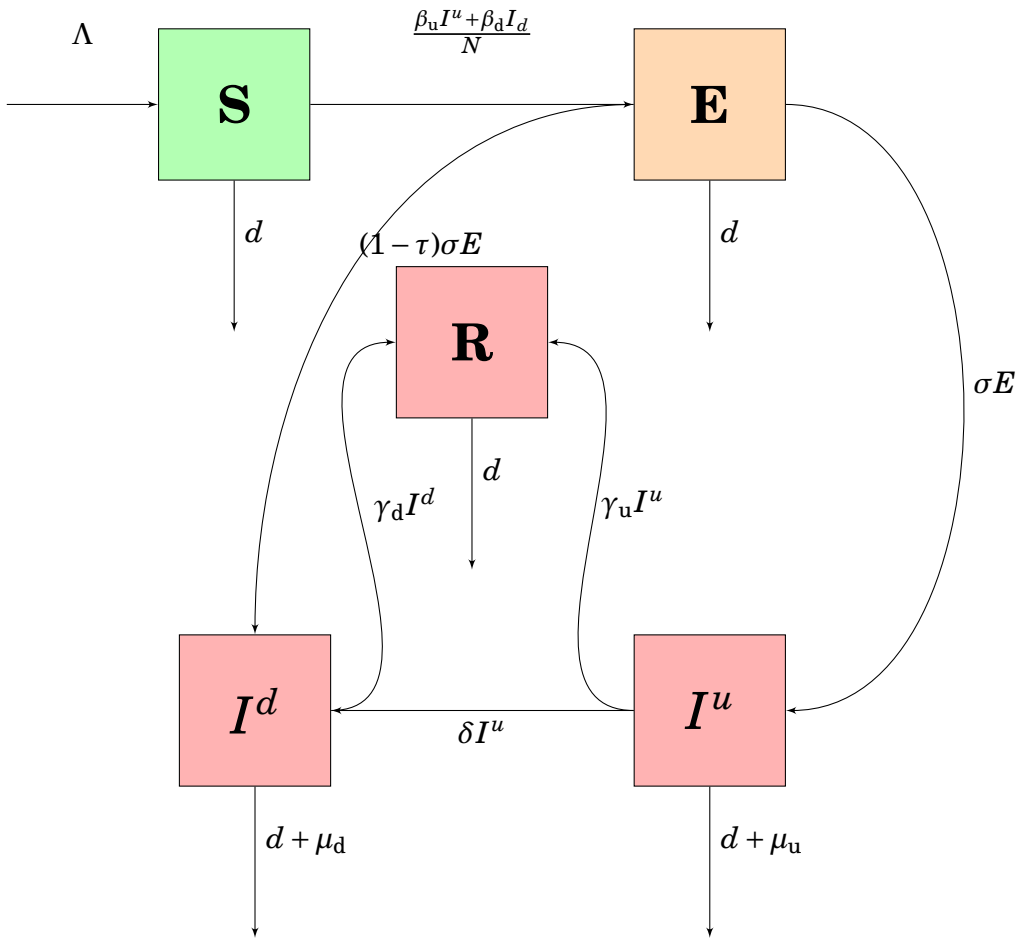


Figure 4.1: Diagram of the SEI^uI^dR model of COVID-19.

4.2 Mathematical analysis of the fractional model: existence, positivity, and stability

In this section, we prove the existence and uniqueness of the solution for the fractional model (4.1), as well as its boundedness and positivity. Additionally, we analyze the basic reproduction number, equilibrium points, and the stability of the system.

4.2.1 Existence and uniqueness of the solution

In this part we prove the existence and uniqueness of solutions of the fractional SEI^uI^dR model (4.1) by applying the fixed point theorem, along with the Picard-Lindelof method.

Let $C\left([0,T],\mathbb{R}^5\right)$ is the Banach space of continuous real valued functions with the norm denoted by $\|\,.\,\|$.

We pose

$$\begin{cases} \psi_1(t,S(t)) = & \Lambda - \frac{(\beta_{\mathrm{u}} I^{\mathrm{u}} + \beta_{\mathrm{d}} I^{\mathrm{d}})S}{N} - dS, \\ \psi_2(t,E(t)) = & \frac{(\beta_{\mathrm{u}} I^{\mathrm{u}} + \beta_{\mathrm{d}} I^{\mathrm{d}})S}{N} - (\sigma + d)E, \\ \psi_3(t,I^u(t)) = & \tau\sigma E - \left(\mu_{\mathrm{u}} + \delta + \gamma_{\mathrm{u}} + d\right) I^{\mathrm{u}}, \\ \psi_4(t,I^d(t)) = & (1-\tau)\sigma E + \delta I^{\mathrm{u}} - \left(\mu_{\mathrm{d}} + \gamma_{\mathrm{d}} + d\right) I^{\mathrm{d}}, \\ \psi_5(t,R(t)) = & \gamma_{\mathrm{u}} I^{\mathrm{u}} + \gamma_{\mathrm{d}} I^{\mathrm{d}} - dR. \end{cases} \tag{4.2}$$

So the system (4.1) becomes

$$\begin{cases} {}^{ABC}D_t^{\alpha} S(t) = \psi_1(t,S(t)); \;\; S(0) = S_0, \\ {}^{ABC}D_t^{\alpha} E(t) = \psi_2(t,E(t)); \;\; E(0) = E_0, \\ {}^{ABC}D_t^{\alpha} I^u(t) = \psi_3(t,I^u(t)); \;\; I^u(0) = I_0^u, \\ {}^{ABC}D_t^{\alpha} I^d(t) = \psi_4(t,I^u(t)); \;\; I^d(0) = I_0^d, \\ {}^{ABC}D_t^{\alpha} R(t) = \psi_5(t,R(t)); \;\; R(0) = R_0. \end{cases} \tag{4.3}$$

By applying the fractional integral described in (1.9) to both sides of (4.3), we obtain

$$\begin{aligned} S(t) - S(0) &= {}^{ABC}I_t^{\alpha}\psi_1(t,S(t)) = \frac{1-\alpha}{M(\alpha)}\psi_1(t,S(t)) + \frac{\alpha}{M(\alpha)\Gamma(\alpha)}\int_0^t (t-x)^{\alpha-1}\psi_1(x,S(x))\,dx, \\ E(t) - E(0) &= {}^{ABC}I_t^{\alpha}\psi_2(t,E(t)) = \frac{1-\alpha}{M(\alpha)}\psi_2(t,E(t)) + \frac{\alpha}{M(\alpha)\Gamma(\alpha)}\int_0^t (t-x)^{\alpha-1}\psi_2(x,E(x))\,dx, \\ I^u(t) - I^u(0) &= {}^{ABC}I_t^{\alpha}\psi_3(t,I^u(t)) = \frac{1-\alpha}{M(\alpha)}\psi_3(t,I^u(t)) + \frac{\alpha}{M(\alpha)\Gamma(\alpha)}\int_0^t (t-x)^{\alpha-1}\psi_3(x,I^u(x))\,dx, \\ I^d(t) - I^d(0) &= {}^{ABC}I_t^{\alpha}\psi_4(t,I^d(t)) = \frac{1-\alpha}{M(\alpha)}\psi_4(t,I^d(t)) + \frac{\alpha}{M(\alpha)\Gamma(\alpha)}\int_0^t (t-x)^{\alpha-1}\psi_4(x,I^d(x))\,dx, \\ R(t) - R(0) &= {}^{ABC}I_t^{\alpha}\psi_5(t,R(t)) = \frac{1-\alpha}{M(\alpha)}\psi_5(t,R(t)) + \frac{\alpha}{M(\alpha)\Gamma(\alpha)}\int_0^t (t-x)^{\alpha-1}\psi_5(x,R(x))\,dx. \end{aligned} \tag{4.4}$$

Denote

$$\begin{cases} k_1 = \left(\beta_{\mathrm{u}} + \beta_{\mathrm{d}} + d\right), \\ k_2 = \sigma + d, \\ k_3 = \mu_{\mathrm{u}} + \delta + \gamma_{\mathrm{u}} + d, \\ k_4 = \mu_{\mathrm{d}} + \gamma_{\mathrm{d}} + d, \\ k_5 = d. \end{cases} \tag{4.5}$$

Theorem 4.1. *If the following conditions are verified*

$$\begin{aligned} &0 \le k_1 < 1, \\ &0 \le k_2 < 1, \\ &0 \le k_3 < 1, \\ &0 \le k_4 < 1, \\ &0 \le k_5 < 1, \end{aligned} \tag{4.6}$$

then the kernels $\psi_1, \psi_2 \psi_3, \psi_4$ *and* ψ_5 *satisfy the Lipschitz condition and contractions mappings.*

Proof. Let S_1 and S_2 be two functions, then

$$\begin{aligned} \| \psi_1(t,S_1) - \psi_1(t,S_2) \| &= \| \left(\frac{\left(\beta_{\mathrm{u}} I^{\mathrm{u}} + \beta_{\mathrm{d}} I^{\mathrm{d}}\right)}{N} + d \right) (S_1(t) - S_2(t)) \| \\ &\le | \left(\beta_{\mathrm{u}} + \beta_{\mathrm{d}} + d\right) | \, \| S_1(t) - S_2(t) \| \\ &\le k_1 \, \| S_1(t) - S_2(t) \| \end{aligned}$$

where k_1 is defined in (4.5). Therefore, ψ_1 satisfy the Lipschitz condition for $0 \le k_1 < 1$, then it is a contraction mapping. Similarly, we can prove that $\psi_1, \psi_2, \psi_3, \psi_4, \psi_5$ are contraction mapping.

$$\begin{aligned} \| \psi_2(t,E_1) - \psi_2(t,E_2) \| &\le k_2 \, \| E_1 - E_2 \|, \\ \| \psi_3(t,I_{d1}) - \psi_2(t,{I^d}_2) \| &\le k_3 \, \| {I^d}_1 - {I^d}_2 \|, \\ \| \psi_4(t,{I^u}_1) - \psi_4(t,{I^u}_2) \| &\le k_4 \, \| {I^u}_1 - {I^u}_2 \|, \\ \| \psi_5(t,R_1) - \psi_5(t,R_2) \| &\le k_5 \, \| R_1 - R_2 \|, \end{aligned}$$

where k_2, k_3, k_4, k_5 are defined in (4.5).

We consider the recursive formula of equation (4.4)

$$\begin{aligned} S_n(t) &= \frac{1-\alpha}{M(\alpha)} \psi_1(t, S_{n-1}(t)) + \frac{\alpha}{M(\alpha)\Gamma(\alpha)} \int_0^t (t-x)^{\alpha-1} \psi_1(x, S_{n-1}(t)) dx, \\ E_n(t) &= \frac{1-\alpha}{M(\alpha)} \psi_2(t, E_{n-1}(t)) + \frac{\alpha}{M(\alpha)\Gamma(\alpha)} \int_0^t (t-x)^{\alpha-1} \psi_2(x, E_{n-1}(t)) dx \\ {I^u}_n(t) &= \frac{1-\alpha}{M(\alpha)} \psi_3(t, {I^u}_{n-1}(t) + \frac{\alpha}{M(\alpha)\Gamma(\alpha)} \int_0^t (t-x)^{\alpha-1} \psi_3(x, {I^u}_{n-1}(t) dx \\ {I^d}_n(t) &= \frac{1-\alpha}{M(\alpha)} \psi_4(t, {I^d}_{n-1}(t)) + \frac{\alpha}{M(\alpha)\Gamma(\alpha)} \int_0^t (t-x)^{\alpha-1} \psi_4(x, {I^d}_{n-1}(t)) dx \\ R_n(t) &= \frac{1-\alpha}{M(\alpha)} \psi_5(t, R_n(t)) + \frac{\alpha}{M(\alpha)\Gamma(\alpha)} \int_0^t (t-x)^{\alpha-1} \psi_5(x, R_{n-1}(t)) dx \end{aligned} \tag{4.7}$$

We make the difference between two consecutive terms we find the following expressions:

$$\begin{aligned}
\omega_1^n = S_n(t) - S_{n-1}(t) &= \frac{1-\alpha}{M(\alpha)}\left(\psi_1(t,S_n(t)) - \psi_1(t,S_{n-1}(t))\right) \\
&+ \frac{\alpha}{M(\alpha)\Gamma(\alpha)}\int_0^t (t-x)^{\alpha-1}[\psi_1(x,S_n(t)) - \psi_1(x,S_{n-1}(t))]dx \qquad (4.8)\\
\omega_2^n = E_n(t) - E_{n-1}(t) &= \frac{1-\alpha}{M(\alpha)}\left(\psi_2(t,E_n(t)) - \psi_2(t,E_n(t))\right) \\
&+ \frac{\alpha}{M(\alpha)\Gamma(\alpha)}\int_0^t (t-x)^{\alpha-1}[\psi_2(x,E_n(t)) - \psi_2(x,E_{n-1}(t))]dx \qquad (4.9)\\
\omega_3^n = {I^u}_n(t) - {I^u}_{n-1}(t) &= \frac{1-\alpha}{M(\alpha)}\left(\psi_3(t,{I^u}_n(t)) - \psi_3(t,{I^u}_{n-1}(t))\right) \\
&+ \frac{\alpha}{M(\alpha)\Gamma(\alpha)}\int_0^t (t-x)^{\alpha-1}[\psi_3(x,{I^u}_n(t)) - \psi_3(x,{I^u}_{n-1}(t))]dx \qquad (4.10)\\
\omega_4^n = {I^d}_n(t) - {I^d}_{n-1}(t) &= \frac{1-\alpha}{M(\alpha)}\left(\psi_4(t,{I^d}_n(t)) - \psi_4(t,{I^d}_{n-1}(t))\right) \\
&+ \frac{\alpha}{M(\alpha)\Gamma(\alpha)}\int_0^t (t-x)^{\alpha-1}[\psi_4(x,{I^d}_n(t)) - \psi_4(x,{I^d}_{n-1}(t))]dx \qquad (4.11)\\
\omega_5^n = R_n(t) - R_{n-1}(t) &= \frac{1-\alpha}{M(\alpha)}\left(\psi_5(t,R_n(t)) - \psi_5(t,R_{n-1}(t))\right) \\
&+ \frac{\alpha}{M(\alpha)\Gamma(\alpha)}\int_0^t (tx)^{\alpha-1}[\psi_5(x,R_n(t)) - \psi_5(x,R_{n-1}(t))]dx \qquad (4.12)
\end{aligned}$$

We can see that

$$\sum_{i=1}^{n}\omega_1^i = S_n(t) - S_0, \quad \sum_{i=1}^{n}\omega_2^i = E_n(t) - E_0, \quad \sum_{i=1}^{n}\omega_3^i = I_n^d(t) - I_0^d,$$
$$\sum_{i=1}^{n}\omega_4^i = I_n^u(t) - I_0^u, \quad \sum_{i=1}^{n}\omega_5^i = R_n(t) - R_0.$$

Apply the norm to equation (4.8) and using the triangular inequality, we obtain

$$\begin{aligned}
\| \omega_1^n \| &= \| S_n(t) - S_{n-1}(t) \| \\
&\leq \frac{1-\alpha}{M(\alpha)} \| \psi_1(t,S_n(t)) - \psi_1(t,S_{n-1}(t)) \| \\
&+ \frac{\alpha}{M(\alpha)\Gamma(\alpha)}\int_0^t (t-x)^{\alpha-1} \| \psi_1(x,S_n(t)) - \psi_1(x,S_{n-1}(t)) \| dx. \qquad (4.13)
\end{aligned}$$

Since ψ_1 satisfy the Lipschitz condition with corresponding constant k_1, we get

$$\| \omega_1^n \| \leq \frac{(1-\alpha)k_1}{M(\alpha)} \| S_n - S_{n-1} \| + \frac{\alpha k_1}{M(\alpha)\Gamma(\alpha)}\int_0^t (t-x)^{\alpha-1} \| S_n - S_{n-1} \| dx, \qquad (4.14)$$

implies that

$$\| \omega_1^n \| \leq \frac{(1-\alpha)k_1}{M(\alpha)} \| \omega_1^{n-1} \| + \frac{\alpha k_1}{M(\alpha)\Gamma(\alpha)}\int_0^t (t-x)^{\alpha-1} \| \omega_1^{n-1} \| dx, \qquad (4.15)$$

on the similar way, we have

$$\| \omega_2^n \| \leq \frac{(1-\alpha)k_2}{M(\alpha)} \| \omega_2^{n-1} \| + \frac{\alpha k_2}{M(\alpha)\Gamma(\alpha)} \int_0^t (t-x)^{\alpha-1} \| \omega_2^{n-1} \| dx \tag{4.16}$$

$$\| \omega_3^n \| \leq \frac{(1-\alpha)k_3}{M(\alpha)} \| \omega_3^{n-1} \| + \frac{\alpha k_3}{M(\alpha)\Gamma(\alpha)} \int_0^t (t-x)^{\alpha-1} \| \omega_3^{n-1} \| dx \tag{4.17}$$

$$\| \omega_4^n \| \leq \frac{(1-\alpha)k_4}{M(\alpha)} \| \omega_4^{n-1} \| + \frac{\alpha k_4}{M(\alpha)\Gamma(\alpha)} \int_0^t (t-x)^{\alpha-1} \| \omega_4^{n-1} \| dx \tag{4.18}$$

$$\| \omega_5^n \| \leq \frac{(1-\alpha)k_5}{M(\alpha)} \| \omega_5^{n-1} \| + \frac{\alpha k_5}{M(\alpha)\Gamma(\alpha)} \int_0^t (t-x)^{\alpha-1} \| \omega_5^{n-1} \| dx \tag{4.19}$$

■

Theorem 4.2. *If there exists a constant $\xi > 0$ such that*

$$\frac{(1-\alpha)k_i}{M(\alpha)} + \frac{k_i \xi^\alpha}{M(\alpha)\Gamma(\alpha)} < 1, \qquad \text{for } i = 1,...,5. \tag{4.20}$$

Then the system (4.1) admits a unique solution.

Proof. From equations (4.15) to (4.19), we find the following inequalities:

$$\| \omega_i^n \| \leq \| \omega_i^0 \| \left[\frac{(1-\alpha)k_i}{M(\alpha)} + \frac{k_i \tau^\alpha}{M(\alpha)\Gamma(\alpha)} \right]^n, \quad \text{for } i = 1,...,5. \tag{4.21}$$

Therefore the existence and continuity of system (4.1). To prove that the above functions are solutions of system (4.1), we assume that

$$S(t) - S(0) = S_n(t) - \upsilon_n^1, \tag{4.22}$$

$$E(t) - E(0) = E_n(t) - \upsilon_n^2, \tag{4.23}$$

$$I^u(t) - I^u(0) = I_n^u(t) - \upsilon_n^3, \tag{4.24}$$

$$I^d(t) - I^u(0) = I_n^d(t) - \upsilon_n^4, \tag{4.25}$$

$$R(t) - R(0) = R_n(t) - \upsilon_n^5. \tag{4.26}$$

Then, we have

$$\| \upsilon_n^1 \| = \| S_n(t) - (S(t) - S(0)) \|, \tag{4.27}$$

$$\| \upsilon_n^2 \| = \| E_n(t) - (E(t) - E(0)) \|, \tag{4.28}$$

$$\| \upsilon_n^3 \| = \| I_n^u(t) - (I^u(t) - I^u(0)) \|, \tag{4.29}$$

$$\| \upsilon_n^4 \| = \| I_n^d(t) - (I^d(t) - I^d(0)) \|, \tag{4.30}$$

$$\| \upsilon_n^5 \| = \| R_n(t) - (R(t) - R(0)) \|. \tag{4.31}$$

From equations (4.4) and (4.7), we have

$$\begin{aligned}\left\|v_n^1(t)\right\| &\leqslant \| \frac{1-\alpha}{M(\alpha)}\left(\psi_1(t,S(t))-\psi_1(t,S_{n-1}\right) \\ &+ \frac{\alpha}{M(\alpha)\Gamma(\alpha)}\int_0^t (t-y)^{\alpha-1}\left(\psi_1(t,S(t))-\psi_1(t,S_{n-1})\mathrm{d}y\right\|, \\ \left\|v_n^1(t)\right\| &\leqslant \frac{1-\alpha}{M(\alpha)}\left\|\psi_1(t,S(t))-\psi_1(t,S_{n-1}\right\| \\ &+ \frac{\alpha}{M(\alpha)\Gamma(\alpha)}\int_0^t (t-y)^{\alpha-1}\left\|\psi_1(t,S(t))-\psi_1(t,S_{n-1})\right\|\mathrm{d}y, \\ &\leqslant \frac{1-\alpha}{M(\alpha)}k_1\left\|S-S_{n-1}\right\| + \frac{t^\alpha}{M(\alpha)\Gamma(\alpha)}k_1\left\|S-S_{n-1}\right\|.\end{aligned} \tag{4.32}$$

By recursively repeating the process, we get

$$\left\|v_n^1\right\| \leqslant \left[\frac{1-\alpha}{M(\alpha)}+\frac{\xi^\alpha}{M(\alpha)\Gamma(\alpha)}\right]^{n+1} k_1^{n+1}N.$$

So, for $\xi > t$ we get

$$\left\|v_n^1\right\| \leqslant \left[\frac{1-\alpha}{M(\alpha)}+\frac{\xi^\alpha}{M(\alpha)\Gamma(\alpha)}\right]^{n+1} k_1^{n+1}N.$$

We take $n \to \infty$ in the previous inequality and find

$$\|v_n^1\| \to 0.$$

In the same way, we demonstrate that

$$\|v_n^2\| \to 0, \quad \|v_n^3\| \to 0, \quad \|v_n^4\| \to 0, \quad \|v_n^5\| \to 0.$$

Thus, the existence of solutions to the system (4.1) is demonstrated.

For the uniqueness of the solution, we assume that there exist two solutions $(S_1,E_1,I_1^u,I_1^d,R_1)$ and $(S_2,E_2,I_2^u,I_2^d,R_2)$ for the system (4.1). Then, we get

As ψ_1, ψ_2, and ψ_3 satisfy the Lipschitz condition, we have:

$$\begin{aligned}\|S_1-S_2\| &\leq \frac{k_1}{M(\alpha)\Gamma(\alpha)}\|S_1-S_2\|\int_0^t (t-x)^{\alpha-1}dx + \frac{(1-\alpha)k_1}{M(\alpha)}\|S_1-S_2\|, \\ \|E_1-E_2\| &\leq \frac{k_2}{M(\alpha)\Gamma(\alpha)}\|E_1-E_2\|\int_0^t (t-x)^{\alpha-1}dx + \frac{(1-\alpha)k_2}{M(\alpha)}\|E_1-E_2\|, \\ \|I_1^u-I_2^u\| &\leq \frac{k_3}{M(\alpha)\Gamma(\alpha)}\|I_1^u-I_2^u\|\int_0^t (t-x)^{\alpha-1}dx + \frac{(1-\alpha)k_3}{M(\alpha)}\|I_1^u-I_2^u\|, \\ \|I_1^d-I_2^d\| &\leq \frac{k_4}{M(\alpha)\Gamma(\alpha)}\|I_1^d-I_2^d\|\int_0^t (t-x)^{\alpha-1}dx + \frac{(1-\alpha)k_4}{M(\alpha)}\|I_1^d-I_2^d\|, \\ \|R_1-R_2\| &\leq \frac{k_5}{M(\alpha)\Gamma(\alpha)}\|R_1-R_2\|\int_0^t (t-x)^{\alpha-1}dx + \frac{(1-\alpha)k_5}{M(\alpha)}\|R_1-R_2\|.\end{aligned}$$

Then

$$\begin{aligned}
\|S_1 - S_2\| \left[1 - \left(\frac{k_1\xi^\alpha}{\alpha\Gamma(\alpha)M(\alpha)} + \frac{(1-\alpha)k_1}{\Gamma(\alpha)}\right)\right] &\leq 0,\\
\|E_1 - E_2\| \left[1 - \left(\frac{k_2\xi^\alpha}{\alpha\Gamma(\alpha)M(\alpha)} + \frac{(1-\alpha)k_2}{\Gamma(\alpha)}\right)\right] &\leq 0,\\
\|I_1^u - I_2^u\| \left[1 - \left(\frac{k_3\xi^\alpha}{\alpha\Gamma(\alpha)M(\alpha)} + \frac{(1-\alpha)k_3}{\Gamma(\alpha)}\right)\right] &\leq 0,\\
\|I_1^d - I_2^d\| \left[1 - \left(\frac{k_4\xi^\alpha}{\alpha\Gamma(\alpha)M(\alpha)} + \frac{(1-\alpha)k_4}{\Gamma(\alpha)}\right)\right] &\leq 0,\\
\|R_1 - R_2\| \left[1 - \left(\frac{k_5\xi^\alpha}{\alpha\Gamma(\alpha)M(\alpha)} + \frac{(1-\alpha)k_5}{\Gamma(\alpha)}\right)\right] &\leq 0.
\end{aligned}$$

Therefore,

$$S_1(t) = S_2(t), E_1(t) = E_2(t), I_1^u(t) = I_2^u(t), I_1^d(t) = I_2^d(t), R_1(t) = R_2(t) \text{for all } t \geqslant 0.$$

Hence the uniqueness of the solution. ■

4.2.2 Nonnegativity of solutions

Since the model describes a total population, it is necessary that all variables of the model (4.1) remain positive for all future times ($t \geq 0$)

Theorem 4.3. *The solutions* (S,E,I^u,I^d,R) *of the system* (4.1) *are all positive for all* $t \geq 0$*, meaning they belong to the set* Θ_1*, where*

$$\Theta_1 = \left\{(S,E,I^u,I^d,R) \in \mathbb{R}^5 : S(t) \geq 0, E(t) \geq 0, I^u(t) \geq 0, I^d(t) \geq 0, R(t) \geq 0\right\}.$$

Proof. Now, we prove that the solutions are non-negative. We begin with the first equation of the system (4.1), which is as follows:

$$\begin{aligned}
{}^{ABC}D_t^\alpha S(t) &= \Lambda - \frac{\left(\beta_u I^u(t) + \beta_d I^d(t)\right)S(t)}{N} - dS(t),\\
&\geq -\left(\beta_u + \beta_d + d\right)S(t).
\end{aligned}$$

Then,

$$^{ABC}D_t^\alpha S(t) \geq -\theta S(t), \tag{4.33}$$

whith $\theta = \beta_u + \beta_d + d$.

By applying the Laplace transform to the inequality (4.33), we obtain

$$\mathscr{L}\{S(t)\}(s) \geq \frac{M(\alpha)S(0)}{M(\alpha)+\theta(1-\alpha)} \cdot \frac{s^{\alpha-1}}{s^{\alpha}+\frac{\theta\alpha}{M(\alpha)+\theta(1-\alpha)}}. \tag{4.34}$$

Applying the inverse Laplace transform and using Formula (1.22), we obtain

$$S(t) \geq \frac{M(\alpha)S(0)}{M(\alpha)+\theta(1-\alpha)} E_{\alpha,1}\left(-t^{\alpha}\frac{\theta\alpha}{M(\alpha)+\theta(1-\alpha)}\right). \tag{4.35}$$

As $S(0) \geq 0$ and $0 < E_{\alpha,1}\left(-t^{\alpha}\frac{\theta\alpha}{M(\alpha)+\theta(1-\alpha)}\right) \leq 1$, therefore $S(t) \geq 0$.

Likewise, we prove $E(t) \geq 0, I^u(t) \geq 0, I^d(t) \geq 0$, and $R(t) \geq 0$, we conclude that the solution will remain in $\mathbb{R}^5_+$.

■

4.2.3 Biologically feasible region of the solution

Next, we establish that the solutions are bounded.

Theorem 4.4. *The biologically feasible domain of the fractional model (4.1) is given by*

$$\Theta_2 := \left\{\left(S,E,I^u,I^d,R\right) \in \mathbb{R}^5_+ : 0 \leq N(t) \leq \frac{\Lambda}{d}\right\},$$

where $N(t) = S(t)+E(t)+I^u(t)+I^d(t)+R(t)$.

Proof. By summing all the equations of the system (4.1), we obtain

$${}^{ABC}D^{\alpha}_t N(t) = \Lambda - dN(t) - \mu_u I^u - \mu_d I^d. \tag{4.36}$$

When there is no disease present in a population ($I^u = I^d = 0$), we have

$${}^{ABC}D^{\alpha}_t N(t) \leq \Lambda - dN(t) \tag{4.37}$$

Applying the Laplace transform to inequality (4.37), we obtain

$$\frac{M(\alpha)s^{\alpha}\mathscr{L}\{N(t)\}(s)}{\alpha+(1-\alpha)s^{\alpha}} + d\,\mathscr{L}\{N(t)\}(s) \leq \Lambda s^{\alpha-(\alpha+1)} + \frac{M(\alpha)N(0)s^{\alpha-1}}{\alpha+(1-\alpha)s^{\alpha}}. \tag{4.38}$$

Then

$$\mathscr{L}\{N(t)\}(s) \leq \frac{1}{M(\alpha)+d(1-\alpha)} \cdot \frac{\Lambda(1-\alpha)s^{\alpha-1}+\Lambda\alpha\, s^{\alpha-(\alpha+1)}+N(0)M(\alpha)s^{\alpha-1}}{s^{\alpha}+\frac{\alpha d}{M(\alpha)+d(1-\alpha)}}. \tag{4.39}$$

From the formula (1.22), we find

(4.40)
$$N(t) \leq \frac{\Lambda \alpha t^{\alpha}}{(1-\alpha)d + M(\alpha)} E_{\alpha,\alpha+1}\left(-\xi t^{\alpha}\right) + \left[\frac{\Lambda(1-\alpha)}{(1-\alpha)d + M(\alpha)} + \frac{M(\alpha)N(0)}{M(\alpha)+(1-\alpha)d}\right] E_{\alpha,1}\left(-\xi t^{\alpha}\right),$$

where $\xi = \frac{d\alpha}{M(\alpha+d(1-\alpha))}$.
We obtain that $\lim_{t\to\infty} N \leq \frac{\Lambda}{d}$. This implies that $N(t), S(t), E(t), I^u(t), I^d(t)$ and $R(t)$ are bounded in Θ_2. ■

4.2.4 Basic reproduction number

The basic reproduction number, $\mathscr{R}_0$, is obtained using the next-generation method [87], which involves calculating the transmission matrix of newly infected cases, denoted as T, and the transition matrix of infections, denoted as Σ, pertaining to the model (4.1). The basic reproduction number, $\mathscr{R}_0$, is then given by $\mathscr{R}_0 = \rho\left(-T\Sigma^{-1}\right)$, where ρ represents the spectral radius. The matrices T and Σ are defined as:

$$T = \begin{pmatrix} 0 & \beta_{\mathrm{d}} & \beta_{\mathrm{d}} \\ 0 & 0 & 0 \\ 0 & 0 & 0 \end{pmatrix}, \quad \Sigma = \begin{pmatrix} -(\sigma+d) & 0 & 0 \\ \tau\sigma & -(\mu_{\mathrm{u}}+\delta+\gamma_{\mathrm{u}}+d) & 0 \\ (1-\tau)\sigma & \delta & -(\mu_{\mathrm{d}}+\gamma_{\mathrm{d}}+d) \end{pmatrix}$$

Therefore, the basic reproduction number for our model is

$$\mathscr{R}_0 = \frac{\beta_{\mathrm{u}}\tau\sigma}{(\sigma+d)(\mu_{\mathrm{u}}+\delta+\gamma_{\mathrm{u}}+d)} + \frac{\beta_{\mathrm{d}}(1-\tau)\sigma}{(\sigma+d)(\mu_{\mathrm{d}}+\gamma_{\mathrm{d}}+d)} + \frac{\beta_{\mathrm{d}}\tau\sigma\delta}{(\sigma+d)(\mu_{\mathrm{u}}+\delta+\gamma_{\mathrm{u}}+d)(\mu_{\mathrm{d}}+\gamma_{\mathrm{d}}+d)}.$$

4.2.5 The Equilibrium points

To find the equilibrium points of the model (4.1), we must solve the following equations

(4.41)
$$\begin{cases} \Lambda - \frac{(\beta_{\mathrm{u}}I^{\mathrm{u}}+\beta_{\mathrm{d}}I^{\mathrm{d}})S}{N} - dS = 0, \\ \frac{(\beta_{\mathrm{u}}I^{\mathrm{u}}+\beta_{\mathrm{d}}I^{\mathrm{d}})S}{N} - (\sigma+d)E = 0, \\ \tau\sigma E - \left(\mu_{\mathrm{u}}+\delta+\gamma_{\mathrm{u}}+d\right)I^{\mathrm{u}} = 0, \\ (1-\tau)\sigma E + \delta I^{\mathrm{u}} - \left(\mu_{\mathrm{d}}+\gamma_{\mathrm{d}}+d\right)I^{\mathrm{d}} = 0, \\ \gamma_{\mathrm{u}}I^{\mathrm{u}} + \gamma_{\mathrm{d}}I^{\mathrm{d}} - dR = 0. \end{cases}$$

First, we determine the disease-free equilibrium $\mathscr{E}_0$, which represents a state in which the entire population is free of infection. The model (4.1) has a disease-free equilibrium

given as follows

$$\mathscr{E}_0 = \left(S_0, E_0, I^u{}_0, I^d{}_0, R_0\right) = \left(\frac{\Lambda}{d}, 0, 0, 0, 0\right). \tag{4.42}$$

Let's now determine the endemic equilibrium expression for our model (4.1), which describes the state in which COVID-19 is prevalent among community members($\mathscr{R}_0 > 1$). Moreover, the model (4.1) has a unique endemic equilibrium, defined as follows

$$\mathscr{E}_1 = \left(S^*, E^*, I^{u*}, I^{d*}, R^*\right), \tag{4.43}$$

with

$$\begin{aligned}
S^* &= \frac{\Lambda - (\sigma + d)E^*}{d} > 0,\\
E^* &= \frac{\Lambda(\mathscr{R}_0 - 1)}{(\sigma + d)(\mathscr{R}_0 - 1) + d\left(1 + \frac{\tau\sigma}{\mu_u + \delta + \gamma_u + d}\left(1 + \frac{\gamma_u}{d}\right) + \frac{(1-\tau)\sigma(\mu_u + \delta + \gamma_u + d) + \tau\sigma d}{\mu_d + \gamma_d + d}\left(1 + \frac{\gamma_d}{d}\right)\right)} > 0,\\
I^{u*} &= \frac{\tau\sigma}{\mu_u + \delta + \gamma_u + d}E^* > 0,\\
I^{d*} &= \frac{\sigma(1-\tau)(\mu_u + \delta + \gamma_u + d) + \tau\sigma\delta}{(\mu_u + \delta + \gamma_u + d)(\mu_d + \gamma_d + d)}E^* > 0,\\
R^* &= \frac{\gamma_d I^{d*} + \gamma_u I^{u*}}{d} > 0.
\end{aligned}$$

Based on our analysis, we can state the following results:

Theorem 4.5.

- *If $\mathscr{R}_0 < 1$, there exists a unique disease-free equilibrium, denoted by $\mathscr{E}_0$.*
- *If $\mathscr{R}_0 > 1$, there exists a unique endemic equilibrium point, denoted by $\mathscr{E}_1$.*

4.2.6 Stability analysis

Theorem 4.6. *The coronavirus-free equilibrium $\mathscr{E}_0$ of model (4.1) is locally asymptotically stable if $\mathscr{R}_0 \leq 1$. When $\mathscr{R}_0 > 1$, $\mathscr{E}_0$ is unstable.*

Proof. The Jacobian matrix of system (4.1) at $\mathscr{E}_0$ is

$$\mathscr{J}(\mathscr{E}_0) = \begin{pmatrix}
-d & 0 & -\beta_u & -\beta_d & 0\\
0 & -(\sigma + d) & \beta_u & \beta_d & 0\\
0 & \tau\sigma & -(\mu_u + \delta + \gamma_u + d) & 0 & 0\\
0 & (1-\tau)\sigma & \delta & -(\mu_d + \gamma_d + d) & 0\\
0 & 0 & \gamma_u & \gamma_d & -d
\end{pmatrix}$$

The eigenvalues of $\mathscr{J}(\mathscr{E}_0)$ are the scalars λ satisfying :

$$\det\left(\mathscr{J}(\mathscr{E}_0)-\lambda I_5\right)=0 \Leftrightarrow \quad (\lambda+d)^2(\lambda^3+a_1\lambda^2+a_2\lambda+a_3)=0,$$

where

$$\begin{aligned}
a_1 &= \mu_{\mathrm{u}}+\delta+\gamma_{\mathrm{u}}+d+\sigma+d+\mu_{\mathrm{d}}+\gamma_{\mathrm{d}}+d>0,\\
a_2 &= (\sigma+d)(\mu_{\mathrm{d}}+\gamma_{\mathrm{d}}+d)+(\sigma+d)(\mu_{\mathrm{u}}+\delta+\gamma_{\mathrm{u}}+d)+(\mu_{\mathrm{d}}+\gamma_{\mathrm{d}}+d)(\mu_{\mathrm{u}}+\delta+\gamma_{\mathrm{u}}+d)\\
&\quad -\beta_{\mathrm{u}}\tau\sigma-\beta_{\mathrm{d}}(1-\tau)\sigma,\\
a_3 &= (\sigma+d)(\mu_{\mathrm{u}}+\delta+\gamma_{\mathrm{u}}+d)(\mu_{\mathrm{d}}+\gamma_{\mathrm{d}}+d)-\beta_{\mathrm{u}}\tau\sigma(\mu_{\mathrm{d}}+\gamma_{\mathrm{d}}+d)-\beta_{\mathrm{d}}\tau\sigma\delta\\
&\quad -\beta_{\mathrm{d}}(1-\tau)\sigma(\mu_{\mathrm{u}}+\delta+\gamma_{\mathrm{u}}+d).
\end{aligned}$$

It is evident that a_1 is positive. Additionally, if $\mathscr{R}_0\leq 1$, then a_2, a_3 and $a_1a_2-a_3$ are also positive. According to the Routh-Hurwitz stability criterion [90], all eigenvalues have negative real parts, which verifies the stability condition of fractional models in the ABC sense, expressed as

$$|\arg(\lambda_i)|=\pi>\frac{\pi}{2}>\frac{\rho\pi}{2},\quad i=1,2,3,4. \tag{4.44}$$

We define Δ as follows

$$\Delta=a_1^2a_2^2+18a_1a_2a_3-4a_2^3-4a_1^3a_3-27a_3^2.$$

To complete the proof, we require the following lemma

Lemma 4.1. *[5] Assume that $\mathscr{R}_0\leq 1$ and one of the following conditions is satisfied:*

1. $\Delta>0$, $a_1>0$, $a_2>0$, *and* $a_1a_2-a_3>0$.
2. $\Delta<0$, $a_1\geq 0$, $a_2\geq 0$, $a_3>0$, *and* $\alpha\in\left(0,\frac{2}{3}\right]$.

Then, the coronavirus-free equilibrium $\mathscr{E}_0$ of the fractional model (4.1) with ABC derivative is locally asymptotically stable. ■

Theorem 4.7. *The endemic equilibrium $\mathscr{E}_1$ of model fractional (4.1) is locally asymptotically stable if $\mathscr{R}_0>1$.*

Proof. The Jacobian matrix of the model (4.1) at $\mathscr{E}_1$ is determined as follows

$$\mathscr{J}(\mathscr{E}_1)=\begin{pmatrix}
C_1 & C_2 & C_3 & C_4 & C_5\\
C_6 & C_7 & C_8 & C_9 & C_{10}\\
0 & \tau\sigma & -(\mu_{\mathrm{u}}+\delta+\gamma+d) & 0 & 0\\
0 & (1-\tau)\sigma & \delta & -(\mu_{\mathrm{d}}+\gamma_{\mathrm{d}}+d) & 0\\
0 & 0 & \gamma_{\mathrm{u}} & \gamma_{\mathrm{d}} & -d
\end{pmatrix}$$

Where

$$
\begin{aligned}
C_1 &= -d - \frac{\beta_{\mathrm{u}} I^{u*}}{N^*}\left(1-\frac{S^*}{N^*}\right) - \frac{\beta_{\mathrm{d}} I^{d*}}{N^*}\left(1-\frac{S^*}{N^*}\right),\\
C_2 &= \frac{\beta_{\mathrm{u}} I^{u*} + \beta_{\mathrm{d}} I^{d*}}{(N^*)^2} S^*,\\
C_3 &= \frac{\beta_{\mathrm{u}} I^{u*} + \beta_{\mathrm{d}} I^{d*}}{(N^*)^2} S^* - \frac{\beta_{\mathrm{u}} S^*}{N^*},\\
C_4 &= \frac{\beta_{\mathrm{u}} I^{u*} + \beta_{\mathrm{d}} I^{d*}}{(N^*)^2} S^* - \frac{\beta_{\mathrm{d}} S^*}{N^*},\\
C_5 &= \frac{\beta_{\mathrm{u}} I^{u*} + \beta_{\mathrm{d}} I^{d*}}{(N^*)^2} S^*,\\
C_6 &= \frac{\beta_{\mathrm{u}} I^{u*}}{N^*}\left(1-\frac{S^*}{N^*}\right) + \frac{\beta_{\mathrm{d}} I^{d*}}{N^*}\left(1-\frac{S^*}{N^*}\right),\\
C_7 &= -\frac{\beta_{\mathrm{u}} I^{u*} + \beta_{\mathrm{d}} I^{d*}}{(N^*)^2} S^* - (\sigma + d),\\
C_8 &= -\frac{\beta_{\mathrm{u}} I^{u*} + \beta_{\mathrm{d}} I^{d*}}{(N^*)^2} S^* + \frac{\beta_{\mathrm{u}} S^*}{N^*},\\
C_9 &= -\frac{\beta_{\mathrm{u}} I^{u*} + \beta_{\mathrm{d}} I^{d*}}{(N^*)^2} S^* + \frac{\beta_{\mathrm{d}} S^*}{N^*},\\
C_{10} &= -\frac{\beta_{\mathrm{u}} I^{u*} + \beta_{\mathrm{d}} I^{d*}}{(N^*)^2} S^*.
\end{aligned}
$$

Then, the characteristic equation of $\mathscr{J}(\mathscr{E}_1)$ is given by:

$$\lambda^5 + b_1\lambda^4 + b_2\lambda^3 + b_3\lambda^2 + b_4\lambda + b_5 = 0,$$

where

$$
\begin{aligned}
b_1 &= \mu_u + \delta + \gamma_u + d + \mu_d + \gamma_d + d - C_7 + C_2 + d,\\
b_2 &= d(\mu_u + \delta + \gamma_u + d + \mu_d + \gamma_d + d - C_7 + C_2 + d) + (\mu_d + \gamma_d + d - C_7)(\mu_u + \delta + \gamma_u + d - C_1)\\
&\quad + C_2(\mu_d + \gamma_d + d) - C_7(\mu_d + \gamma_d + d) - C_1(\mu_u + \delta + \gamma_u + d)\\
&\quad + \tau\sigma(C_3 - C_8) + (\mu_d + \gamma_d + d - C_2)C_2,\\
b_3 &= d(\mu_d + \gamma_d + d - C_7)(\mu_u + \delta + \gamma_u + d - C_1) + d\,C_2(\mu_d + \gamma_d + d) - d\,C_7(\mu_d + \gamma_d + d)\\
&\quad - d\,C_1(\mu_u + \delta + \gamma_u + d) + d\,\tau\sigma(C_3 - C_8) + d(\mu_d + \gamma_d + d - C_2)C_2\\
&\quad - C_{10}\tau\sigma\gamma_u - (1-\tau)\sigma\delta\gamma_d C_{10} + \gamma_u\tau\sigma C_5 + (1-\tau)\sigma\gamma_d C_5\\
&\quad - (\mu_d + \gamma_d + d)(\mu_u + \delta + \gamma_u + d - C_1)C_7 - (\mu_u + \delta + \gamma_u + d)(\mu_d + \gamma_d + d - C_7)C_1\\
&\quad - (\mu_d + \gamma_d + d - C_1)\tau\sigma C_8 + (\mu_d + \gamma_d + d - C_2)((\mu_d + \gamma_d + d)C_2 + \tau\sigma C_3)\\
&\quad - (\mu_d + \gamma_d + d)C_2^2,\\
b_4 &= -d(\mu_d + \gamma_d + d)(\mu_u + \delta + \gamma_u + d - C_1)C_7 - d(\mu_u + \delta + \gamma_u + d)(\mu_d + \gamma_d + d - C_7)C_1\\
&\quad - d(\mu_d + \gamma_d + d - C_1)\tau\sigma C_8 + d(\mu_d + \gamma_d + d - C_2)((\mu_d + \gamma_d + d)C_2 + \tau\sigma C_3)\\
&\quad - d(\mu_d + \gamma_d + d)C_2^2\\
&\quad - C_{10}\tau\sigma\gamma_u(\mu_d + \gamma_d + d - C_1) - C_{10}\tau\sigma\delta\gamma_d - (1-\tau)\sigma\gamma_d C_{10}(\mu_u + \delta + \gamma_u + d - C_1)\\
&\quad + C_1\delta\gamma_d\tau\sigma + \gamma_u\tau\sigma C_5(\mu_d + \gamma_d + d - C_6) + (1-\tau)\sigma\gamma_d C_5(\mu_u + \delta + \gamma_u + d - C_6)\\
&\quad - C_2(\mu_d + \gamma_d + d)((\mu_d + \gamma_d + d)C_2 + C_3\tau\sigma) + C_1C_7(\mu_u + \gamma_u + d)(\mu_d + \gamma_d + d)\\
&\quad + (\mu_d + \gamma_d + d)C_1C_8\tau\sigma,\\
b_5 &= -d\,C_2(\mu_d + \gamma_d + d)((\mu_d + \gamma_d + d)C_2 + C_3\tau\sigma) + dC_1C_7(\mu_u + \gamma_u + d)(\mu_d + \gamma_d + d)\\
&\quad + d(\mu_d + \gamma_d + d)C_1C_8\tau\sigma + C_1C_{10}\tau\sigma\delta\gamma_d + C_1C_{10}\tau\sigma\gamma_u(\mu_d + \gamma_d + d)\\
&\quad + C_1(1-\tau)\sigma\gamma_d C_{10}(\mu_d + \gamma_d + d) - C_6\delta\gamma_d\tau\sigma C_5 - C_6C_5\gamma_u\tau\sigma(\mu_d + \gamma_d + d)\\
&\quad - (1-\tau)\sigma\gamma_d\,C_5\,C_6(\mu_u + \delta + \gamma_u + d).
\end{aligned}
$$

It is evident that $b_1 > 0$, and if $b_i > 0$ for all $i = 2,\ldots,5$, and if the following conditions are verified:

$$
\Delta_1 = \begin{vmatrix} b_1 & 1 \\ b_3 & b_2 \end{vmatrix} > 0, \quad \Delta_2 = \begin{vmatrix} b_1 & 1 & 0 \\ b_3 & b_2 & b_1 \\ b_5 & b_4 & b_3 \end{vmatrix} > 0, \quad \Delta_3 = \begin{vmatrix} b_1 & 1 & 0 & 0 \\ b_3 & b_2 & b_1 & 1 \\ b_5 & b_4 & b_3 & b_2 \\ 0 & 0 & b_5 & b_4 \end{vmatrix} > 0,
$$

Then the endemic equilibrium $\mathscr{E}_1$ of the fractional model (4.1) is locally asymptotically stable.

■

4.3 Fractional control and sensitivity analysis of the SEI^uI^dR epidemic model

This section is divided into two subsections. The first focuses on "Sensitivity analysis", where we examine the responsiveness of model parameters and their impact on system behavior. The second subsection introduces "Fractional control optimization", where the fractional calculus approach is applied to optimize the control of the proposed model, providing a more flexible framework for dynamics and stability improvements.

4.3.1 Sensitivity analysis of $\mathscr{R}_0$

The sensitivity indices of $\mathscr{R}_0$ with respect to the parameters of the model in (4.1) are as follows:

$$\zeta_{\beta_u}^{\mathscr{R}_0} := \frac{\partial \mathscr{R}_0}{\partial \beta_u} \times \frac{\beta_u}{\mathscr{R}_0} = \frac{\tau\sigma\beta_u}{(\sigma+d)(\mu_u+\delta+\gamma_u+d)\mathscr{R}_0},$$

$$\zeta_{\beta_d}^{\mathscr{R}_0} := \frac{\partial \mathscr{R}_0}{\partial \beta_d} \times \frac{\beta_d}{\mathscr{R}_0} = \left[(1-\tau)+\frac{\tau\delta}{\mu_u+\delta+\gamma_u+d}\right] \times \frac{\beta_d\sigma}{\mathscr{R}_0(\sigma+d)(\mu_d+\gamma_d+d)},$$

$$\begin{aligned}\zeta_{\tau}^{\mathscr{R}_0} := \frac{\partial \mathscr{R}_0}{\partial \tau} \times \frac{\tau}{\mathscr{R}_0} &= -\frac{\beta_d\sigma\tau}{(\sigma+d)(\mu_d+\gamma_d+d)\mathscr{R}_0}\left[\frac{\delta}{\mu_u+\delta+\gamma_u+d}-1\right] \\ &\quad + \frac{\tau\sigma\beta_u}{\mathscr{R}_0(\mu_u+\delta+\gamma_u+d)(\sigma+d)},\end{aligned}$$

$$\zeta_{\sigma}^{\mathscr{R}_0} := \frac{\partial \mathscr{R}_0}{\partial \sigma} \times \frac{\sigma}{\mathscr{R}_0} = \frac{d}{\sigma+d},$$

$$\zeta_{d}^{\mathscr{R}_0} := \frac{\partial \mathscr{R}_0}{\partial d} \times \frac{d}{\mathscr{R}_0} = -\frac{d}{\sigma+d} - \frac{d\cdot\sigma\cdot\beta_d\cdot\left(1-\tau+\frac{\tau\cdot\delta}{\mu_u+\delta+\gamma_u+d}\right)}{R_0\cdot(\sigma+d)\cdot(\mu_d+\gamma_d+d)^2} - \frac{d\cdot\sigma\cdot\tau\cdot\left(\beta_u+\frac{\beta_d\cdot\delta}{\mu_d+\gamma_d+d}\right)}{R_0\cdot(\sigma+d)\cdot(\mu_u+\delta+\gamma_u+d)^2},$$

$$\begin{aligned}\zeta_{\delta}^{\mathscr{R}_0} := \frac{\partial \mathscr{R}_0}{\partial \delta} \times \frac{\delta}{\mathscr{R}_0} &= \frac{\delta\tau\sigma}{\mathscr{R}_0(\sigma+d)(\mu_u+\delta+\gamma_u+d)} \\ &\quad \times \left[\frac{\beta_d}{\mu_d+\gamma_d+d} - \frac{\beta_u}{\mu_u+\delta+\gamma_u+d} - \frac{\beta_d\delta}{(\mu_u+\delta+\gamma_u+d)(\mu_d+\gamma_d+d)}\right],\end{aligned}$$

$$\zeta_{\mu_u}^{\mathscr{R}_0} := \frac{\partial \mathscr{R}_0}{\partial \mu_u} \times \frac{\mu_u}{\mathscr{R}_0} = -\frac{\mu_u\tau\sigma}{(\sigma+d)(\mu_u+\delta+\gamma_u+d)\mathscr{R}_0} \times \left[\beta_u+\frac{\beta_d\delta}{\mu_d+\gamma_d+d}\right],$$

$$\zeta_{\mu_d}^{\mathscr{R}_0} := \frac{\partial \mathscr{R}_0}{\partial \mu_d} \times \frac{\mu_d}{\mathscr{R}_0} = -\frac{\mu_d\sigma\beta_d}{(\sigma+d)(\mu_d+\gamma_d+d)\mathscr{R}_0} \times \left[(1-\tau)+\frac{\tau\delta}{\mu_u+\delta+\gamma_u+d}\right],$$

$$\zeta_{\gamma_u}^{\mathscr{R}_0} := \frac{\partial \mathscr{R}_0}{\partial \gamma_u} \times \frac{\gamma_u}{\mathscr{R}_0} = -\frac{\gamma_u\tau\sigma}{(\sigma+d)(\mu_u+\delta+\gamma_u+d)\mathscr{R}_0} \times \left[\beta_u+\frac{\beta_d\delta}{\mu_d+\gamma_d+d}\right],$$

$$\zeta_{\gamma_d}^{\mathscr{R}_0} := \frac{\partial \mathscr{R}_0}{\partial \gamma_d} \times \frac{\gamma_d}{\mathscr{R}_0} = -\frac{\gamma_d\sigma\beta_d}{(\sigma+d)(\mu_d+\gamma_d+d)\mathscr{R}_0} \times \left[(1-\tau)+\frac{\tau\delta}{\mu_u+\delta+\gamma_u+d}\right].$$

For variables not present in the expression of $\mathscr{R}_0$, the sensitivity index is zero. Based on

Parameters	Sensitivity Index
β_{d}	0.0711
β_{d}	0.9289
τ	-4.0099
σ	0.0826
d	-0.6638
δ	0.5441
μ_{u}	-0.0020
μ_{d}	-0.0030
γ_{u}	-0.3335
γ_{d}	-0.5591

Table 4.1: Sensitivity indices of various model parameters.

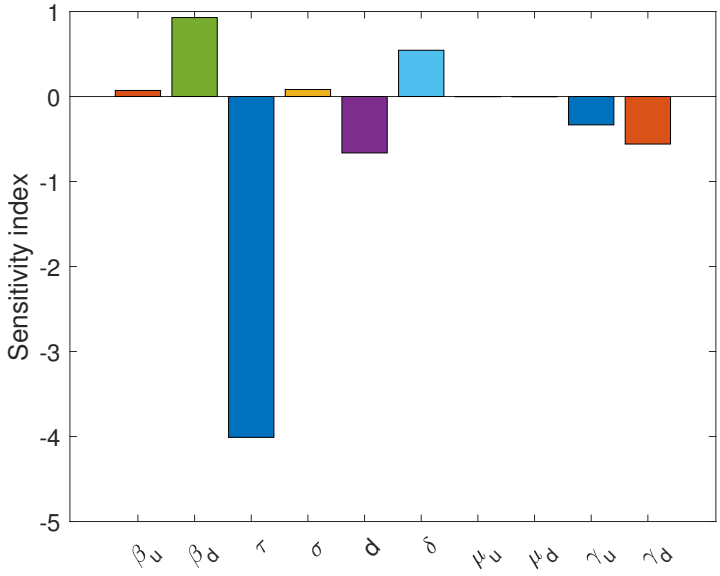


Figure 4.2: Bar plot representing the sensitivity indices of various model parameters.

the data presented in Table 4.1 and Figure 4.2, the variables with the highest observed sensitivity are β_{u}, β_{d}, τ, and δ, which show the highest sensitivity indices, whether positive or negative. A positive sensitivity index indicates that an increase in the parameter value leads to an increased spread of infection, while a negative sensitivity index indicates that an increase in the parameter value reduces the spread of infection.

For instance, β_{d}, which represents the transmission rate within hospital settings or locations designated for isolating patients, has a positive sensitivity index. This implies that an increase in β_{d} leads to a greater spread of the disease within these settings. Similarly, δ, the rate at which undetected cases are confirmed through PCR tests and

transition to the detected category, also has a positive sensitivity index. This means that a higher δ will result in more cases being detected, thereby influencing the system's dynamics.

Conversely, parameters such as the proportion of virus-exposed individuals who become infected but remain undetected exhibit negative sensitivity indices. This means that an increase in this proportion leads to a decrease in the overall infection spread, as it may slow down the progression by reducing the number of undetected cases transitioning to the infected state. Similarly, the negative sensitivity indices for γ_{u} and γ_{d} suggest that increasing these parameters helps to reduce the spread of the disease.

4.3.2 Formulation of fractional control optimization for the SEI^uI^dR model

Based on the sensitivity analysis described in the previous subsection, where β_{u} and β_{d} were identified as the most sensitive parameters, we chose u_1 to represent the control variable for preventing SEI^uI^dR transmission within the community. This control variable aims to reduce contact between susceptible individuals and infected individuals, whether detected or undetected. Furthermore, the fractional SEI^uI^dR model (4.1), after incorporating the optimal control u_1, is as follows:

$$
\begin{cases}
{}^{ABC}D_t^{\alpha} S(t) = \Lambda - (1-u_1)\frac{\beta_{\mathrm{u}} I^{\mathrm{u}} + \beta_{\mathrm{d}} I^{\mathrm{d}}}{N} S - dS, \\
{}^{ABC}D_t^{\alpha} E(t) = (1-u_1)\frac{(\beta_{\mathrm{u}} I^{\mathrm{u}} + \beta_{\mathrm{d}} I^{\mathrm{d}})S}{N} - (\sigma + d)E, \\
{}^{ABC}D_t^{\alpha} I^{\mathrm{u}}(t) = \tau\sigma E - \left(\mu_{\mathrm{u}} + \delta + \gamma_{\mathrm{u}} + d\right) I^{\mathrm{u}}, \\
{}^{ABC}D_t^{\alpha} I^{\mathrm{d}}(t) = (1-\tau)\sigma E + \delta I^{\mathrm{u}} - \left(\mu_{\mathrm{d}} + \gamma_{\mathrm{d}} + d\right) I^{\mathrm{d}}, \\
{}^{ABC}D_t^{\alpha} R(t) = \gamma_{\mathrm{u}} I^{\mathrm{u}} + \gamma_{\mathrm{d}} I^{\mathrm{d}} - dR.
\end{cases}
\tag{4.45}
$$

With the initial conditions $S(0) = S_0 \geq 0, E(0) = E_0 \geq 0, I^u(0) = I_0^u \geq 0, I^d(0) = I_0^d \geq 0, R(0) = R_0 \geq 0$. The objective function is defined as follows:

$$
\min J(u_1(t)) = \int_0^T A_1 E(t) + A_2 I^u(t) + A_3 I^d(t) + \frac{1}{2} A_4 u_1^2(t) dt,
$$

where A_1, A_2, A_3 and A_4 are positive weight coefficients, with A_4 ensuring the units of the integrand are consistent, and T represents the final time.
The associated feasible control domain is

$$
\mathscr{B} = \{u_1(t) \mid 0 \leq u_1(t) \leq 1, t \in [0, T]\}
$$

The Hamiltonian for our optimal control system (4.45) is defined as

$$\begin{aligned}\mathscr{H} =& A_1E + A_2I^u + A_3I^d + \frac{1}{2}\left(A_4u_1^2\right)\\ &+ \lambda_S\left[\Lambda - (1-u_1)\frac{\beta_uI^u + \beta_{\mathrm{d}}I^d}{N}S - dS\right]\\ &+ \lambda_E\left[(1-u_1)\frac{\beta_uI^u + \beta_{\mathrm{d}}I^d}{N}S - (\sigma+d)E\right]\\ &+ \lambda_u\left[\tau\sigma E - \left(\gamma_{\mathrm{u}} + d + \delta\right)I^u\right]\\ &+ \lambda_d\left[(1-\tau)\sigma E + \delta I^u - \left(\gamma_{\mathrm{d}} + d\right)I^d\right]\\ &+ \lambda_R\left[\gamma_{\mathrm{u}}I^u + \gamma_{\mathrm{d}}I^d - dR\right],\end{aligned} \tag{4.46}$$

where $\lambda_S, \lambda_E, \lambda_d, \lambda_u$ and λ_R are the adjoint variables. According on Pontryagin's minimum principle [73], we can state the following theorem.

Theorem 4.8. *The optimal control u_1^*, along with the corresponding solutions $S_*, E_*, I_*^u, I_*^d, R^*$, minimize the objective functional $J(u_1)$ over the set $\mathscr{B}$. There exist adjoint variables $\lambda_S, \lambda_E, \lambda_u, \lambda_d, \lambda_R$, satisfying transversality conditions $\lambda_i(T) = 0$, such that*

$$\begin{aligned}{}^{ABC}D_t^{\alpha}\lambda_S =& (1-u_1)\frac{\left(\beta_uI_*^{\mathrm{u}} + \beta_dI_*^{\mathrm{d}}\right)(\lambda_S - \lambda_E)}{N_*} + d\lambda_S\\ &+ (1-u_1)\left(\beta_uI_*^{\mathrm{u}} + \beta_dI_*^{\mathrm{d}}\right)\frac{(\lambda_S - \lambda_E)}{N_*^2}S_*,\end{aligned} \tag{4.47}$$

$$\begin{aligned}{}^{ABC}D_t^{\alpha}\lambda_E =& -A_1 - (1-u_1)\left(\beta_uI_*^{\mathrm{u}} + \beta_dI_*^{\mathrm{d}}\right)\frac{(\lambda_S - \lambda_E)}{N_*^2}S_*\\ &+ (\sigma+d)\lambda_E - \tau\sigma\lambda_u - (1-\tau)\sigma\lambda_d,\end{aligned} \tag{4.48}$$

$$\begin{aligned}{}^{ABC}D_t^{\alpha}\lambda_u =& -A_2 + (1-u_1)\left(\beta_uI_*^{\mathrm{u}} + \beta_dI_*^{\mathrm{d}}\right)S\frac{(\lambda_E - \lambda_S)}{N_*^2}\\ &+ (1-u_1)\frac{\beta_uS_*(\lambda_E - \lambda_S)}{N} + (\mu_u + \gamma_u + \delta + d)\lambda_u - \delta\lambda_d - \gamma_u\lambda_R,\end{aligned} \tag{4.49}$$

$$\begin{aligned}{}^{ABC}D_t^{\alpha}\lambda_d =& -A_3 + (1-u_1)\left(\beta_uI_*^{\mathrm{u}} + \beta_dI_*^{\mathrm{d}}\right)S\frac{(\lambda_E - \lambda_S)}{N_*^2}\\ &+ (1-u_1)\frac{\beta_dS_*(\lambda_E - \lambda_S)}{N_*} + (\mu_d + \gamma_d + d)\lambda_d - \gamma_d\lambda_R,\end{aligned} \tag{4.50}$$

$${}^{ABC}D_t^{\alpha}\lambda_R = (1-u_1)\frac{\left(\beta_uI_*^{\mathrm{u}} + \beta_dI_*^{\mathrm{d}}\right)(\lambda_E - \lambda_S)S_*}{N_*^2} - d\lambda_R. \tag{4.51}$$

Additionally, the corresponding optimal control u_1^* is expressed as

$$u_1^* = \min\left\{1, \max\left(0, \frac{(\beta_uI_*^{\mathrm{u}} + \beta_dI_*^{\mathrm{d}})(\lambda_E - \lambda_S)S_*}{A_4N_*}\right)\right\}. \tag{4.52}$$

Proof. We apply Pontryagin's maximum principle [73] to address the COVID-19 optimal control problem (4.45), which is formulated as follows.

$$
\begin{aligned}
&{}_{t}^{ABC}D_{T}^{\alpha}\lambda_S(t)=\frac{\partial\mathcal{H}}{\partial S},\quad {}_{t}^{ABC}D_{T}^{\alpha}\lambda_E(t)=\frac{\partial\mathcal{H}}{\partial E},\quad {}_{t}^{ABC}D_{T}^{\alpha}\lambda_u(t)=\frac{\partial\mathcal{H}}{\partial I^u},\\
&{}_{t}^{ABC}D_{T}^{\alpha}\lambda_d(t)=\frac{\partial\mathcal{H}}{\partial I^d},\quad {}_{t}^{ABC}D_{T}^{\alpha}\lambda_R(t)=\frac{\partial\mathcal{H}}{\partial R},
\end{aligned}
\tag{4.53}
$$

with transversality conditions

$$\lambda_S(T)=0,\quad \lambda_E(T)=0,\quad \lambda_{I^u}(T)=0,\quad \lambda_{I^d}(T)=0,\quad \lambda_R(T)=0.$$

To derive equation (4.52), we apply the following condition.

$$\frac{\partial\mathcal{H}}{\partial \mathrm{u}_1}=0.$$

■

Parameter	Value	Source
Λ	300.38	Assumed
β_u	0.10138	[39]
β_d	5.7436	Assumed
d	0.0450	[39]
τ	0.92506	[39]
σ	0.5	[39]
μ_u	4.2×10^{-4}	[39]
μ_d	3.7×10^{-4}	[39]
γ_d	0.06859	[39]
γ_u	0.07	[39]
δ	1.8110×10^{-7}	[39]

Table 4.2: Parameter values for the fractional model SEI^uI^dR.

4.4 Numerical simulations

In this section, we apply the Taoufik–Atangana scheme, as previously described, to the COVID-19 model with the fractional ABC derivative (4.1). The scheme presented in equation (1.39) is implemented for our model (4.1), leading to the following algorithm.

$$
\begin{aligned}
S(t_{n+1}) &= S(0) + \frac{1-\alpha}{M(\alpha)}\psi_1(t_n, S(t_n)) + \frac{\alpha}{M(\alpha)}\sum_{j=0}^{n}\left[\frac{h^\alpha \psi_1(t_k, z(t_k))}{\Gamma(\alpha+2)}\times\right.\\
&\quad \{(n-k+2+\alpha)(n+1-k)^\alpha - (n-k+2+2\alpha)(n-k)^\alpha\}\\
&\quad \left. -\frac{h^\alpha \psi_1(t_{k-1}, z(t_{k-1}))}{\Gamma(\alpha+2)}\{(n+1-k)^{\alpha+1} - (n-k+1+\alpha)(n-k)^\alpha\}\right],\\
E(t_{n+1}) &= E(0) + \frac{1-\alpha}{M(\alpha)}\psi_2(t_n, z(t_n)) + \frac{\alpha}{M(\alpha)}\sum_{k=0}^{n}\left[\frac{h^\alpha \psi_2(t_k, z(t_k))}{\Gamma(\alpha+2)}\times\right.\\
&\quad \{(n-k+2+\alpha)(n+1-k)^\alpha - (n-k+2+2\alpha)(n-k)^\alpha\}\\
&\quad \left. -\frac{h^\alpha \psi_1(t_{k-1}, z(t_{k-1}))}{\Gamma(\alpha+2)}\{(n+1-k)^{\alpha+1} - (n-k+1+\alpha)(n-k)^\alpha\}\right],\\
I^u(t_{n+1}) &= I^u(0) + \frac{1-\alpha}{M(\alpha)}\psi_3(t_n, z(t_n)) + \frac{\alpha}{M(\alpha)}\sum_{k=0}^{n}\left[\frac{h^\alpha \psi_3(t_k, z(t_k))}{\Gamma(\alpha+2)}\times\right.\\
&\quad \{(n-k+2+\alpha)(n+1-k)^\alpha - (n-k+2+2\alpha)(n-k)^\alpha\}\\
&\quad \left. -\frac{h^\alpha \psi_1(t_{k-1}, z(t_{k-1}))}{\Gamma(\alpha+2)}\{(n+1-k)^{\alpha+1} - (n-k+1+\alpha)(n-k)^\alpha\}\right],\\
I^d(t_{n+1}) &= I^d(t_0) + \frac{1-\alpha}{M(\alpha)}\psi_4(t_n, z(t_n)) + \frac{\alpha}{M(\alpha)}\sum_{k=0}^{n}\left[\frac{h^\alpha \psi_4(t_k, z(t_k))}{\Gamma(\alpha+2)}\times\right.\\
&\quad \{(n-k+2+\alpha)(n+1-k)^\alpha - (n-k+2+2\alpha)(n-k)^\alpha\}\\
&\quad \left. -\frac{h^\alpha \psi_1(t_{k-1}, z(t_{k-1}))}{\Gamma(\alpha+2)}\{(n+1-k)^{\alpha+1} - (n-k+1+\alpha)(n-k)^\alpha\}\right],\\
R(t_{n+1}) &= R(0) + \frac{1-\alpha}{M(\alpha)}\psi_5(t_n, z(t_n)) + \frac{\alpha}{M(\alpha)}\sum_{k=0}^{n}\left[\frac{h^\alpha \psi_5(t_k, z(t_k))}{\Gamma(\alpha+2)}\times\right.\\
&\quad \{(n-k+2+\alpha)(n+1-k)^\alpha - (n-k+2+2\alpha)(n-k)^\alpha\}\\
&\quad \left. -\frac{h^\alpha \psi_5(t_{k-1}, z(t_{k-1}))}{\Gamma(\alpha+2)}\{(n+1-k)^{\alpha+1} - (n-k+1+\alpha)(n-k)^\alpha\}\right],
\end{aligned}
$$

where ψ_1,ψ_2, ψ_3,ψ_4 and ψ_5 are given in 4.2.

4.4.1 Effect of the ABC derivative on model dynamics

In this section, we explore the dynamics of the SEI^dI^uR model using the Taoufik–Atangana numerical scheme. The parameter values employed in the simulations are presented in Table 4.2. We incorporate the ABC fractional derivative with varying orders $\alpha = (1, 0.95, 0.85, 0.75)$ to analyze its impact on the model's behavior, as illustrated in Figure 4.3. The trajectories of the compartments $S(t)$, $E(t)$, $I_u(t)$, $I_d(t)$,

and $R(t)$ converge to the equilibrium point $\mathscr{E}_1 = (1.0574 \times 10^3, 4.6385 \times 10^2, 9.9784 \times 10^2, 1.5260 \times 10^2, 1.7848 \times 10^3)$ when $\mathscr{R}_0 = 1.9306 > 1$. This observation indicates that $\mathscr{E}_1$ is locally asymptotically stable.

The curves in subfigures 4.3(a)-4.3(e) demonstrate that as the fractional order α decreases, both the infection rate and the peak incidence of the disease decline. This highlights the significant impact that fractional derivatives can have on understanding and managing coronavirus transmission. Unlike the integer-order derivative ($\alpha = 1$), the fractional model incorporates a memory effect that deepens our understanding of the model's stability and long-term dynamics, which are essential for evaluating outbreak potential and the effectiveness of control strategies. Larger α values (closer to 1) indicate weaker memory effects, resulting in faster dynamics, while smaller α values introduce a stronger memory effect, thereby slowing the progression of the disease over time.

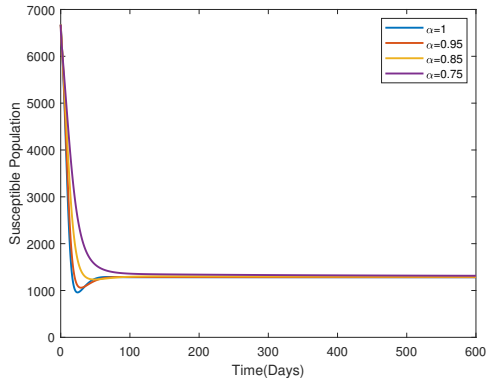
Additionally, to examine how the parameters β_u and τ affect the dynamics of the exposed, detected infected, and undetected infected populations in a COVID-19 model, we vary these parameters across different rates and present the resulting simulations. Graphical representations are shown for three values of $\alpha = (0.95, 0.85, 0.75)$.

Figure 4.4 illustrates that increasing τ (the fraction of individuals who are exposed to the virus and become infected without being detected) to its baseline value leads to a substantial reduction in the exposed population. Additionally, for each value of τ, a decrease in α causes both the peak of the exposed population to drop and its occurrence to be delayed. This outcome highlights the effect of a stronger memory effect, which slows the spread and reduces the number of exposed individuals at any given time. The same behavior is observed in the compartments of infected undetected, as shown in Figure 4.5, and in the infected detected Figures in 4.6.

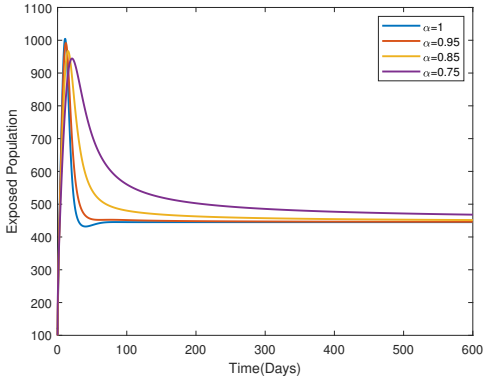
Figure 4.7 depicts the progression of the exposed population over time for varying values of β_u (the community transmission rate) and the three indicated α values. We observe that a higher β_u leads to a significantly larger exposed population and faster dynamics, particularly when $\alpha = 0.95$. As α decreases, the memory effect slows the spread, resulting in smaller and more delayed peaks, regardless of the value of β_u. The same behavior is observed in the compartments shown in Figures 4.8 and 4.9.

4.4.2 Numerical simulation of the control problem

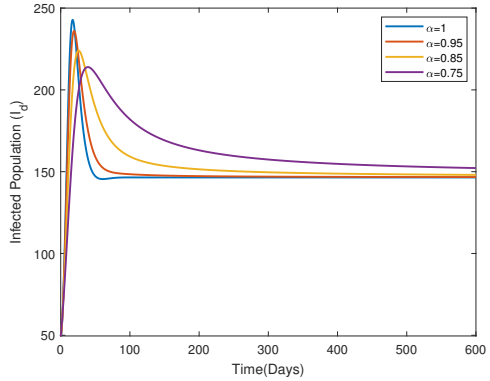
This section presents the results of the numerical simulations conducted for the proposed fractional model, both with and without controls. The Taoufik scheme was applied to simulate the adjoint variables. The parameter values are listed in Table 4.2. The weights



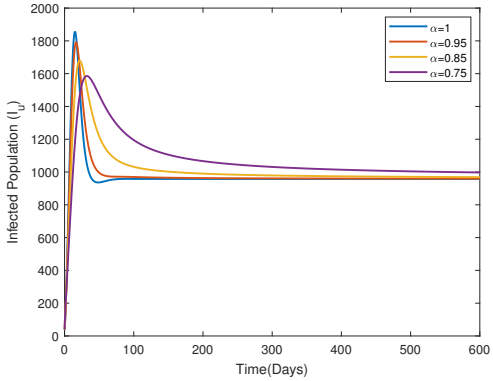
(a) Susceptible population



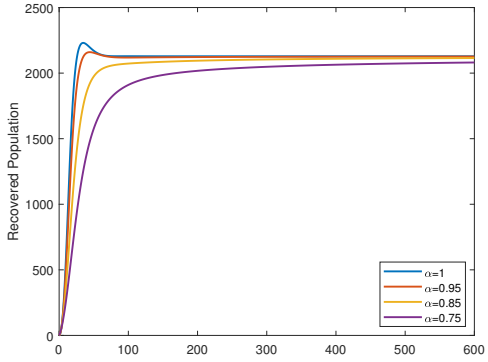
(b) Exposed population



(c) Infected detected population



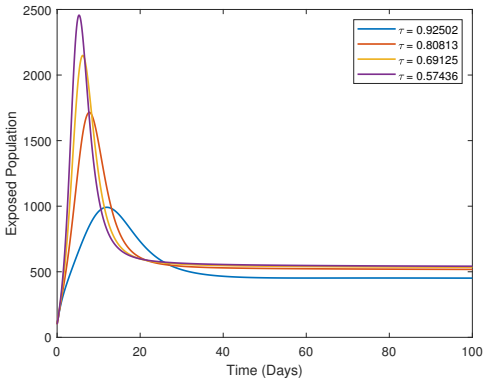
(d) Infected undetected population



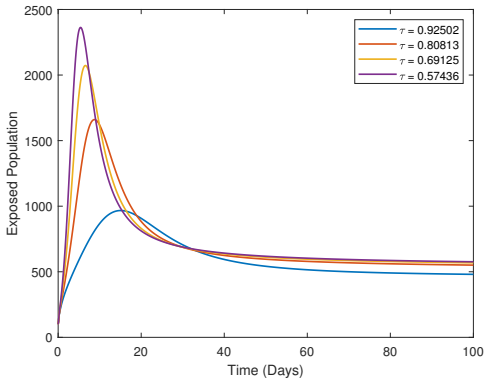
(e) Recovered individuals

Figure 4.3: Dynamics of the SEI^dI^uR model over time (in years) for various values of α using the Taoufik–Atangana scheme.

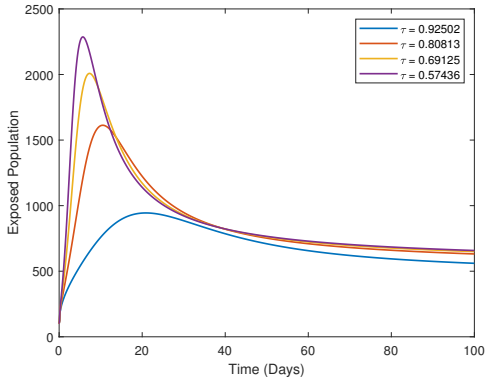
and balancing coefficients were set as follows: $A_1 = 1$, $A_2 = 1$, $A_3 = 1$, and $A_4 = 1000$. The simulation was carried out with a time step of $h = 0.01$ and a fractional order of $\alpha = 0.85$. From the results in Fig. 4.10, we observed that under the optimal control



(a) Exposed population for $\alpha = 0.95$



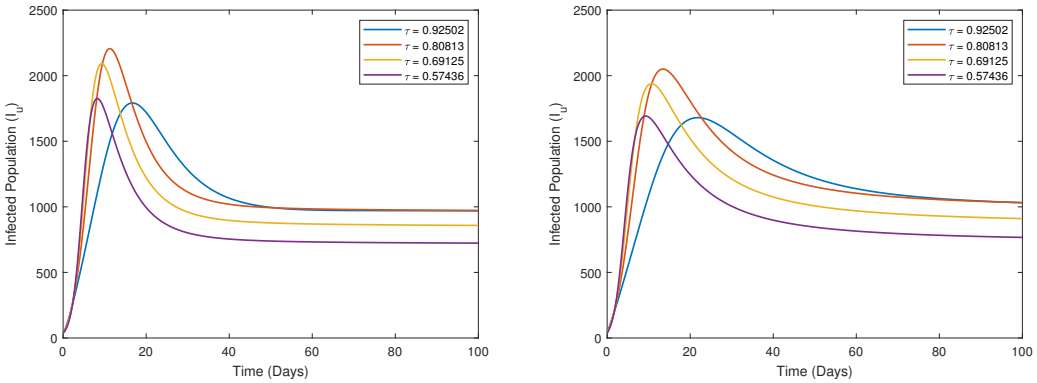
(b) Exposed population for $\alpha = 0.85$



(c) Exposed population for $\alpha = 0.75$

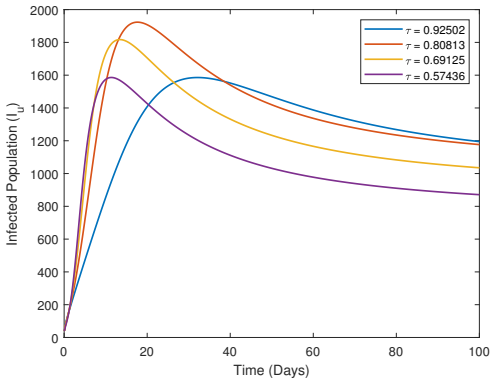
Figure 4.4: The effect of τ on the dynamics of the exposed population.

u_1, there is a significant reduction in the number of exposed individuals, as well as a considerable decrease in both the infected undetected and detected populations, leading to a substantial reduction in the number of virus carriers. This demonstrates that the optimal control strategy can effectively mitigate the spread of COVID-19.



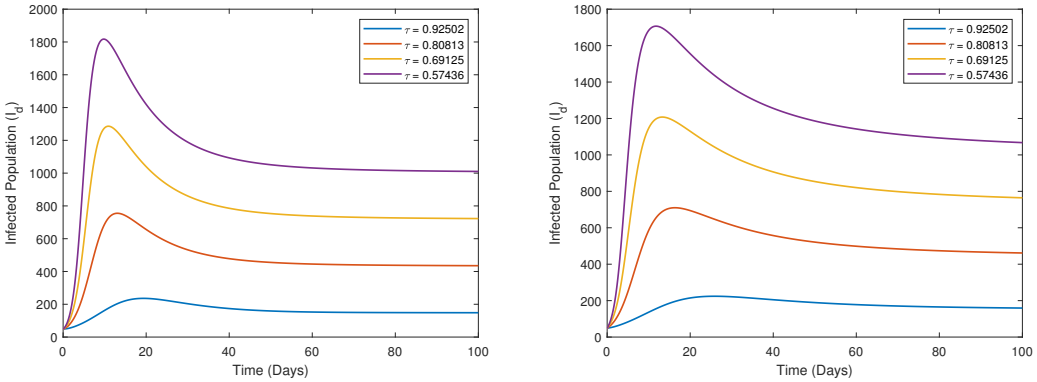
(a) Infected undetected population for α = 0.95

(b) Infected undetected population for α = 0.85

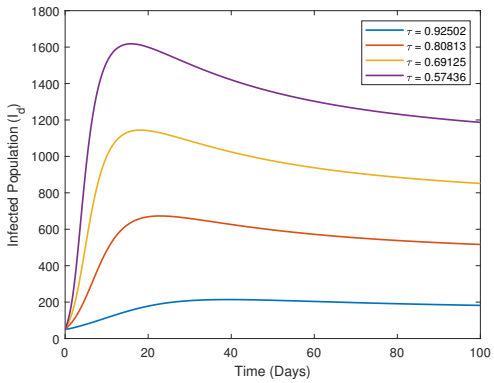


(c) Infected undetected population for α = 0.75

Figure 4.5: The effect of τ on the dynamics of the infected undetected population for different values of α.

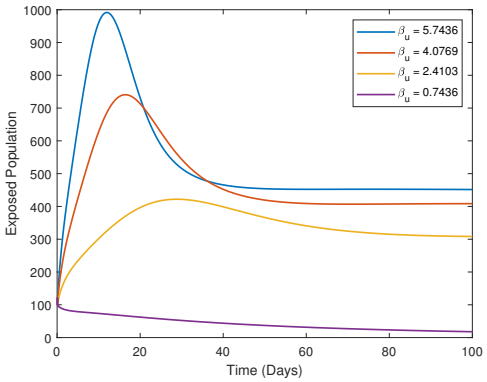


(a) Infected detected population for $\alpha = 0.95$ (b) Infected detected population for $\alpha = 0.85$

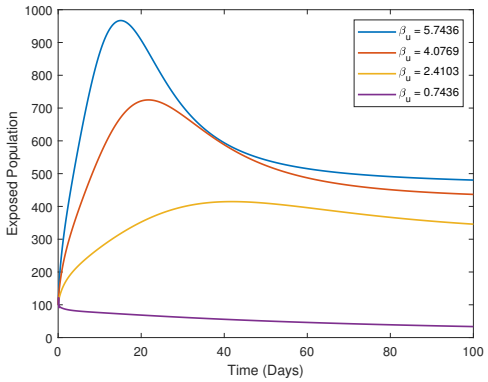


(c) Infected detected population for $\alpha = 0.75$

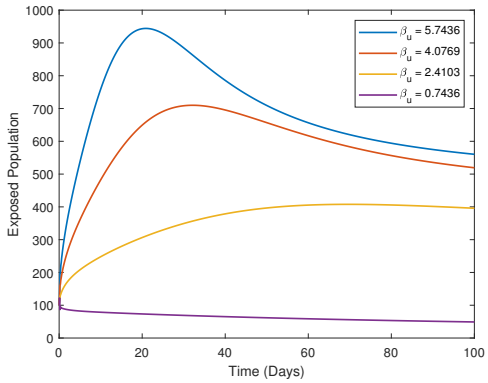
Figure 4.6: The effect of τ on the dynamics of the infected detected population for different values of α.



(a) Exposed population for $\alpha = 0.95$

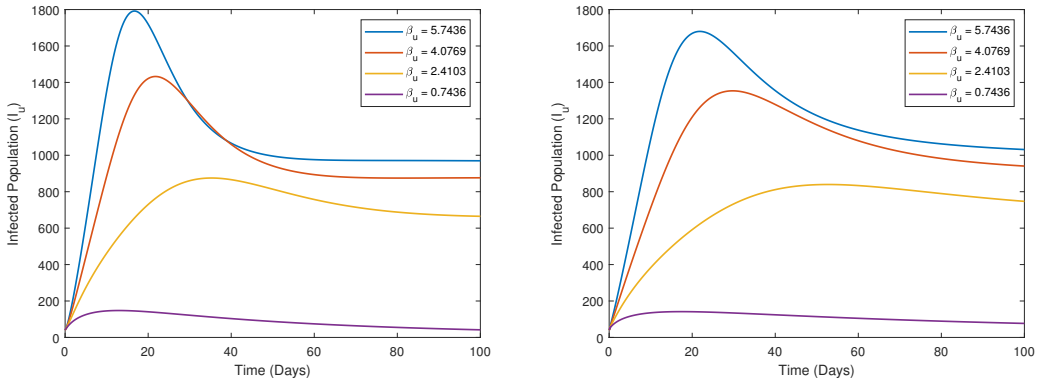


(b) Exposed population for $\alpha = 0.85$



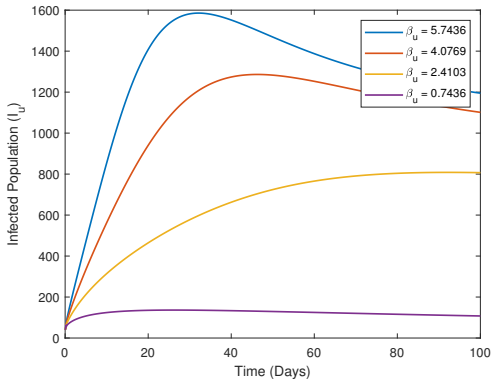
(c) Exposed population for $\alpha = 0.75$

Figure 4.7: The effect of the transmission rate within the community β_u on the dynamics of the exposed population for different values of the fractional order α.



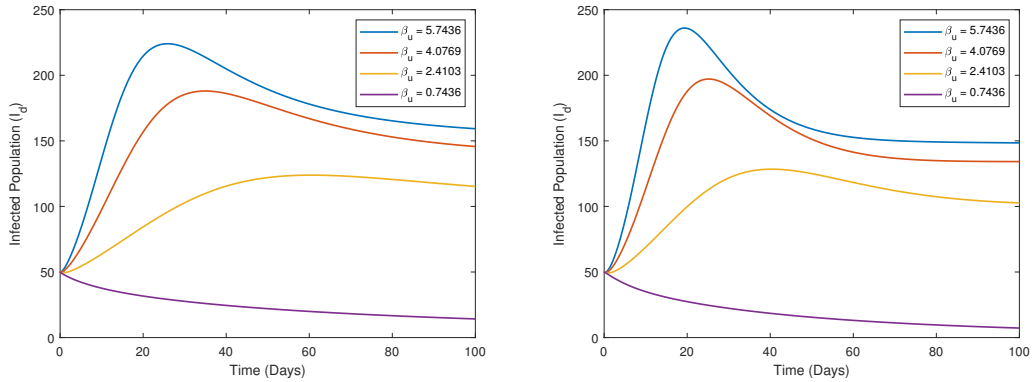
(a) Infected undetected population for α = 0.95

(b) Infected undetected population for α = 0.85

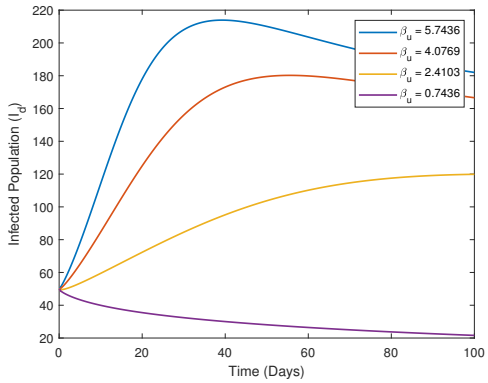


(c) Infected undetected population for α = 0.75

Figure 4.8: The effect of the transmission rate within the community β_u on the dynamics of the infected undetected population for different values of α.

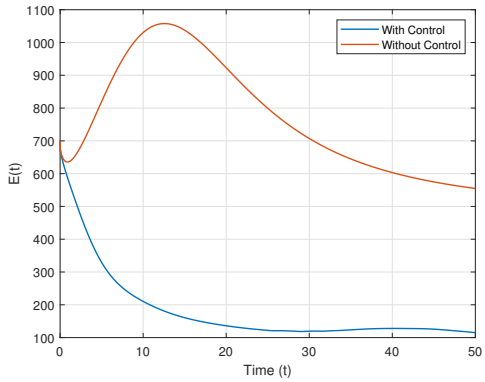


(a) Infected detected population for $\alpha = 0.95$ (b) Infected detected population for $\alpha = 0.85$

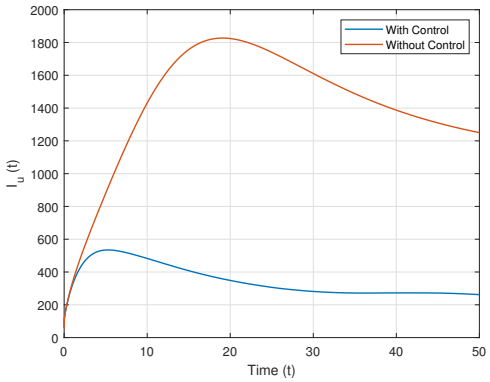


(c) Infected detected population for $\alpha = 0.75$

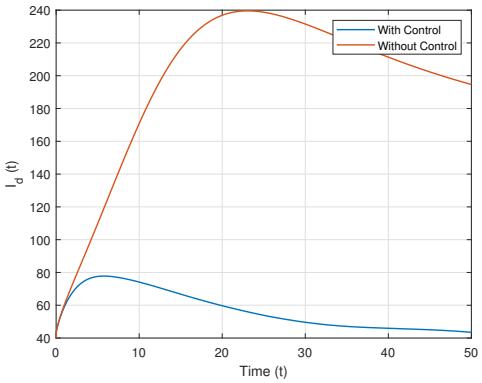
Figure 4.9: The effect of the transmission rate within the community β_u on the dynamics of the infected detected population for different values of α.



(a) Exposed population.



(b) Infected undetected population.



(c) Infected detected population.

Figure 4.10: Comparison of the evolution of COVID-19 dynamics with and without Control.

4.5 Conclusion

In this chapter, we developed a fractional SEI^uI^dR model for COVID-19 using the ABC fractional derivative to examine the impact of fractional orders on disease dynamics. We established the existence and uniqueness of solutions and identified the biologically feasible region for the model. Our analysis demonstrated that the model is locally asymptotically stable at the disease-free equilibrium when $\mathscr{R}_0 < 1$ and at the endemic equilibrium when $\mathscr{R}_0 > 1$. Sensitivity analysis revealed that τ and β_{d} are critical parameters for controlling the disease's spread. Additionally, we introduced an optimal control strategy designed to reduce disease transmission by minimizing contact between susceptible individuals and both undetected and detected infected populations. Numerical findings indicated that fractional-order models converge more slowly toward stable states compared to integer-order models, offering a more nuanced perspective on disease progression. The optimal control strategy was found to significantly reduce the spread of the pandemic. These findings provide important guidance for policymakers in devising effective strategies to curb the spread of COVID-19.

CONCLUSION AND FUTURE PERSPECTIVES

This thesis comprehensively examined the dynamics of various infectious diseases using compartmental models with fractional derivatives, focusing on both Caputo and ABC types. Rigorous mathematical analyses were conducted across all models, including proofs of existence, uniqueness, boundedness, and positivity of the solution, as well as stability and sensitivity analysis of model parameters used. Additionally, numerical simulations were used to validate these theoretical results and to explore model behavior across various fractional orders.

First, the study investigated an SIA model for HIV/AIDS transmission to assess the influence of migration. Results demonstrated that migration significantly contributes to epidemic spread, amplifying transmission across regions. By employing fractional derivatives, the model provided deeper insights into transmission dynamics, capturing the slow progression of HIV to AIDS more accurately than traditional models. Specifically, we found that the time for individuals affected by AIDS to reach a steady state is approximately 50 years, aligning well with observed HIV progression timelines. A key contribution of this thesis is the comparative analysis of the Caputo and ABC approaches within the HIV model, evaluating each derivative's impact on convergence and predictive capacity. Findings showed that the Caputo derivative achieved faster convergence, while the ABC derivative, with its non-local properties, converged more gradually. This distinction highlights the ABC approach's potential to capture long-term memory effects in disease progression, offering an extended perspective on the chronic nature of HIV/AIDS.

Second, we analyze an SIP model for a marine parasite-induced disease using both Caputo and ABC derivatives, finding that both exhibit similar numerical trends in this context. This suggests that the Caputo and ABC kernels shape the model's behavior in comparable ways. In contrast, our HIV/AIDS model shows a more noticeable difference between the derivatives, particularly when the fractional order is reduced to 0.65. This disparity likely stems from initial conditions and parameters in the marine parasite model that are less suited to highlighting differences between the derivatives. These

findings underscore the importance of real-world data in selecting the most suitable kernel for accurate modeling.

Lastly, this thesis examined a novel COVID-19 model incorporating the ABC derivative and considering two types of infected classes: detected and non-detected. With an optimal control strategy designed to minimize infection rates by raising awareness among the population. The findings highlight the role of the ABC derivative in capturing the complex population dynamics over time, showing a delayed convergence compared to the integer-order derivative. Additionally, varying the fractional order results in distinct peaks in the dynamics. On the other hand, the control strategy (awareness-raising) leads to a significant reduction in both the exposed population and the infected individuals, whether detected or undetected.

Overall, this thesis presents a study on eco-epidemiological and epidemiological modeling using non-integer order derivatives, focusing specifically on the Caputo and ABC types. Through rigorous mathematical and numerical analysis, along with constructive proofs, we have illuminated the complex behavior of the systems studied, leading to a deeper understanding of the role of fractional approaches. However, these findings shed light on several open questions and future perspectives:

- Extend the application of fractional models to other infectious diseases, such as emerging influenza strains or zoonotic viruses, which exhibit complex and evolving dynamics. This would deepen our understanding of diseases with unpredictable transmission patterns, enhancing preparedness for future outbreaks.

- Integrate fractional calculus with machine learning to improve predictive accuracy, particularly for real-time parameter estimation and model adaptation. This combination would enable dynamic adjustments based on incoming data, enhancing the reliability of forecasts for complex disease dynamics.

- Incorporate real-world data to improve the alignment between model predictions and observed measurements, leading to more accurate and reliable results.

- Introduce spatial diffusion to capture the effects of geographic spread and localized interactions on disease transmission. Coupling this with optimal control strategies could enable targeted interventions, improving resource allocation and containment efforts in specific regions.

BIBLIOGRAPHY

[1] M. A. ABDULWASAA, M. S. ABDO, K. SHAH, T. A. NOFAL, S. K. PANCHAL, S. V. KAWALE, AND A. H. ABDEL ATY, *Fractal-fractional mathematical modeling and forecasting of new cases and deaths of covid-19 epidemic outbreaks in india*, Results in Physics, 20 (2021), p. 103702.

[2] F. J. ADROHER-AUROUX AND R. BENÍTEZ-RODRÍGUEZ, *Anisakiasis and anisakis: An underdiagnosed emerging disease and its main etiological agents*, Research in veterinary science, 132 (2020), pp. 535–545.

[3] M. AGARWAL AND V. VERMA, *Modeling and analysis of the spread of an infectious disease cholera with environmental fluctuations*, Applications and Applied Mathematics: An International Journal (AAM), 7 (2012), p. 27.

[4] N. AGUILA-CAMACHO, M. A. DUARTE-MERMOUD, AND J. A. GALLEGOS, *Lyapunov functions for fractional order systems*, Communications in Nonlinear Science and Numerical Simulation, 19 (2014), pp. 2951–2957.

[5] E. AHMED, A. EL-SAYED, AND H. A. EL-SAKA, *On some routh–hurwitz conditions for fractional order differential equations and their applications in lorenz, rössler, chua and chen systems*, Physics Letters A, 358 (2006), pp. 1–4.

[6] A. A. ALDERREMY, K. M. SAAD, J. F. GÓMEZ-AGUILAR, S. ALY, D. KUMAR, AND J. SINGH, *New models of fractional blood ethanol and two-cell cubic autocatalator reaction equations*, Mathematical Methods in the Applied Sciences, 46 (2023), pp. 7767–7778.

[7] H. ALIZADEH, A. SHARIFI, S. DAMANBAGH, H. NAZARNIA, AND M. NAZARNIA, *Impacts of the covid-19 pandemic on the social sphere and lessons for crisis management: a literature review*, Natural Hazards, 117 (2023), pp. 2139–2164.

[8] A. ALKHAZZAN, P. JIANG, D. BALEANU, H. KHAN, AND A. KHAN, *Stability and existence results for a class of nonlinear fractional differential equations with singularity*, Mathematical Methods in the Applied Sciences, 41 (2018), pp. 9321–9334.

[9] M. S. ALQARNI, M. ALGHAMDI, T. MUHAMMAD, A. S. ALSHOMRANI, AND M. A. KHAN, *Mathematical modeling for novel coronavirus (covid-19) and control*, Numerical Methods for Partial Differential Equations, 38 (2022), pp. 760–776.

[10] O. AMER, *The impact of fish parasites on human health*, Journal of the Egyptian Society of Parasitology, 44 (2014), pp. 249–274.

[11] S. ANNAS, M. I. PRATAMA, M. RIFANDI, W. SANUSI, AND S. SIDE, *Stability analysis and numerical simulation of seir model for pandemic covid-19 spread in indonesia*, Chaos, solitons & fractals, 139 (2020), p. 110072.

[12] O. O. APENTENG, P. P. OSEI, N. A. ISMAIL, AND A. CHIABAI, *Analysing the impact of migration on hiv/aids cases using epidemiological modelling to guide policy makers*, Infectious Disease Modelling, 7 (2022), pp. 252–261.

[13] T. M. ATANACKOVIC, S. PILIPOVIC, B. STANKOVIC, AND D. ZORICA, *Fractional calculus with applications in mechanics: wave propagation, impact and variational principles*, John Wiley & Sons, 2014.

[14] A. ATANGANA AND D. BALEANU, *New fractional derivatives with nonlocal and non-singular kernel: theory and application to heat transfer model*, arXiv preprint arXiv:1602.03408, (2016).

[15] W. ATOKOLO, R. O. AJA, S. E. ANIAKU, I. S. ONAH, AND G. C. MBAH, *Approximate solution of the fractional order sterile insect technology model via the laplace–adomian decomposition method for the spread of zika virus disease*, International Journal of Mathematics and Mathematical Sciences, 2022 (2022).

[16] C. BAISHYA, S. J. ACHAR, P. VEERESHA, AND D. PRAKASHA, *Dynamics of a fractional epidemiological model with disease infection in both the populations*, Chaos: An Interdisciplinary Journal of Nonlinear Science, 31 (2021).

[17] D. BALEANU, K. DIETHELM, E. SCALAS, AND J. J. TRUJILLO, *Fractional calculus: models and numerical methods*, vol. 3, World Scientific, 2012.

[18] R. Begum, O. Tunç, H. Khan, H. Gulzar, and A. Khan, *A fractional order zika virus model with mittag–leffler kernel*, Chaos, Solitons and Fractals, 146 (2021), p. 110898.

[19] D. C. Behringer, K. D. Lafferty, and B. R. Silliman, *Marine disease ecology*, Oxford University Press, USA, 2020.

[20] D. Bernoulli and D. Chapelle, *Essai d'une nouvelle analyse de la mortalité causée par la petite vérole, et des avantages de l'inoculation pour la prévenir*, (2023).

[21] D. L. Cantrell, M. L. Groner, T. Ben-Horin, J. Grant, and C. W. Revie, *Modeling pathogen dispersal in marine fish and shellfish*, Trends in Parasitology, 36 (2020), pp. 239–249.

[22] M. Caputo, *Linear models of dissipation whose q is almost frequency independent—ii*, Geophysical Journal International, 13 (1967), pp. 529–539.

[23] M. Caputo and M. Fabrizio, *A new definition of fractional derivative without singular kernel*, Progress in Fractional Differentiation & Applications, 1 (2015), pp. 73–85.

[24] L. Cardoso, F. Dos Santos, and R. Camargo, *Analysis of fractional-order models for hepatitis b*, Computational and Applied Mathematics, 37 (2018), pp. 4570–4586.

[25] A. Chikrii and I. Matychyn, *Riemann–liouville, caputo, and sequential fractional derivatives in differential games*, Advances in dynamic games: theory, applications, and numerical methods for differential and stochastic games, (2011), pp. 61–81.

[26] N. Chitnis, J. M. Hyman, and J. M. Cushing, *Determining important parameters in the spread of malaria through the sensitivity analysis of a mathematical model*, Bulletin of mathematical biology, 70 (2008), pp. 1272–1296.

[27] M. Coccia, *The impact of first and second wave of the covid-19 pandemic in society: comparative analysis to support control measures to cope with negative effects of future infectious diseases*, Environmental Research, 197 (2021), p. 111099.

[28] R. Darling and J. Newman, *On the short-time behavior of porous intercalation electrodes*, Journal of the Electrochemical society, 144 (1997), p. 3057.

[29] K. D. DEANE, J. O. PARKHURST, AND D. JOHNSTON, *Linking migration, mobility and hiv*, Tropical Medicine & International Health, 15 (2010), pp. 1458–1463.

[30] D. L. DEANGELIS, R. GOLDSTEIN, AND R. V. O'NEILL, *A model for tropic interaction*, Ecology, 56 (1975), pp. 881–892.

[31] O. DIEKMANN, J. A. P. HEESTERBEEK, AND J. A. J. METZ, *On the definition and the computation of the basic reproduction ratio r 0 in models for infectious diseases in heterogeneous populations*, Journal of mathematical biology, 28 (1990), pp. 365–382.

[32] K. DIETHELM AND N. J. FORD, *Analysis of fractional differential equations*, Journal of Mathematical Analysis and Applications, 265 (2002), pp. 229–248.

[33] K. DIETHELM, N. J. FORD, AND A. D. FREED, *A predictor-corrector approach for the numerical solution of fractional differential equations*, Nonlinear Dynamics, 29 (2002), pp. 3–22.

[34] J. ESBJÖRNSSON, M. MILD, F. MÅNSSON, H. NORRGREN, AND P. MEDSTRAND, *Hiv-1 molecular epidemiology in guinea-bissau, west africa: origin, demography and migrations*, PloS one, 6 (2011), p. e17025.

[35] L. EULER, *De progressionibus transcendentibus seu quarum termini generales algebraice dari nequeunt*, Commentarii academiae scientiarum Petropolitanae, (1738), pp. 36–57.

[36] FAO, *The State of World Fisheries and Aquaculture 2020*, Food and Agriculture Organization of the United Nations, 2020.

[37] J. B. J. FOURIER, *Théorie analytique de la chaleur*, vol. 1, Gauthier-Villars, 1888.

[38] M. S. GOTTLIEB, H. M. SCHANKER, P. T. FAN, A. SAXON, J. D. WEISMAN, I. POZALSKI, ET AL., *Pneumocystis pneumonia—los angeles*, Mmwr, 30 (1981), pp. 250–2.

[39] A. A. HAMOU, R. R. RASUL, Z. HAMMOUCH, AND N. ÖZDEMIR, *Analysis and dynamics of a mathematical model to predict unreported cases of covid-19 epidemic in morocco*, Computational and Applied Mathematics, 41 (2022), p. 289.

[40] D. Harvell, R. Aronson, N. Baron, J. Connell, A. Dobson, S. Ellner, L. Gerber, K. Kim, A. Kuris, H. McCallum, et al., *The rising tide of ocean diseases: unsolved problems and research priorities*, Frontiers in Ecology and the Environment, 2 (2004), pp. 375–382.

[41] R. Herrmann, *Fractional calculus: an introduction for physicists*, World Scientific, 2011.

[42] Y.-H. Hsieh and S.-P. Sheu, *The effect of density-dependent treatment and behavior change on the dynamics of hiv transmission*, Journal of Mathematical Biology, 43 (2001), pp. 69–80.

[43] H.-F. Huo, R. Chen, and X.-Y. Wang, *Modelling and stability of hiv/aids epidemic model with treatment*, Applied Mathematical Modelling, 40 (2016), pp. 6550–6559.

[44] J. Huo, H. Zhao, and L. Zhu, *The effect of vaccines on backward bifurcation in a fractional order hiv model*, Nonlinear Analysis: Real World Applications, 26 (2015), pp. 289–305.

[45] H. Joshi, S. Lenhart, K. Albright, and K. Gipson, *Modeling the effect of information campaigns on the hiv epidemic in uganda*, Math. Biosci. Eng, 5 (2008), pp. 757–770.

[46] N. Kai Diethelm, N. Ford., and A. J. D. Freed, *Detailed error analysis for a fractional adams method*, Numerical algorithms, 36 (2004), pp. 31–52.

[47] W. O. Kermack and A. G. McKendrick, *A contribution to the mathematical theory of epidemics*, Proceedings of the royal society of london. Series A, Containing papers of a mathematical and physical character, 115 (1927), pp. 700–721.

[48] H. Khan, K. Alam, H. Gulzar, S. Etemad, and S. Rezapour, *A case study of fractal-fractional tuberculosis model in china: Existence and stability theories along with numerical simulations*, Mathematics and Computers in Simulation, 198 (2022), pp. 455–473.

[49] H. Khan, C. Tunç, and A. Khan, *Stability results and existence theorems for nonlinear delay-fractional differential equations with φ_p^*-operator*, 2020.

[50] H. KHEIRI AND M. JAFARI, *Fractional optimal control of an hiv/aids epidemic model with random testing and contact tracing*, Journal of Applied Mathematics and Computing, 60 (2019), pp. 387–411.

[51] A. KILBAS A, H. M. SRIVASTAVA, AND J. J. TRUJILLO, *Theory and applications of fractional differential equations*, vol. 204, elsevier, 2006.

[52] S. F. LACROIX, *Traité du calcul différentiel et du calcul intégral*, vol. 1, JBM Duprat, 1797.

[53] J. L. LAGRANGE, *Sur une nouvelle espèce de calcul rélatif à la différentiation & à l'intégration des quantités variables*, Académie royale des sciences et belles lettres, 1775.

[54] P. S. LAPLACE, *Théorie analytique des probabilités*, Courcier, 1820.

[55] A. V. LETNIKOV, *Theory of differentiation with an arbtraly indicator*, Matem Sbornik, 3 (1868), pp. 1–68.

[56] C. LI AND Y. MA, *Fractional dynamical system and its linearization theorem*, Nonlinear Dynamics, 71 (2013), pp. 621–633.

[57] W. LIN, *Global existence theory and chaos control of fractional differential equations*, Journal of Mathematical Analysis and Applications, 332 (2007), pp. 709–726.

[58] X. LIU AND L. YANG, *Stability analysis of an seiqv epidemic model with saturated incidence rate*, Nonlinear analysis: real world applications, 13 (2012), pp. 2671–2679.

[59] A. J. LYNCH, S. J. COOKE, A. M. DEINES, S. D. BOWER, D. B. BUNNELL, I. G. COWX, V. M. NGUYEN, J. NOHNER, K. PHOUTHAVONG, B. RILEY, ET AL., *The social, economic, and environmental importance of inland fish and fisheries*, Environmental Reviews, 24 (2016), pp. 115–121.

[60] J. T. MACHADO, V. KIRYAKOVA, AND F. MAINARDI, *Recent history of fractional calculus*, Communications in nonlinear science and numerical simulation, 16 (2011), pp. 1140–1153.

[61] F. MAINARDI, *Fractional calculus and waves in linear viscoelasticity: an introduction to mathematical models*, World Scientific, 2022.

[62] A. MARCHAUD, *Sur les dérivées et sur les différences des fonctions de variables réelles*, Journal de Mathematiques Pures et Appliquees, 6 (1927), pp. 337–425.

[63] D. MATIGNON, *Stability results for fractional differential equations with applications to control processing*, in Computational engineering in systems applications, vol. 2, Citeseer, 1996, pp. 963–968.

[64] K. S. MILLER AND B. ROSS, *An introduction to the fractional calculus and fractional differential equations*, (No Title), (1993).

[65] Z. MUKANDAVIRE, W. GARIRA, AND J. TCHUENCHE, *Modelling effects of public health educational campaigns on hiv/aids transmission dynamics*, Applied Mathematical Modelling, 33 (2009), pp. 2084–2095.

[66] P. A. NAIK, J. ZU, AND K. M. OWOLABI, *Global dynamics of a fractional order model for the transmission of hiv epidemic with optimal control*, Chaos, Solitons & Fractals, 138 (2020), p. 109826.

[67] H. NAJAFI, S. ETEMAD, N. PATANARAPEELERT, J. K. K. ASAMOAH, S. REZAPOUR, AND T. SITTHIWIRATTHAM, *A study on dynamics of cd4+ t-cells under the effect of hiv-1 infection based on a mathematical fractal-fractional model via the adams-bashforth scheme and newton polynomials*, Mathematics, 10 (2022), p. 1366.

[68] T. F. NONNENMACHER AND R. METZLER, *Applications of fractional calculus techniques to problems in biophysics*, Applications of fractional calculus in physics, (2000), pp. 377–427.

[69] Z. M. ODIBAT AND S. MOMANI, *An algorithm for the numerical solution of differential equations of fractional order*, Journal of Applied Mathematics & Informatics, 26 (2008), pp. 15–27.

[70] Z. M. ODIBAT AND N. T. SHAWAGFEH, *Generalized taylor's formula*, Applied Mathematics and Computation, 186 (2007), pp. 286–293.

[71] I. PODLUBNY, *The laplace transform method for linear differential equations of the fractional order*, arXiv preprint funct-an/9710005, (1997).

[72] I. PODLUBNY, *Fractional differential equations: an introduction to fractional derivatives, fractional differential equations, to methods of their solution and some of their applications*, Elsevier, 1998.

[73] L. S. PONTRYAGIN, *Mathematical theory of optimal processes*, Routledge, 2018.

[74] B. RIEMANN, *Versuch einer allgemeinen auffassung der integration und differentiation*, Gesammelte Werke, 62 (1876).

[75] R. ROSS, *The prevention of malaria*, John Murray, 1911.

[76] S. G. SAMKO, *Fractional integrals and derivatives*, Theory and applications, (1993).

[77] E. SCALAS, R. GORENFLO, AND F. MAINARDI, *Fractional calculus and continuous-time finance*, Physica A: Statistical Mechanics and its Applications, 284 (2000), pp. 376–384.

[78] C. J. SILVA AND D. F. TORRES, *A tb-hiv/aids coinfection model and optimal control treatment*, arXiv preprint arXiv:1501.03322, (2015).

[79] H. SUN, W. CHEN, AND Y. CHEN, *Variable-order fractional differential operators in anomalous diffusion modeling*, Physica A: Statistical Mechanics and its Applications, 388 (2009), pp. 4586–4592.

[80] H. SUN, Y. ZHANG, D. BALEANU, W. CHEN, AND Y. CHEN, *A new collection of real world applications of fractional calculus in science and engineering*, Communications in Nonlinear Science and Numerical Simulation, 64 (2018), pp. 213–231.

[81] Y. TIAN AND X. LIU, *Global dynamics of a virus dynamical model with general incidence rate and cure rate*, Nonlinear Analysis: Real World Applications, 16 (2014), pp. 17–26.

[82] M. TOUFIK AND A. ATANGANA, *New numerical approximation of fractional derivative with non-local and non-singular kernel: application to chaotic models*, The european physical journal plus, 132 (2017), pp. 1–16.

[83] N. H. TUAN, H. MOHAMMADI, AND S. REZAPOUR, *A mathematical model for covid-19 transmission by using the caputo fractional derivative*, Chaos, Solitons & Fractals, 140 (2020), p. 110107.

[84] S. ULLAH AND M. A. KHAN, *Modeling the impact of non-pharmaceutical interventions on the dynamics of novel coronavirus with optimal control analysis with a case study*, Chaos, Solitons & Fractals, 139 (2020), p. 110075.

[85] U.S. Food and Drug Administration, *Fda takes key action in fight against covid-19 by issuing emergency use authorization for first covid-19 vaccine*, December 11 2020. Accessed: September 17, 2024.

[86] N. K. Vaidya and J. Wu, *Hiv epidemic in far-western nepal: effect of seasonal labor migration to india*, BMC Public Health, 11 (2011), pp. 1–11.

[87] P. Van den Driessche and J. Watmough, *Reproduction numbers and sub-threshold endemic equilibria for compartmental models of disease transmission*, Mathematical biosciences, 180 (2002), pp. 29–48.

[88] C. Vargas-De-León, *Volterra-type lyapunov functions for fractional-order epidemic systems*, Communications in Nonlinear Science and Numerical Simulation, 24 (2015), pp. 75–85.

[89] J.-J. Wang, J.-Z. Zhang, and Z. Jin, *Analysis of an sir model with bilinear incidence rate*, Nonlinear Analysis: Real World Applications, 11 (2010), pp. 2390–2402.

[90] X.-y. Wang, Y.-j. He, and M.-j. Wang, *Chaos control of a fractional order modified coupled dynamos system*, Nonlinear Analysis: Theory, Methods & Applications, 71 (2009), pp. 6126–6134.

[91] H. Weyl, *Bemerkungen zum begriff des differentialquotienten gebrochener ordnung*, Vierteljschr. Naturforsch. Gesellsch. Zurich, 62 (1917), pp. 296–302.

[92] W. H. O. (WHO), *Who's covid-19 response timeline*. https://www.who.int/emergencies/diseases/novel-coronavirus-2019/interactivetimeline/#category-Information, 2022. Available from: https://www.who.int/emergencies/diseases/novel-coronavirus-2019/interactivetimeline/#category-Information.

[93] J. Wu, B. Tang, N. L. Bragazzi, K. Nah, and Z. McCarthy, *Quantifying the role of social distancing, personal protection and case detection in mitigating covid-19 outbreak in ontario, canada*, Journal of mathematics in industry, 10 (2020), pp. 1–12.

[94] X.-J. Yang, *General fractional derivatives: theory, methods and applications*, Chapman and Hall/CRC, 2019.

[95] ÀLEX GIMÉNEZ-ROMERO, A. GRAU, I. E. HENDRIKS, AND M. A. MATIAS, *Modelling parasite-produced marine diseases: The case of the mass mortality event of pinna nobilis*, Ecological Modelling, 459 (2021), p. 109705.